Closed Loop Geothermal System Design

by

Ali Ghavidel

A thesis
presented to the University of Waterloo
in fulfillment of the
thesis requirement for the degree of
Doctor of Philosophy
in
Civil Engineering

Waterloo, Ontario, Canada, 2022

© Ali Ghavidel 2022

Examining Committee Membership

The following served on the Examining Committee for this thesis. The decision of the Examining Committee is by majority vote.

External Examiner:	Dr. Hartmut Hollander Professor, Dept. of Civil Eng, University of Manitoba
Supervisor(s):	Dr. Maurice B. Dusseault Professor, Dept. of Earth and Environmental Sciences, University of Waterloo Dr. Robert Gracie Associate Professor, Dept. of Civil and Environmental Eng, University of Waterloo
Internal Member:	Dr. Shunde Yin Associate Professor, Dept. of Civil and Environmental Eng, University of Waterloo
Internal Member:	Dr. Dipanjan Basu Associate Professor, Dept. of Civil and Environmental Eng, University of Waterloo
Internal-External Member:	Dr. Roydon Fraser Professor, Dept. of Mechanical and Mechatronics Eng, University of Waterloo

Author's Declaration

I hereby declare that I am the sole author of this thesis. This is a true copy of the thesis, including any required final revisions, as accepted by my examiners.

I understand that my thesis may be made electronically available to the public.

Abstract

In contrast to other renewable sources (e.g., wind and solar) that may only be intermittently available throughout a day or year, geothermal resources provide a carbon-free and sustainable source of energy for base-load operations during the whole year with only a minor land-use requirement. Geothermal resources can be used for electricity generation, ideally combined with direct heat, which is valuable in cold seasons/areas.

Hot Dry Rocks (HDRs) at various depths present the largest portion of potential geothermal resources across the world. Great depths in low temperature gradient regions and the absence of sufficient natural fluid and permeability present challenges to extraction of heat from HDRs. An Enhanced Geothermal System (EGS) has been the only practical approach to the heat extraction from HDRs. However, the interaction between the injected cold fluid and hot rock mass in the stimulated fractured reservoir commonly leads to substantial challenges, uncertainties, and risks such as high-magnitude induced seismicity, circulating fluid loss, aquifer contamination, and short-circuiting.

A relatively new method, known as the Closed Loop Geothermal System (CLGS) has recently been introduced as an alternative to the EGS approach, which can significantly reduce the risks associated with EGSs. In CLGSs, the fluid is circulated in a closed-loop well system and produces an approximately constant level of heat over a long time (> 30 years); however, a rapid decline in the outlet fluid temperature from the reservoir, one of the main drawbacks of CLGSs, is putting the commercial viability of such systems in doubt. No solution has yet been presented to prevent such a rapid drop in the produced fluid temperature from CLGSs. The final outputs of the whole system, i.e., both heat and electricity generation, coupled with the reservoir system, have not been studied. Furthermore, previous studies have neglected realistic assumptions, such as reservoir evaluation with a non-constant flux and fluid temperature along the wells, non-constant ambient temperature for electricity generation, etc.

This paper-based PhD research is dedicated to designing the CLGS for an acceptable level of electrical power production, in addition to addressing the mentioned gaps, in three main objectives. The first objective, fulfilled in Chapter 2, is to develop a semi-analytical solution for a single-well CLGS to accurately and quickly estimate the production fluid (water) temperature over time for a wide range of practical reservoir parameters without requiring computational cost. Ten reservoir characteristics (including rock and fluid properties, well length and diameter, and injection flow rate) are reduced to three dimensionless parameters, in which realistic boundary conditions are assumed in the analysis, e.g., a non-constant fluid temperature and heat flux. An axisymmetric Finite Element

Method (FEM) program is developed to evaluate the production fluid temperature though transient conduction in the rock mass and conductive-convective heat transfer within and between the rock and fluid. The Response Surface Method (RSM) and power laws are used to present the relationship between output fluid temperatures and times as a function of dimensionless parameters, providing an empirical approximate solution for the mathematical model that can be used in a way similar to analytical solutions. The empirical solution has the advantages of ease and expediency of evaluations, as is often required for the optimization of systems.

The second objective, addressed in Chapter 3, is to design a water-based multilateral-horizontal-well CLGS for optimum heat and electrical power production, by coupling a FEM reservoir simulator with a surface Organic Rankine Cycle (ORC). The design parameters are the number of wells, interwell spacing, well length and diameter, injection flow rate, energy losses along the wells, and ORC working and cooling fluid mass flow rates. The study evaluates how these parameters affect the evolution of the spatial distribution of the temperature of the rock mass, the circulation fluid temperature leaving the reservoir, and the rate of electrical power generation with seasonal variations in surface air temperature. Moreover, the impacts of non-constant ambient air surface temperature and non-constant fluid temperature on electrical power generation are assessed - two variables not previously well studied together but having significant impact on system performance.

The third objective, realized in Chapter 4, is to assess heat and electrical power production from a CLGS with supercritical CO_2 (SCO_2) or water circulating in a hexagonal array of horizontal wells in HDR. The analysis is based on a coupled Finite Volume Method (FVM)/FEM/ORC model, evaluating compressible temperature-dependent pipe flow of water and SCO_2 in the wells and transient conductive-convective heat transfer within and between the rock and fluid, and electricity generation at a non-constant ambient air temperature. The performances of the system are evaluated for different numbers of wells and total injection and ORC mass flow rates to determine the best range of these parameters for optimum heat and electrical power production.

To sum up the research findings, temperature evolution of the reservoir over a wide range of realistic properties is not influenced significantly by the rock and fluid properties, injection flow rate, or well length and diameter, being a function of time only for constant initial rock mass and injection fluid temperatures. Therefore, in a CLGS with a hexagonal array of horizontal wells, the distance between wells beyond which the performance of a hexagonal array of wells is practically indistinguishable from that of a single isolated well is 200 m over 30 years; i.e., the produced fluid temperature is practically unaffected by heat extraction from neighboring wells, regardless of reservoir properties. When using smaller interwell spacing (100 m), the system shows only a small impact ($\sim 1\%$) after 30 years of

heat production. The circulating fluid in CLGS experiences rapid temperature rise, decline and transition periods in less than a year before becoming approximately stable for a long time. Circulating SCO_2 instead of water yields higher production temperatures but less energy content because of the lower volumetric heat capacity of SCO_2 under production conditions. Both water-based and SCO_2-based systems are able to generate considerable amounts of combined heat and electricity (3-4 MW) for over 30 years, which are valuable in northern Canadian communities. Water-based CLGS may be more attractive than SCO_2-based system, as fewer horizontal wells are needed for the same level of power generation (lower drilling costs). Operation costs of SCO_2-based systems would be reduced by thermosyphoning. The system produces the highest electrical power output during cold months and the lowest electrical output during warm ones.

Acknowledgements

I would like to thank my supervisors, Dr. Maurice Dusseault and Dr. Robert Gracie, for their sincere support and encouragement. I also thank the committee members for reviewing this thesis.

Dedication

To the memory of my beloved mother and father who were expecting this day.
To my wife and my family for all their love and sacrifices.

Table of Contents

List of Figures xii

List of Tables xvi

1 Introduction 1

1.1 An Introduction to Geothermal Energy and Heat Extraction Methods . . . 3

1.2 Evaluation of Geothermal Systems . . . 5

1.3 Closed Loop Geothermal System (CLGS) . . . 9

1.4 Motivations . . . 11

1.5 Research Objectives and Methodologies . . . 12

2 Transient Heat Transfer in a Horizontal Well in Hot Dry Rock–Model, Solution, and Response Surfaces for Practical Inputs 15

2.1 Introduction . . . 17

2.2 Methodology . . . 19

2.2.1 Finite Element Method Implementation . . . 25

2.3 Results and Discussions . . . 27

2.4 Conclusion . . . 33

3 Design Parameters Impacting Electricity Generation From Horizontal Multilateral Closed-Loop Geothermal Systems in Hot Dry Rock 41

3.1 Introduction . . . 43

3.2 CLGS Configuration, Models, and Governing Equations 45
3.2.1 CLGS Configuration 45
3.2.2 Reservoir FEM Model and Governing Equations 46
3.2.3 ORC Model and Governing Equations 49
3.3 CLGS Design 49
3.3.1 Reservoir Design (Distance Between Horizontal Wells) 51
3.3.2 The Impacts of Ambient Temperature on Electricity Production . . 57
3.3.3 ORC Properties (Working and Cooling Fluid Mass Flow Rates) . . 60
3.3.4 Number of Wells and Geometry 61
3.3.5 Energy/Head Loss 66
3.4 Conclusion 68

4 Energy From Horizontal Multilateral Closed Loop Geothermal Systems Using Supercritical CO_2 or Water 70

4.1 Introduction 72
4.2 CLGS Configuration and Model Description 74
4.3 Governing Equations 75
4.3.1 Heat transfer in the rock mass 75
4.3.2 Pipe flow for compressible and incompressible fluids 76
4.3.3 Heat transfer for compressible and incompressible fluids 78
4.3.4 Organic Rankine Cycle (ORC) 79
4.4 Results and Discussions 80
4.4.1 Temperature, pressure, and density distribution of SCO_2 along the wells 81
4.4.2 The CLGS performance using SCO_2 compared to water as circulating fluids 85
4.5 Conclusion 105

5 Conclusions, Publications, and Future Works **107**

5.1 Conclusions 108

5.2 Summary of Design Parameters and Assumptions of the Model 110

5.3 CLGS Assessment in Canada 111

5.4 Publications 114

5.4.1 Journal papers 114

5.4.2 Conference presentations 114

5.5 Future Works 115

References **116**

APPENDICES **131**

A Appendix1 **132**

A.1 Numerical Solution Strategy 132

A.2 Organic Rankine Cycle Model 133

List of Abbreviations **141**

List of Figures

1.1 A schematic view of the CLGS with ORC. 11

2.1 Primary circuit schematic view. The power plant is established close to the production well. 20

2.2 The model comprises the fluid domain (Ω_f) within the horizontal wellbore and the rock mass domain (Ω_s). 22

2.3 Axisymmetric model domain with fine meshes on the well wall and coarse meshes on far field boundaries. Colours represent the rock temperature after some time heat production. 26

2.4 Left graph: the outlet fluid temperature over time. Right graph: the fluid temperature along the wellbore at three different times: (a) the first month, (b) the third month, and (c) the fourth year. 29

2.5 Sensitivity study of the effects of dimensionless parameters (α, β, γ) on the outlet fluid temperature over time. 35

2.6 Contour plots of the dimensionless output fluid temperature at different times (years 1, 2, 3, 4) in α and γ space ($D = 0.4m, L = 1000m$). 36

2.7 Contour plots of times (years) at different given dimensionless output fluid temperatures in α and γ space ($D = 0.4m, L = 1000m$). 38

2.8 Power law fit results versus numerical results for different α and γ. 39

2.9 Assessment of two potential geothermal cases using FEM and RS models; case 1 (2 legs with low flow rate and small diameter) versus case 2 (single leg with high flow rate and large diameter). 40

3.1 The closed loop geothermal system (CLGS) with multiple horizontal wells. 46

3.2 The CLGS with two sets of multilateral wells for increasing the system's efficiency. 47

3.3 Schematic diagram of an ideal Rankine cycle (T-s diagram and components). 50

3.4 Schematic presentation of R_{safe} and R_{opt} in two dimensional view for a single horizontal well. 53

3.5 Cross-section view of a single isolated horizontal well and a hexagonally distributed array of horizontal wells of CLGS. 54

3.6 The rock temperature changes in the radial direction from horizontal well (near the injection well) for a wide practical range of geometric, rock and fluid properties (dimensionless numbers α and γ) over time. 55

3.7 The outlet fluid temperature of a single isolated well and an array of wells for $R = 50\ m$ and $R = 100\ m$, indicating $100\ m$ is a reasonable distance between wells ($R_{opt} = 50\ m$). 56

3.8 Electricity generation from a closed loop geothermal system (CLGS), assuming constant (the first graph) and non-constant ambient temperature (the second graph). 57

3.9 Electricity generation for different amounts of working and cooling mass flow rates, assuming ORC parameters as constant values (highlighted green area represents the optimum mass flow rates). 62

3.10 Negligible effects of different well diameters on the outlet fluid temperature and outlet electricity from a closed loop geothermal system, over time. . . 63

3.11 Electricity generation from CLGS with 1 and 2 km horizontal wells during cold months (November, December, January, and February) of the second year for different amounts of injection flow rates and the number of wells. . 64

3.12 Electricity generation from CLGS with 1 and 2 km horizontal wells during April and October of the second year for different amounts of injection flow rates and the number of wells. 65

3.13 Energy loss per kilometer along a horizontal well for different well diameters, injection flow rates, and absolute roughness. 67

4.1 Schematic diagram of the CLGS with multiple horizontal wells in an hexagonal array and an ideal Rankine cycle (T-s diagram and its components). . 75

4.2 Circular inclined pipe flow components. 79

4.3 Temperature distribution of circulating SCO_2 along the wells for the CLGS with the injection temperature of 35 ^oC and flow rate of 4 m^3/min after 2 years. 83
4.4 The temperature of the produced SCO_2 from the reservoir over time. . . . 84
4.5 Density of SCO_2 at different temperatures and pressures along the injection, horizontal, and production well. 86
4.6 Temperature distribution of circulating SCO_2 along the wells compared to that of water for the same CLGS with the same injection and reservoir conditions after the second year. 87
4.7 The difference between the production fluid temperature from the reservoir over time, assuming SCO_2 and water as circulating fluids. 88
4.8 (First graph) The St number, and (Second graph) the Bi number of water and SCO_2 along the wells. 89
4.9 The temperature distribution of circulating SCO_2 along a single well at the second year for two different total injection flow rates (2 and 4 m^3/min). . 91
4.10 The production SCO_2 temperature at the production well at the surface for different injection flow rates over time. 92
4.11 The production SCO_2 temperature for different number of horizontal wells (with a length of 1 km) at a constant total injection flow rate of 6 m^3/min. 93
4.12 The produced SCO_2 and water temperature at the production well for different total injection flow rates and the number of horizontal wells at the second year (with characteristics used in Table 4.1). 94
4.13 The rate of heat extraction from SCO_2-based and water-based CLGSs for different total injection flow rates and the number of horizontal wells after two years (Reservoir characteristics of Table 4.1 with the injection temperature of 35 ^oC and the initial reservoir temperature of 150 ^oC). 95
4.14 The outlet electrical power from a water-based CLGS with 6 horizontal wells and the total injection flow rate of 10 m^3/min for different values of working and cooling mass flow rates during warm seasons (minimum) and warm seasons (maximum) of the second year. 97
4.15 The outlet electrical power from a SCO_2-based CLGS with 6 horizontal wells and the total injection flow rate of 10 m^3/min for different values of working and cooling mass flow rates during warm seasons (minimum) and cold seasons (maximum) of the second year. 98

4.16 The produced electrical power from a water-based CLGS with a total injection flow rate of 10 m^3/min and 6 horizontal well under non-constant ambient temperature ($\dot{m}_{wf} = 50\ kg/s$, $\dot{m}_{cf} = 180\ kg/s$). 100

4.17 The produced electrical power from a water-based CLGS with a total injection flow rate of 10 m^3/min and 6 horizontal well under non-constant ambient temperature. ORC working fluid mass flow rate of 50 kg/s and cooling fluid mass flow rate of 150 kg/s during October to April and 300 kg/s during May to September. 101

4.18 The produced electrical power from a SCO_2-based CLGS with a total injection flow rate of 10 m^3/min and 6 horizontal well under non-constant ambient temperature. ORC working fluid mass flow rate of 40 kg/s and cooling fluid mass flow rate of 150 kg/s during October to April and 250 kg/s during May to September. 102

4.19 The outlet electrical power from water-based CLGS for different total injection flow rates and number of horizontal wells in the second year, with ORC working fluid mass flow rate of 50 kg/s and cooling fluid mass flow rate of 150 and 300 km/s during cold and warm months, respectively (reservoir properties from Table 4.1, injection temperature 35 ^oC, rock temperature 150 ^oC). 103

4.20 The outlet electrical power from water-based CLGS for different total injection flow rates and number of horizontal wells in the second year, with ORC working fluid mass flow rate of 40 kg/s and cooling fluid mass flow rate of 150 and 250 km/s during cold and warm months, respectively (reservoir properties from Table 4.1, injection temperature 35 ^oC, rock temperature 150 ^oC). 104

5.1 The difference between two water-based CLGSs located in low (60 $^oC/km$) and high (75 $^oC/km$) geothermal gradient places. 112

5.2 The difference between two water-based CLGSs with the assumption of two different thermal conductivity for the reservoir granite rock of 0.9 and 3 W/mK. 113

A.1 Schematic diagram of an ideal Rankine cycle (T-s diagram and components). 134

A.2 Isentropic and real work of turbine and pump. 137

A.3 The evaporator diagram T-S and T-q. 140

List of Tables

2.1 The rock mass and fluid properties 28

2.2 Dimensionless parameters ranges based on practical ranges of system's properties. 28

2.3 The power-law fit coefficients and goodness of fit table at given years for different D and L. 31

2.4 The general power-law fit coefficients at given years, valid for all range of D, L, and dimensionless parameters (α and γ). 32

2.5 The power-law fit coefficients and goodness of fit table at given temperatures ($D = 0.4m, L = 1000m$). 32

2.6 The rock mass and fluid properties of two potential geothermal cases' characteristics. 35

2.7 Two potential geothermal cases' characteristics. 37

3.1 Typical range of physical properties of granite and water and potential ranges of CLGS design and operation parameters [1]. 54

3.2 Dimensionless parameters ranges based on practical ranges of reservoir properties. 55

3.3 The reservoir rock of the Utah FORGE site, fluid (water), and ORC properties used in the analysis. 58

3.4 Monthly average surface air temperature of the region of the Utah FORGE site [2]. 59

4.1 Characteristics of the reservoir based on data from the Utah FORGE site data [3]. 81

4.2 ORC properties used in the analysis for SCO_2-based and water-based CLGSs. . 96

4.3 Monthly average surface air temperature used for electricity generation from ORC [2]. 96

A.1 Symbols used for ORC model 135

Chapter 1

Introduction

In this chapter, an overview of geothermal systems is provided. Different methods of heat and electricity production from geothermal systems are briefly discussed, followed by an introduction to different methods for geothermal reservoir evaluation. Subsequently, Closed Loop Geothermal Systems (CLGSs) are discussed in detail. In the last stage, research motivations, objectives, and methodologies used to carry out the research are elaborated.

1.1 An Introduction to Geothermal Energy and Heat Extraction Methods

The world is experiencing rapid growth in global population, increasing demand in different energy sectors. Due to the considerable growth in modern technology, energy consumption heavily relies on the modern form of energy, and appropriate energy resources are required to meet this global demand. The world has already seen peak consumption of different energy resources (wood, coal, and oil), and now it is experiencing, or may already have experienced, the transition from peak oil to natural gas [4]. Over the last decades, humans have encountered the consequences of the extreme usage of fossil-fuels, such as greenhouse-gas emissions, environmental impacts, and global climate change [5]. Therefore, switching from fossil fuels to renewable and low carbon energy resources is urgently needed to tackle the environmental challenges, as two thirds of carbon dioxide emissions are related to energy consumption. Although a significant energy transition has not been possible so far, it is becoming possible through technological innovation, falling costs, and competitiveness among renewable energy sources; however, it is not occurring fast enough to meet agreed-to targets [4, 6].

Among various energy sources, geothermal energy, in contrast to other sources which are dependent on climate variation and are not sustainable for base load operations, provides a clean, carbon-free, reliable, and sustainable source of energy. Although not strictly a renewable resource in the engineering time scale for a given project, available geothermal sources in Earth's crust can be viewed as a renewable energy source at a scale of about a thousand years due to slow replenishing of heat from the Earth's mantle through conductive heat transfer.

Geothermal energy could be an appropriate source for both electricity generation and direct heat, especially in cold regions, where the electricity is used to generate heat through a low-efficiency process, or in remote areas, where the fuel or electricity delivery is difficult and costly. The stored heat energy in the upper 10 km of the Earth's crust is theoretically $\sim 1.3 \times 10^{27} J$ [7]. The total worldwide installed capacity of geothermal electricity generation has substantially increased from 0.2 GW in 1950 to 12.7 GW in 2015 [7, 8], and it could produce 1400 $TWh/year$ by 2050, which is about 3.5% of global electricity generation [8].

Different classifications have been presented for geothermal energy resources based on the reservoir depth, reservoir or output geothermal fluid (geofluid) temperature, reservoir geological type, and end use purposes. In reservoir depth classification, geothermal energy resources vary from shallow depth sediments saturated with warm or hot groundwater or dry steam, to lower grade heat energy stored in rocks at moderate depth (1-4 km), to Hot

Dry Rock (HDR) 5-10 km deep [9]. Temperature based classification divides the resources into three common categories: low-temperature (<80 ^oC) medium-temperature (80-150 ^oC), and high-temperature (>150^oC) resources (otherwise termed low-grade, medium-grade and high-grade) [9]. Classification based on the geological types of reservoir is also common, and it divides geothermal energy resources into three main categories – convective (hydrothermal) systems, conductive systems, and deep aquifers – with some subdivisions related to use [10].

In primary definition of geothermal resources (i.e., hot, shallow, steam-generating fluids), traditional geothermal resources are locally distributed only around the Ring of Fire (the circum-Pacific volcanic belt).. However, HDRs are widely available across the world at various depths and present a huge potential resource for geothermal energy at accessible depths. It has been estimated that HDRs may represent approximately 10 million quads ($1\,quad = 1.06 \times 10^{18} Joules$) of heat energy [11]. However, the absence of sufficient natural fluid, low-permeability rock, and great depth in some areas with low temperature gradients present challenges to the extraction of heat from HDRs [12].

Technology developments have led to relatively new concepts for heat extraction from HDRs, known as Enhanced Geothermal System (EGS), Closed Loop Geothermal System (CLGS), and Open Loop Geothermal System (OLGS), all of which can be designed in different configurations.

In an EGS, one injection well is drilled to a desired depth in HDR, then, the rock mass properties are enhanced by hydraulic stimulation (hydrofracturing or hydroshearing), creating pathways through which a fluid can be circulated to extract heat. The heat exchange volume and area may be further enhanced by multiple long wellbores, including inclined or horizontal ones. An extraction well is drilled to intersect with the fractured reservoir, completing the circulation loop from the injection well to the extraction well. To extract heat, cold water is injected into the system at the injection well, and gains heat as it passes through the reservoir. The hot fluid is then extracted at the production well. The produced hot geothermal fluid is used for electricity generation or direct use purposes at the surface and is then reinjected into the reservoir in a cycle. EGS methods have been widely studied in the literature [13, 14, 15, 16, 17, 18, 19]. Issues of concern in EGS development include heat transfer rate and efficiency, short-circuiting, well stimulation and integrity, and induced seismicity.

An OLGS is an alternative method to EGS for heat extraction from HDRs, in which a closed-end horizontal well is drilled into HDR [20, 21, 22]. Injection and production pathways for the fluid flow are in the same well but in separate tubes and in different directions. This system can be more practical for abandoned horizontal wells in high

temperature oil and gas reservoirs, though currently, no commercial project has been built or tested based on this system.

A CLGS is a new approach to produce heat from HDRs using horizontal wells [23]. In this approach, the injection, horizontal, and production wells form a U-shape closed loop system in the reservoir. The horizontal section may include multiple wells with different lengths. Horizontal wells must be long enough to provide sufficient time and volume for the injected fluid to heat up to an appropriate temperature. A CLGS is isolated from the environment and has the advantage of significantly reducing the risks of seismicity, water loss, and aquifer contamination.

1.2 Evaluation of Geothermal Systems

The evaluation of geothermal systems in a broad view includes different areas of geology (site characterization and selection), geophysics, geochemistry (monitoring, scaling and reactions), geomechanics (drilling, reservoir management, and seismic activity management), and power plant design, all associated with environmental impacts, financial concerns, and policy aspects. An accurate evaluation of the products of a geothermal system is one of the primary steps of a project, affecting the feasibility of the whole system.

The technical evaluation of geothermal systems mainly includes two parts: assessing the subsurface reservoir and the surface facilities. Subsurface reservoir analyses include different aspects of the rock and fluid, drilling process, geometry design, etc., and the surface evaluation assesses the facilities such as power plants in terms of power generation. The reservoir and power plant evaluation methods are discussed in the following.

Reservoir evaluation of geothermal systems encompasses a multiphysics problem due to the interactions between the injected cold fluid and hot dry rock. The problem includes several mutual processes: heat transfer within and between the rock and fluid, fluid flow, chemical reactions, and solid deformations [24, 25, 26, 27, 28, 17]. The mutual effects of these processes cause several issues, such as stress changes, volume shrinkage, reactivation of preexisting fractures or the creation of new ones, seismic events, fracture aperture alteration, changes in permeability, casing issues, etc.

Assessing the mechanical behavior of deep reservoir rock becomes complicated if all *in situ* conditions are considered. Cold-fluid injection into the reservoir may lead to rock matrix thermoelastic shrinkage and a higher fluid pressure in the rock mass (especially for EGS, where the fluid is in direct contact with the rock). Pressure changes and cooling involve massive stress redistribution, leading to regions of reduced normal stress, increased

shear stress, existing fracture aperture increases [29], and secondary small crack creation [30]. These effects can cause fault reactivation and induced seismic activity, together forming one of the main concerns of geothermal projects [13]. Temperature changes in the rock mass and fluid are due to mutual effects of transient heat transfer processes within and between the rock and fluid. Heat transfer processes in geothermal reservoirs include conductive or conductive-convective processes in the rock mass depending on the rock matrix situation (with or without porosity and permeability), conductive-convective process in the fluid, and convective heat transfer between the rock and fluid. Fluid flow analysis (pressure and velocity fields) becomes challenging depending on the geothermal reservoir type and fluid properties. For example, if the injected fluid is compressible like supercritical CO2 (SCO2) or the reservoir is fractured like an EGS reservoir.

Evaluating the mutual and simultaneous impacts of all the aforementioned complex issues on each other (temperature, pressure, deformation) requires a coupled Thermo-Hydro-Mechanical (THM) analysis, if chemical reactions are ignored. Depending on the problem, the objective focus of THM evaluation can either be the whole process, a combination of its parts, or individual parts themselves, namely thermal, hydrological, or mechanical. Although analytical methods have been part of the approach to coupled problems, besides their deep and comprehensible representation of the problem, they have the drawback of many simplifications due to the highly sophisticated situation in the reservoir, which may be too complex to address in a purely analytical solution of regular geometry.

Numerical coupled models, therefore, are necessary for presenting more precise and reliable results by considering all possible real assumptions. THM modeling is commonly built upon the two basic partial coupling mechanisms using continuum mechanics principles [31]: 1) thermoelasticity of solids (T-M), which defines the interaction between the stress-deformation and temperature fields through thermal stress and expansion, and 2) poroelasticity theory (H-M), which describes the interaction between the deformability and permeability fields of porous media. Interaction among fluid flow, heat transfer, and deformation in THM coupling are formulated based on the conservation of mass, energy, and momentum, leading to three inter-related (coupled) partial differential equations (PDEs).

Either continuum or discrete approaches can be used to solve the coupled sets [31]. Continuum approaches have been commonly used for continuous problems and include various numerical methods, such as Finite Element Method (FEM), Boundary Element Method (BEM), Finite Difference Method (FDM), and Finite Volume Method (FVM) [32, 33, 34, 35, 36, 37]. Discrete approaches, on the other hand, are commonly applied for problems with discontinuities (faults, fractures) that are presumed to dominate overall behavior. This approach commonly uses Discrete Element Method (DEM) [38, 39, 40] and Discrete Fracture Network (DFN) method [41, 42].

The choice between using the continuum or the discrete approach is not based on rigid guidelines; rather, it depends on the scale of the problem, especially for rock mechanics problems. For instance, in the presence of a limited number of discontinuities in a large-scale rock mass, blocks surrounded by fractures may be treated as block components in a discrete element modeling approach, but may themselves contain many smaller fractures that are "ignored" to restrict the computational complexity of the problem.

Among the important numerical methods for rock mass modeling, FEM [43] is one of the most well-known numerical tools in engineering computation due to its versatility and flexibility in handling material inhomogeneity and non-linearity. FEM is also suitable for complex geometries and boundary conditions; however, its use is generally limited to modeling small deformations with constant boundary conditions in the far-field [31]. BEM, unlike FEM, automatically simulates the far field effects, but is considered inappropriate for modeling strongly non-linear material behavior, for elastoplastic rock problems, and for cases that have strongly variable permeability with stress. The advantages of DEM is its inherent capability of modeling large scale deformation, but it carries the disadvantage of being incapable of easily modeling far-field elastic effects in the way that FEM does; as well a rock matrix cannot be considered permeable in this method [31]. However, to take advantage of both methods, hybrid methods can be applied, depending on the nature of the problem.

The focus of this research is CLGS design in deep HDRs. Since HDRs have very low porosity-permeability and natural fractures, FEM and FVM, the most powerful tools in the continuum methods, are used to evaluate the heat transfer and fluid flow processes in a reservoir of interest. The reservoir of a CLGS can be created in HDR regions with no faults. Furthermore, the fluid in the wells is not in direct contact with the few existing fractures. Therefore, the role of the fractures and faults in mechanical part becomes less important in the analysis and is ignored in reservoir evaluation. However, due to the considerable rock shrinkage over the long term, mechanical deformations can be evaluated in terms of probable seismic activities, which is beyond the scope of this study.

Moving from the subsurface reservoir, we now consider the surface use of the hot outlet fluid from geothermal systems. Electrical power generation and direct heat are two of the most in-demand forms of energy. Three types of power plants are commonly used for electrical power generation at the surface from geothermal systems: flash steam, dry steam, and binary cycle. Along with these, in some cases, combined systems and hybrid technologies may also be used to produce electricity [44, 45].

Dry steam power plants are commonly used for high temperature resources ($>175^oC$) [46, 47]. In these power plants, the fluid is already in vapor form due to the elevated

temperature of the resource and thus is able to drive the turbine directly. The extracted vapor may then be condensed to water and pumped back into the reservoir. Dry steam power plants are scarce worldwide because of the limited number of high quality resources. Nonetheless, they have played a significant role in the growth of geothermal power in countries such as the US, Italy, Japan, and Indonesia [46].

Flash steam power plants are used for medium to high temperature geothermal reservoirs ($\sim$150-175^oC), where the extraction fluid is a mixture of water and vapor (wet steam) [46, 47]. High-pressure hot water enters a separator, where the pressure is reduced, and the water is transformed into steam, which drives the turbine to generate electricity. Then, the steam is condensed to water and returned to the geothermal reservoir to be reused in a closed loop. Flash steam power plants are widely used nowadays and may contain one or two liquid/vapor separators.

Binary power plants are widely used for electricity generation from low temperature geothermal sources ($<$150^oC) [48]. These power plants have two separate cycles – the geothermal fluid (geofluid) is circulated in the primary cycle and heats a low-boiling-point working fluid circulating in the secondary cycle. For low temperature geothermal resources, flash and dry steam power plants are not feasible. An appropriate reservoir temperature range for binary power plants is 120-150 ^oC, which prevents scaling and corrosion from a practical operational point of view [49]. However, these power plants can work at lower temperatures of between 85 ^oC and 170 ^oC [9].

Binary cycle power plants use the advantages of the lower boiling points and higher vapor pressure of various secondary volatile working fluids. The geofluid at temperature T_i heats up a working fluid with a boiling point $<T_i$ through a heat exchanger. The geofluid is piped back into the reservoir after leaving the heat exchanger, and the working fluid drives the turbine [48]. If the geofluid consists of steam and hot liquid mixture, first, a separator is used to separate the mixture's two phases. The hot separated liquid is used to heat the working fluid through the exchangers. However, since the steam has a higher temperature, it is used in two steps to increase the efficiency of the system: first, it drives a turbine, and then, after leaving the turbine, its temperature is still high enough so that it heats a working fluid in the exchangers.

Working fluids used in binary cycle power plants can be divided into pure substances or a mixture of these substances, e.g., propane, isobutane, pentane, hexane, ammonia, special products (with labels such as R22, R113, R114), and ammonia-water solutions. These substances have environmental impacts and need to be assessed carefully due to their toxicity or safety hazards. However, the greenhouse gas emission potential and water consumption are minor in binary power plants due to the closed-loop cycle [48].

There are two main types of binary cycles: the Organic Rankine Cycle (ORC) and the Kalina cycle. The ORC uses organic fluids such as alkanes (e.g., butane, isobutane, pentane, propane) or commercial synthetic refrigerants (e.g., R245fa) [50]. The ORC is commercially widespread [51] and can be used in various types of resources, especially low temperature resources [52]. The Kalina cycle uses an ammonia-water mixture fluid instead of a pure working fluid and simply is a modified Rankine cycle developed by Kalina in 1982 [53]. Using a mixture of ammonia and water has the advantage of maximizing the heat extraction rate due to the variable boiling point of the working fluid, depending on the percentages of its components [54, 55].

An ideal Rankine cycle engine is comprised of a turbine, generator, condenser, pump, and evaporator. The working fluid undergoes various thermodynamic processes as it passes through the components. A detailed discussion of the thermodynamic processes of the working fluid can be found in the literature [56, 48, 47, 57, 58].

The selection of an appropriate working fluid is an important issue in Rankine cycles, affecting the system's efficiency [52], and it requires analyzing the thermodynamic properties and safety and the environmental impacts of potential working fluids, in addition to the geofluid properties and ambient temperature [47]. A variety of approaches can be found in the literature investigating the working fluid selection for binary power plants [59, 60, 52] under various conditions.

The research described in this thesis focuses on designing a CLGS, including the subsurface reservoir and an ORC. The CLGS and the reason for interest in it will be discussed in the following sections.

1.3 Closed Loop Geothermal System (CLGS)

The concept of a Closed Loop Geothermal System (CLGS) was introduced by the Technical University of Berlin for use in geothermal energy extraction from deep underground reservoirs [23]. Figure 1.1 illustrates the technology scheme of the CLGS. This system can be divided into two main sections: a subsurface reservoir, consisting of vertical and horizontal wells; and surface facilities, commonly a binary power plant (i.e., ORC).

The reservoir of a CLGS is comprised of an injection well connected to a production well by horizontal wells, forming a U-shape closed loop system. To extract heat from the system, a fluid is circulated through it from the injection well to the production well. The circulating fluid absorbs heat as it passes through the wells. The hot production fluid at the surface is used to generate electricity and/or deliver direct heat for different sectors

(e.g., residential, industrial, agricultural), followed by transportation and re-entry to the injection well through a pipeline.

One of the drawbacks of the CLGS is that the circulating fluid cannot maintain high production temperatures over time because of the small contact surface between the circulating fluid and HDR and slow conductive heat transfer in the rock mass [23, 61, 62]. To compensate for the disadvantage of this rapid decline in the production temperature, the reservoir can be designed in different configurations. The horizontal section may include multiple wells with different lengths (1-10 km) to provide sufficient volume and time for the circulating fluid to heat up to an appropriate temperature. The limits of the dimensions with regard to depth and horizontal extension are established by the drilling technology limits.

The wells in the system can be either open hole or cased. The vertical sections are commonly cased due to the drilling process. The horizontal section is usually chemically sealed to prevent circulating fluid losses through the system [23, 63]. Therefore, the heat extraction is performed without any physical interaction between the circulating fluid and the surrounding formation except heat transfer in the closed system.

An ORC is commonly used for electrical power generation at surface facilities due to low to medium temperature resources. In the ORC, the hot production fluid from the reservoir (in the primary cycle) heats up a low boiling-point working fluid (in the secondary cycle) through heat exchangers. The working fluid circulation through the ORC components (turbine, condenser, pump, and evaporator) leads to power generation.

The working fluid reaches a high-temperature/pressure state in the evaporator by receiving heat and enters the turbine as saturated or superheated vapor after leaving the evaporator. The high-temperature/pressure of working fluid leads to producing mechanical work by expanding and rotating the turbine connected to a generator, which produces electricity. The pressure of the working fluid drops through leaving the turbine. The low-pressure working fluid loses heat through the condenser through indirect contact with a cooling fluid like water or air. The working fluid pressure is increased to the evaporator working pressure using a pump. Then it enters into the evaporator, completing the secondary closed loop cycle [64].

A CLGS has several advantages in comparison to the other traditional/available technologies of geothermal systems for heat extraction from the deep underground (hydrothermal system and EGS): (i) unlike hydrothermal systems, which require the presence of sufficient permeability and hot fluid in the reservoir, CLGS can be implemented in most areas, independent of the geographical and geological location. The functionality of a CLGS is based merely on the underground temperature gradient, followed by the main

limiting factors, including the state of the drilling technology and the associated costs. (ii) The fluid circulation in a closed loop without any physical interaction with the surrounding rocks significantly reduces the risks of seismicity, fluid loss, and aquifer contamination. The common risks of scaling in the pipes and precipitation in the pore spaces in the reservoir rocks for hydrothermal or EGS systems are not significant problems, easing the CLGS installation process. (iii) The forecast of the system is highly reliable over very long periods of time because there is no influence of the reservoir liquid paths. In contrast, there are many uncertainties in energy production evaluation from EGS and hydrothermal systems due to the sophisticated multiphysics problems in their reservoirs, such as short circuiting, pore space/fracture aperture changes and flow condition changes.

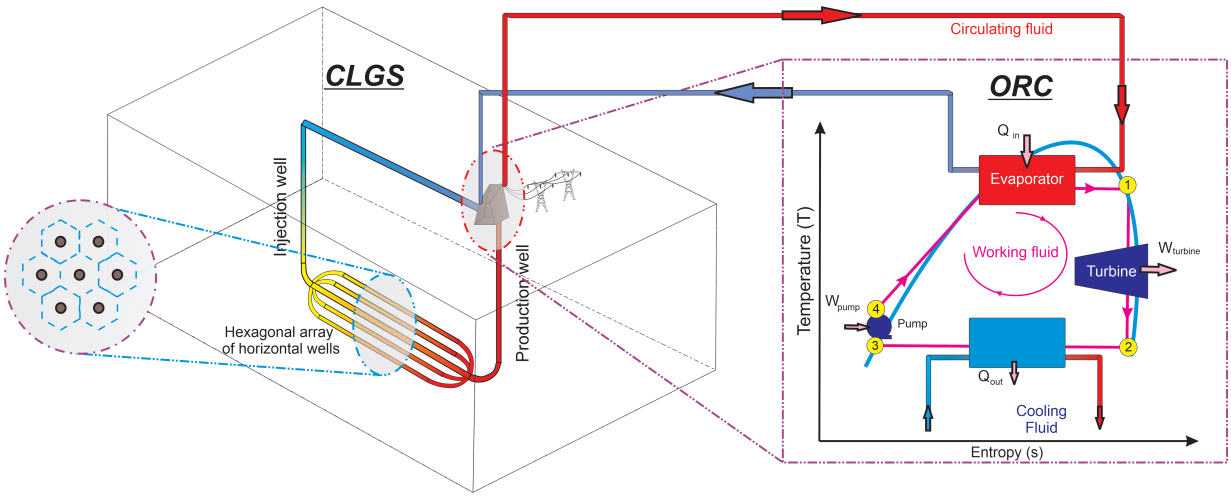

Figure 1.1: A schematic view of the CLGS with ORC.

1.4 Motivations

Among geothermal resources, contrary to locally distributed traditional geothermal resources, HDRs are widely available across the world at various depths, presenting the largest portion of potential geothermal resources for heat and electricity generation [11]. However, great depths in low temperature gradient regions and the absence of sufficient natural fluid and permeability present challenges to the extraction of heat from HDRs [12].

Until recently, the EGS method has been the only practical approach to heat extraction from HDRs. EGS does offer considerable heat production; however, interaction between

the cold injected fluid and hot rock in the artificial fractured reservoir created by hydraulic stimulation leads to serious challenges such as high-magnitude induced seismicity, circulating fluid loss, aquifer contamination, and short-circuiting of fluid flow.

A new method, known as CLGS, has recently been proposed as an alternative method to EGS for heat extraction from HDRs. The CLGS can significantly reduce the risks discussed for the EGS method because in a CLGS, the fluid circulates in a U-shape closed-loop well system [23, 63]. Very few studies in the literature have discussed the CLGS [61, 23]. This system can produce an approximately constant level of heat over a long time (> 30 years); however, a rapid initial decline in the outlet fluid temperature from the reservoir is one of the main drawbacks of CLGSs, putting the commercial viability of such systems in doubt. Previous studies [23, 61, 20, 22] suffer from a lack of a solution to keep the outlet temperature at higher levels. Moreover, to the author's knowledge, no study has evaluated the whole system, i.e., coupling the reservoir and power plant with realistic assumptions, such as reservoir evaluation with non-constant flux and fluid temperature along the wells, horizontal section with multiple horizontal wells, non-constant ambient temperature, etc.

Motivated by these issues, this PhD research is dedicated to designing a CLGS by developing a coupled reservoir/ORC model in terms of optimizing the heat and electricity generation through a parametric study and assuming all realistic assumptions mentioned above. This study is not intended to directly provide a design process for a single case, but to explore aspects of the engineering science that are needed, eventually, for design and finding which parameters are the most important. The main purpose is to find the optimum ranges of the first order reservoir and ORC parameters in terms of maximum heat and electricity generation. The design parameters include flow rates in the wells and the ORC, length, diameter, interwell spacing, and the number of horizontal wells. For higher outlet energy production, the use of SCO_2 as the compressible fluid circulating in the wells is also assessed and compared to water.

1.5 Research Objectives and Methodologies

In this section, the research objectives and methodologies employed to accomplish the objectives are presented.

1: Develop a semi-analytical solution for CLGS to evaluate the output fluid temperature for a wide range of systems characteristics over time

Dimensionless forms of the governing equations are derived, including conduction in the

rock, convection between the wellbore rock and the fluid, and advection and conduction in the fluid along the well. Ten material and geometric parameters are reduced to three dimensionless parameters. The ranges of the dimensionless parameters are identified based on realistic bounds of the material properties (the rock and fluid), geometric parameters (the well length and diameter), and injection flow rates. An axisymmetric FEM program is developed and yields the solution for the temperature of the rock mass and fluid over time. The Response Surface Method (RSM) and power laws are used to present the relationship between output fluid temperatures and times as a function of dimensionless parameters. The power law models provide an empirical approximate solution for the mathematical model and can be used in a way similar to analytical solutions – to accurately and rapidly compute the temperature-time histories of practical geothermal systems. The objective is fulfilled in Chapter 2 of the thesis, and has been published as the following journal article:

Ghavidel, A., Gracie, R., & Dusseault, M.B. (2021). Transient Heat Transfer in a Horizontal Well in Hot Dry Rock–Model, Solution, and Response Surfaces for Practical Inputs. *Applied Thermal Engineering*, 117158.

2: Design CLGS for first-order system (reservoir, wells, ORC) characteristics in terms of maximum outlet fluid temperature and electrical power by developing a coupled reservoir/ORC model for the whole CLGS

A coupled FEM/ORC model is developed for a parametric study of CLGS design with multiple lateral horizontal wells, drilled in HDRs. The model solves the problem of transient heat production in the reservoir and electricity generation evaluation at the surface. The design parameters include interwell spacing, length, diameter, and the number of horizontal wells, injection flow rate, energy losses along the wells, and ORC working and cooling fluid mass flow rates. The model evaluates how these parameters affect the evolution of the spatial distribution of the temperature of the rock mass, the circulation fluid temperature leaving the reservoir, and the rate of electrical power generation with seasonal variations in surface air temperature. The goal is to find the optimum range for the mentioned parameters so that the system delivers the maximum outlet temperature and electrical power. The objective is accomplished in Chapter 3, which has been published as the following journal article:

Ghavidel, A., Gracie, R., & Dusseault, M.B. (2022). Design Parameter Impacting Electricity Generation From Horizontal Multilateral Closed-Loop Geothermal Systems in Hot Dry Rock. *Geothermics*.

3: Evaluate heat and electrical power production from CLGS using compressible supercritical CO_2 compared to incompressible water

A coupled FVM/FEM/ORC model is developed for a CLGS with supercritical CO_2

(SCO_2) and water circulating in a vertical and hexagonal array of horizontal wells in Hot Dry Rock (HDR) to evaluate heat and electrical power production. The FVM/FEM program evaluates incompressible/compressible fluid flow and transient heat transfer within and between the rock and circulating fluids (SCO_2 and water) in the wells. The FVM/FEM CLGS heat transfer simulator is linked to an ORC to evaluate electrical power and heat generation. The goal is to first, compare the production temperature, heat, and electrical power for using SCO_2 and water and second, to find an optimum range of the number of wells and injection flow rates for optimum heat and electrical power production under non-constant ambient temperature. Natural circulation due to thermosyphon effects in SCO_2-based CLGS is also assessed. This objective is fulfilled in Chapter 4, which is currently under review for publication by:

Ghavidel, A., Dusseault, M.B., & Gracie, R. (2022). Energy From Horizontal Multilateral Closed Loop Geothermal Systems Using Supercritical CO_2 or Water. *Geothermics*.

Chapter 2

Transient Heat Transfer in a Horizontal Well in Hot Dry Rock–Model, Solution, and Response Surfaces for Practical Inputs

This chapter is based on the following journal article:

Ghavidel, A., Gracie, R., & Dusseault, M. (2021). Transient Heat Transfer in a Horizontal Well in Hot Dry Rock–Model, Solution, and Response Surfaces for Practical Inputs. *Applied Thermal Engineering*, 117158.

In this journal paper I was the first author and was responsible for the writing of the article. The paper was edited by Dr. Gracie and Dr. Dusseault. I also developed the mathematical and computational formulation and the numerical code.

2.1 Introduction

This chapter presents a solution to the geothermal problem of transient heat production from hot dry rocks using a horizontal well. Switching from fossil fuels to renewable and low carbon energy sources can play an important role in addressing potential environmental challenges. Geothermal heat could be a source of steady, clean, carbon-free, reliable and sustainable energy.

Geothermal heat can be used for electricity generation and for direct use; this can result in greater thermodynamic efficiency. The estimated amount of available heat in the earth varies using different methodologies; although the predicted amount varies based on the definitions and the methods used, all agree that it is a huge number [65, 66, 67, 68, 9]. The total worldwide installed capacity of geothermal electricity generation has increased from 0.2 GW in 1950 to 12.7 GW in 2015 [7, 8]. Geothermal heat could provide 1400 TWh of electrical energy by 2050, about 3.5% of global electricity demand, avoiding about 800 Mt of CO_2 emissions from fossil fuels per year [8]. Geothermal energy use has grown rapidly in many countries such as the United States, the Philippines, Indonesia, Turkey, New Zealand, and Iceland [69]. Direct power generation from dry and wet steam sources has increased to more than 82 countries from 28 in 1995 [70, 71]. Geothermal energy is already a viable source of power; in addition, direct geothermal heat use is increasing in industry and direct habitat heating.

Unlike traditional geothermal resources (i.e., hot, shallow, steam-generating fluids), which are locally distributed, Hot Dry Rocks (HDRs), without fluids and flow paths, are widely available across the world at various depths and present a remarkable potential resource for geothermal energy. By far the largest portion of geothermal resources in the world are in HDRs at accessible depths, approximately 10 million quads ($1\,quad = 1.06 \times 10^{18} Joules$) [11]. Until recently, the existence of a high temperature source at a drillable depth (<2-3 km), the presence of porous and permeable rock, and the availability of sufficient volumes of hot fluid have been the three intertwined and necessary basic parameters of commercializable geothermal power resources. Although areas with high thermal gradient anomalies are found in many HDR regions, the absence of sufficient natural fluid, low-permeability rock, and great depth present challenges to the extraction of heat from HDRs [12].

Technology developments have led to a relatively new concept for heat energy extraction from HDRs, known as an Enhanced Geothermal System (EGS), where the rock mass properties are enhanced by multiple well hydraulic stimulation (hydrofracturing or hydroshearing) with a circulating fluid provided to access the heat. The heat exchange volume

and area may be further enhanced by longer multiple wellbores, including inclined or horizontal wellbores. Although no full-scale commercial projects greater than 10 MW are yet built, the EGS approach may be able to overcome the challenges discussed above. EGS is far less efficient than shallow (<2-3 km) steam sources in terms of power generation and is certain to remain so, but it is far more widely applicable geographically.

A new approach, known as Closed Loop Geothermal System (CLGS), was proposed to produce heat from both hydrothermal systems and HDRs using horizontal wells [23]. The same approach is currently (2020) being tested at full-scale, in Canada. In this approach, horizontal wellbores connect an injection well to a production well, forming a U-shape closed loop. The horizontal wellbores must be long enough to give sufficient time for the injected fluid to be heated to an appropriate temperature. CLGS is isolated from the environment and has the advantage of significantly reducing risks in green-house gas (GHG) emissions, seismicity, water loss, and aquifer contamination. Heat production from CLGS was assessed by Song *et al.,* [61] using numerical methods; however, the boundary condition on the well wall for updating the rock and fluid temperature is simply assumed to be a function of temperature gradient, which can have a significant impact on the outlet fluid temperature over time. The chapter is also limited to specific well geometry characteristics and rock and fluid properties. There is a need for models with fewer assumptions and a need for solutions to these models for a wide range of practical system and rock properties.

Ground Heat Exchangers (GHEs) are another type of closed-loop systems, widely used at shallow depths for space heating and industrial applications. GHEs have been extensively studied with various analytical and semi-analytical solutions [72, 73, 74, 75, 76, 77, 78, 79]. Although GHEs are types of closed-loop systems and related to CLGS, GHEs are sufficiently different from CLGS that models and solutions used for GHEs are not directly applicable to CLGS. Closed-loop GHEs are commonly classified in two categories: U-pipes, comprising a pair of straight pipes, connected with a U-turn at the bottom [80]; and concentric or coaxial pipes, as simple as one straight pipe inside a bigger diameter pipe or as more complex configurations, such as the cylindrical heat source [81], the ring-coil source [82], the helical-line source [83, 84, 85], and the spiral source [86, 87]. Since the upward and downward flowing pipes are very close together, there is heat transfer between these pipes, affecting the overall system efficiency. While the CLGS systems considered here are also U-shaped, flow within the well is one way and the vertical segments of the well are separated by a long (+1 km) horizontal section. Thus, the interaction between vertical segments is negligible and so the models and the solutions available for GHE are not directly appropriate for CLGS. Furthermore, many of the analytical solutions for GHEs are valid for a specific time and space scale; these studies also use empirical constants, which need to be determined by experimental and computational data [88]. In yet other studies, the

models used only evaluated the rock temperature, while assuming constant heat flow rate, constant temperature, or temperature gradient at the wellbore [81, 89]. Thus, while there are numerous existing models for GHEs, they are not directly applicable to the system of interest.

As geothermal systems become more important, many efforts have been made to evaluate the heat transfer process in different conditions and configurations. However, only a few studies have evaluated CLGS so far for specific rock and system properties. Hence, a comprehensive study is needed to evaluate the heat production of CLGS for a wide range of practical well and rock and fluid characteristics. This chapter develops a semi-analytical solution to evaluate the output fluid temperature of a uniform diameter horizontal wellbore for a wide range of system characteristics (such as well diameter and length, injection flow rate, and rock and fluid properties) over time (years). Dimensionless forms of the governing partial differential equations (PDEs) are derived to evaluate the impact of first-order parameters and better understand their impact on the output fluid temperature. Then, a finite element method (FEM) program is developed to evaluate the advection-diffusion heat transfer process from the rock mass to the fluid flowing along the horizontal wellbore. The Response Surface Method (RSM) and power laws are used to present the relationship between output fluid temperatures and times as a function of dimensionless parameters. The power law models provide an empirical approximate solution for the mathematical model and can be used in a way similar to analytical solutions. The empirical solution has the same advantages over FEM as analytical solution – ease and expediency of evaluations, as is often required for optimization of systems.

2.2 Methodology

Heat extraction from a horizontal wellbore is similar to a buried-pipe system that acts as a heat exchanger or radiator (Figure 2.1). This system consists of two vertical wells (injection and production), connected by a long horizontal wellbore, forming a U-shape circuit, referred to as the primary circuit. The horizontal wellbore length accesses enough rock volume for heat energy harvesting. The circulating fluid enters the injection well, heating up during passage through the horizontal wellbore, and hot fluid is extracted at the production well. At the surface, this hot fluid is assumed to pass through a heat exchanger to provide thermal energy to a secondary circuit for power generation or direct heat use. The output fluid from the heat exchanger then moves through a surface pipeline, connecting the power plant to the injection well, and is recirculated through the primary circuit to minimize heat wastage.

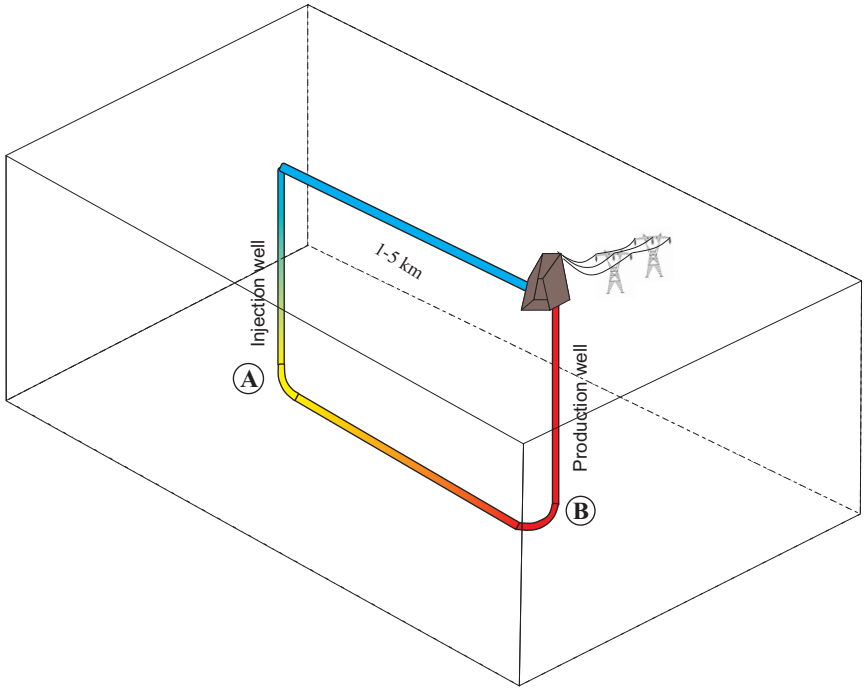

Figure 2.1: Primary circuit schematic view. The power plant is established close to the production well.

The energy output is a function of exit temperature and flow rate. Considering a constant flux, the output fluid temperature is the key factor that determines the quantity of output energy. Commercially successful energy production is challenging in this system because of the small contact surface between the fluid and HDR (the wellbore wall). To increase the output fluid temperature, several approaches can be explored, such as drilling multiple horizontal wellbores, increasing horizontal wellbore length, and increasing the wellbore diameter. However, these solutions cannot be applied without evaluating simultaneous effects of all parameters that affect the output fluid temperature – including the rock mass and fluid characteristics that must be evaluated to guide functionally optimum choices. Here, the thermal behavior of the primary circuit in the ground is explored, without addressing questions related to cost of drilling and other capital expenditures.

Being a coupled transient heat transfer problem affected by several parameters, the output temperature and flow rate cannot be evaluated analytically. On the other hand, if numerical methods are used, many realizations are required, generating large amounts of data for interpretation and presentation. A semi-analytical solution is proposed for a

single horizontal wellbore to analyze and understand the effects of each parameter on the energy production. First, dimensionless forms of the governing equations are derived; then, a finite element code is developed to solve the dimensionless governing equations.

The semi-analytical solution is presented for the domain shown in Figure 2.2. "Semi-analytical" term here represents deriving a dimensionless form analytically and solving the dimensionless form of the governing equations numerically. In the current model, the heat gain/loss due to the vertical segments of the loop system is neglected. Song et *al.*, 2018, [61] have demonstrated that the heat gain/loss from the vertical sections is small compared to the heat gained in the horizontal sections. This assumption is expected to improve with the length of the horizontal well and in systems in which multiple horizontal wells are connected to a single set of vertical wells, the significance of heat gain/loss from the vertical wells will be reduced further. This simplified schematic view includes the rock mass domain (Ω_s) and horizontal wellbore, which includes the fluid domain (Ω_f).

Having very low porosity and permeability, HDRs (e.g., granite) are commonly considered homogeneous, isotropic, impermeable, and rigid rock masses. Transient heat transfer in such a domain is governed by conservation of energy

$$\rho_s c_s \frac{\partial T_s(x,y,z,t)}{\partial t} = k_s \nabla^2 T_s(x,y,z,t) \tag{2.1}$$

in which ρ_s is the bulk density, c_s is the specific heat capacity, k_s is the thermal conductivity, T_s is the rock mass temperature, and t is time. The domain is subject to initial and boundary conditions

$$\begin{aligned} T_s(x,y,z,0) &= T_s^0 \quad \text{on} \quad \Omega_s \\ T_s(x,y,z,t) &= T_s^0 \quad \text{on} \quad \Gamma_T \\ -k_s \boldsymbol{\nabla} T_s(x,y,z,t) \cdot \mathbf{n} &= \bar{q}_c \quad \text{on} \quad \Gamma_{q_c} \\ k_s \boldsymbol{\nabla} T_s \cdot \mathbf{n} + h(T_s(x,y,z,t) - T_f(x,y,z,t)) &= 0 \quad \text{on} \quad \Gamma_{q_h} \end{aligned} \tag{2.2}$$

in which $\boldsymbol{\nabla} \equiv (\frac{\partial}{\partial x}\hat{e}_x + \frac{\partial}{\partial y}\hat{e}_y + \frac{\partial}{\partial z}\hat{e}_z)$ is the Del operator, $\mathbf{n} = (n_x\hat{e}_x + n_y\hat{e}_y + n_z\hat{e}_z)$ is the normal vector, Ω_s is the rock mass domain, and h and T_f are the convective heat transfer coefficient and fluid temperature. The Dirichlet boundary, Γ_T, is subjected to a prescribed temperature, T_s^0, and the Neumann boundary, $\Gamma_q = \Gamma_{q_c} \cup \Gamma_{q_h}$, is subjected to two types of heat flux: constant surface heat flux, $\bar{q}_c$, on Γ_{q_c}, and convective surface heat flux, on Γ_{q_h}– the horizontal wellbore wall, on which the fluid temperature is updated based on the rock temperature over time.

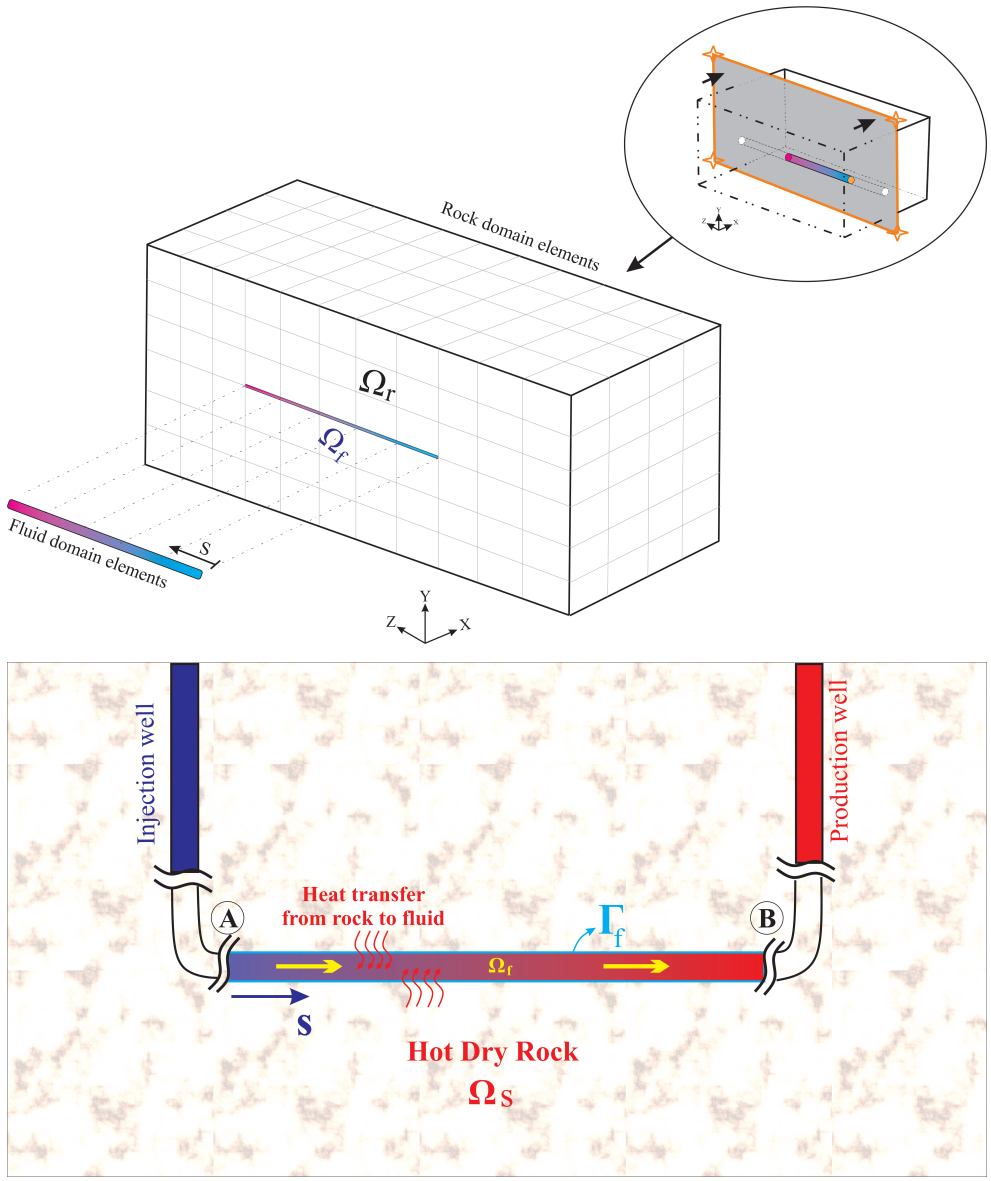

Figure 2.2: The model comprises the fluid domain (Ω_f) within the horizontal wellbore and the rock mass domain (Ω_s).

A Newtonian fluid is injected into the horizontal wellbore at a volumetric flow rate of Q and at a temperature of T_f^{inj}. Heat transfer within the fluid in the wellbore due to advection, diffusion, and heat from the rock mass is governed by

$$-\rho_f c_f u A \frac{\partial T_f(s,t)}{\partial s} + A k_f \frac{\partial^2 T_f(s,t)}{\partial s^2} + \pi D h (T_s(s,t) - T_f(s,t)) = 0, s \in [0, L] \tag{2.3}$$

in which k_f, ρ_f, c_f, u, and T_f are thermal conductivity, bulk density, specific heat capacity, velocity, and fluid temperature. $A = \frac{1}{4}\pi D^2$ is the horizontal wellbore area, and D and L are the diameter and length of the horizontal wellbore. The initial and boundary conditions are:

$$\begin{aligned} T_f(s,0) &= T_f^{inj} \\ T_f(0,t) &= T_f^{inj} \\ \left.\frac{\partial T_f(s,t)}{\partial s}\right|_{s=L} &= 0 \end{aligned} \tag{2.4}$$

Conductive heat transfer in the rock mass is slow, while advection-diffusion heat transfer in fluid is fast. Therefore, heat transfer in the rock mass is assumed as a transient process, whereas quasi-steady state is considered for heat transfer in the fluid because of disparity in timescales analysis [90]. Quasi-steady state does not mean that temperature in the fluid does not change over time, but the time-dependent terms within the governing equations may be neglected.

It is possible to recast the governing equations in dimensionless form. The dimensionless temperatures and spatial coordinates in the rock mass and fluid are defined as

$$\hat{T}_f = \frac{T_f - T_f^{inj}}{T_s^0 - T_f^{inj}}, \hat{T}_s = \frac{T_s - T_f^{inj}}{T_s^0 - T_f^{inj}}, \hat{x} = \frac{x}{L}, \hat{y} = \frac{y}{L}, \hat{z} = \frac{z}{L}, \hat{s} = \frac{s}{L}, \hat{t} = \frac{t}{\tau} \tag{2.5}$$

The scaling factor for time, τ, is a free parameter to be chosen in an intelligent way later. The dimensionless form of the governing equation for heat transfer in the rock mass is

$$\frac{\partial \hat{T}_s}{\partial \hat{t}} = \kappa \nabla^2 \hat{T}_s \tag{2.6}$$

This diffusion equation is subject to the following initial and boundary conditions:

$$
\begin{aligned}
\hat{T}_s\left(\hat{x},\hat{y},\hat{z},0\right) &= 1 \quad \text{on} \quad \Omega_s \\
\hat{T}_s\left(\hat{x},\hat{y},\hat{z},\hat{t}\right) &= 1 \quad \text{on} \quad \Gamma_{T_s} \\
-\kappa\boldsymbol{\nabla}\hat{T}_s(\hat{x},\hat{y},\hat{z},\hat{t})\cdot\mathbf{n} &= \hat{q}_c \quad \text{on} \quad \Gamma_{q_c} \\
\kappa\boldsymbol{\nabla}\hat{T}_s\cdot\mathbf{n}+\gamma(\hat{T}_s(\hat{x},\hat{y},\hat{z},\hat{t})-\hat{T}_f(\hat{x},\hat{y},\hat{z},\hat{t})) &= 0 \quad \text{on} \quad \Gamma_{q_h}
\end{aligned}
\tag{2.7}
$$

with the following dimensionless parameters in the rock mass

$$
\kappa = \frac{k_s\tau}{\rho_s c_s L^2}; \gamma = \frac{h\tau}{\rho_s c_s L} \tag{2.8}
$$

The dimensionless form of the governing equation for heat transfer in the fluid is

$$
-\frac{\partial\hat{T}_f}{\partial\hat{s}} + \beta\frac{\partial^2\hat{T}_f}{\partial\hat{s}^2} + \alpha\left(\hat{T}_s - \hat{T}_f\right) = 0, \hat{s}\in[0,1] \tag{2.9}
$$

which is subject to the following initial and boundary conditions:

$$
\begin{aligned}
\hat{T}_f\left(\hat{s},0\right) &= 0 \\
\hat{T}_f(0,\hat{t}) &= 0 \\
\left.\frac{\partial\hat{T}_f(\hat{s},\hat{t})}{\partial\hat{s}}\right|_{\hat{s}=1} &= 0
\end{aligned}
\tag{2.10}
$$

The dimensionless parameters in the fluid are

$$
\alpha = \frac{4hL}{\rho_f c_f u D}; \beta = \frac{k_f}{\rho_f c_f u L} \tag{2.11}
$$

Let $\kappa = 1$ from Eq.2.8; this yields

$$
\tau = \frac{\rho_s c_s L^2}{k_s} \tag{2.12}
$$

Since κ is relevant only to conductive heat transfer in the rock mass, assuming $\kappa = 1$ leads to the same thermal conductivity for all cases, and indeed the thermal conductivity

for different zero-porosity rocks varies over a limited range. Finally, the three dimensionless parameters remain and can be expressed in terms of well-known dimensionless numbers:

$$\alpha = \frac{4hL}{\rho_f c_f u D} = 4\frac{L}{D}St; \quad \beta = \frac{k_f}{\rho_f c_f u L} = \frac{1}{Pe}; \quad \gamma = \frac{hL}{k_s} = 2\frac{L}{D}Bi \tag{2.13}$$

$$St = \frac{Nu}{RePr} = \frac{h}{\rho_f c_f u}; \quad Pe = \frac{\rho_f c_f u L}{k_f}; \quad Bi = \frac{hD}{2k_s}; \tag{2.14}$$
$$Nu = \frac{hD}{k_f}; \quad Re = \frac{\rho_f u D}{\mu_f}; \quad Pr = \frac{c_f \mu_f}{k_f}$$

in which St is the Stanton number, Pe is the Peclet number, Bi is the Biot number, Nu is the Nusselt number, Re is the Reynolds number, and Pr is the Prandtl number. α is related to the ratio of the rate of convective heat transfer from the rock mass to the fluid versus advective heat transfer in the fluid along the wellbore. In other words, α represents the rate of heat absorbed by the fluid from the rock mass; a higher value of α results in a higher rate of convective heat transfer to the fluid (i.e., consequently a higher output temperature over time). β represents the ratio of the rate of conductive versus advective heat transfer in the fluid along the wellbore. Based on physical interpretation, it is expected that β has a negligible impact on the output fluid temperature because conductive heat transfer in the fluid is much smaller than advective heat transfer. γ is associated with the ratio of the rate of convective heat transfer from the rock mass to the fluid versus conductive heat transfer in the rock mass. In other words, γ determines the heat depletion rate from the rock mass; a higher value of γ accelerates the depletion rate, and in turn the output fluid temperature is expected to drop quickly with time. The convective heat transfer coefficient is defined as a dependent variable using the Ditus-Boelter correlation, the well-known heat transfer correlations of normally sized channels, as below [91]

$$Nu = 0.023 Re^{0.8} Pr^{0.4} \tag{2.15}$$

2.2.1 Finite Element Method Implementation

An axisymmetric FEM code was developed. The rock temperature field is discretized using 6-node quadratic triangular elements. The mesh for the rock is refined around the wellbore, as illustrated in Figure 2.3. The fluid temperature field is discretized using 2 node linear line elements. The discrete equations for conservation of energy in the rock

mass are obtained using a standard Galerkin FEM. The semi-discrete equations for the conservation of the energy in the fluid are obtained using a Least Squares FEM, as the standard Galerkin approach is unstable for advection-dominated problems, as considered here. Numerical time integration is performed using the Crank-Nicolson ($\theta = 0.5$) scheme with a time step of one day.

Figure 2.3 illustrates the model geometry and mesh configuration in axisymmetric coordinates. Colours represent the rock temperature after some time of heat production. Fine meshes were defined around the horizontal well, and coarse meshes were used near the far field boundaries. The outer boundaries are placed far enough from the horizontal well to avoid boundary condition effects on simulation results. In the current model, the vertical temperature gradient in the rock mass is neglected. This is a reasonable assumption since the horizontal well is assumed to be located at a constant depth and the region about the well affected by heat transfer is relatively small, as shown in Figure 2.3. Thus, natural temperature gradient effects are expected to be second order.

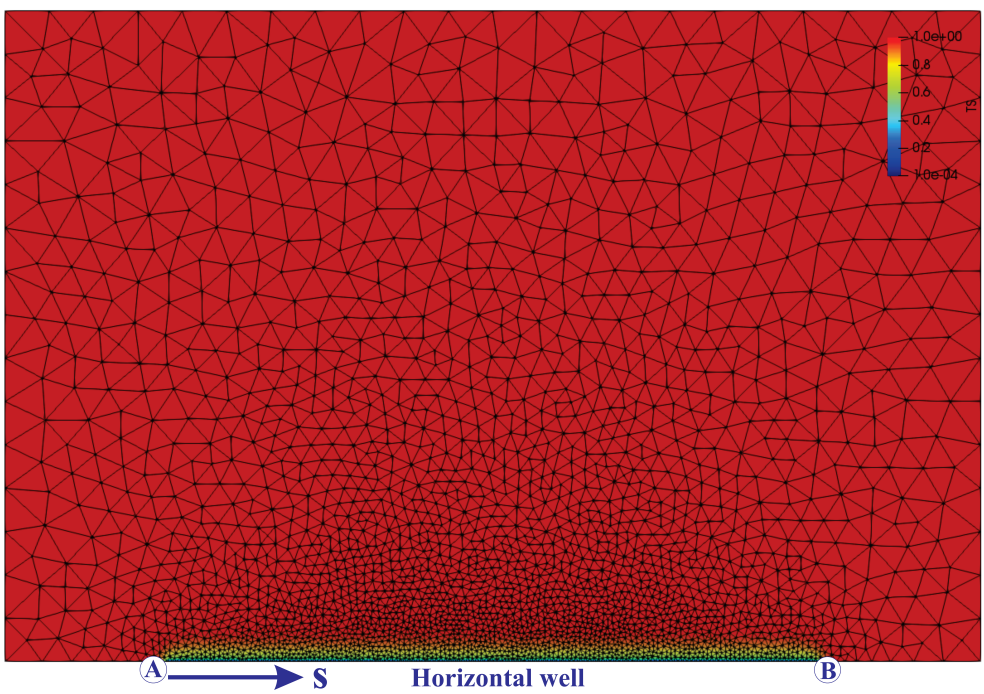

Figure 2.3: Axisymmetric model domain with fine meshes on the well wall and coarse meshes on far field boundaries. Colours represent the rock temperature after some time heat production.

Since the mathematical model developed is transient and couples the fluid and rock temperature, analytical solutions to this problem are non-trivial and are not readily derived. Currently, there does not exist an analytical solution for this problem. The mathematical model has not been validated by experiments or comparison to field data, though this is desirable in the future. The FEM program has been extensively verified.

2.3 Results and Discussions

The closed-loop system (for heat production from HDRs by circulating fluid) comprises two vertical wells (injection and production) and a horizontal wellbore. The main portion of heat transfer from the rock mass to the circulating fluid occurs along the horizontal wellbore [61]. Since HDRs have very low permeability, only rock mass conductive heat transfer is possible, and advection-diffusion dominates the heat transfer from the rock mass to the fluid in the horizontal wellbore.

The rock mass and fluid properties can vary for different HDRs and circulating fluids. The horizontal wellbore length and diameter can also vary depending on the engineering design requirements. Consequently, evaluating the output fluid temperature for all parameters' ranges is difficult.

To narrow the parameters' ranges, the rock mass and fluid are chosen to be specific: granite (i.e., with porosity less than 1%) and water (i.e., fresh water up to saturated NaCl brine). The horizontal wellbore length (L) and diameter (D), and fluid velocity (u) are first-order parameters that can be varied for engineering design purposes. Table 2.1 illustrates the parameters' ranges used for this study. The convective heat transfer coefficient (h) ranges using Equation 2.15 and laboratory results [92] are the same range.

Although narrowing the parameters' ranges results in easier evaluation, the number of parameters is still high, making interpretation difficult. Using the dimensionless parameters, derived in the previous section, decreases the output fluid temperature dependency on ten parameters to three parameters (α, β, γ). Possible ranges for these three dimensionless parameters are presented in Table 2.2 based on the properties given in Table 2.1.

The fluid temperature increases along the wellbore mainly due to convective heat transfer, which is the predominant heat transfer mechanism within the wellbore. After some time, the output temperature (at constant Q) begins to decrease because the contribution of the conductive heat transfer in the rock mass is slow and cannot replenish heat loss on the wellbore wall. Figure 2.4 shows the output fluid temperature over time (the left graph)

Table 2.1: The rock mass and fluid properties

Properties	**Variable**	**Units**	**Value**	**Reference**
Rock density	ρ_s	kg/m^3	2500–3010	[93, 94]
Specific heat capacity of rock	c_s	J/kgK	790–950	[95, 96, 97, 98]
Rock thermal conductivity	k_s	W/mK	0.96–3.62	[93, 95, 99, 100, 101]
Fluid density (water)	ρ_f	kg/m^3	950-1200	[102, 103]
Specific heat capacity of fluid	c_f	J/kgK	3200–4180	[103, 104]
Fluid thermal conductivity	k_f	W/mK	0.6–0.7	[105, 103]
Fluid dynamic viscosity	μ_f	$Pa.s$	2.8×10^{-4}–8×10^{-4}	[105]
Horizontal wellbore diameter	D	m	0.2–0.4	
Horizontal wellbore length	L	m	500–2000	
Fluid velocity	u	m/s	0.5-3	
Convective heat transfer coefficient	h	W/m^2K	1200–13000	[92, 91]

Table 2.2: Dimensionless parameters ranges based on practical ranges of system's properties.

Parameter	**Minimum**	**Maximum**
$\alpha = 4\frac{L}{D}St$	1	3×10^{2}
$\beta = \frac{1}{Pe}$	2×10^{-11}	9×10^{-10}
$\gamma = 2\frac{L}{D}Bi$	7×10^{4}	3×10^{7}

and the fluid temperature along the wellbore (the right graph) at three different times for specific dimensionless parameters.

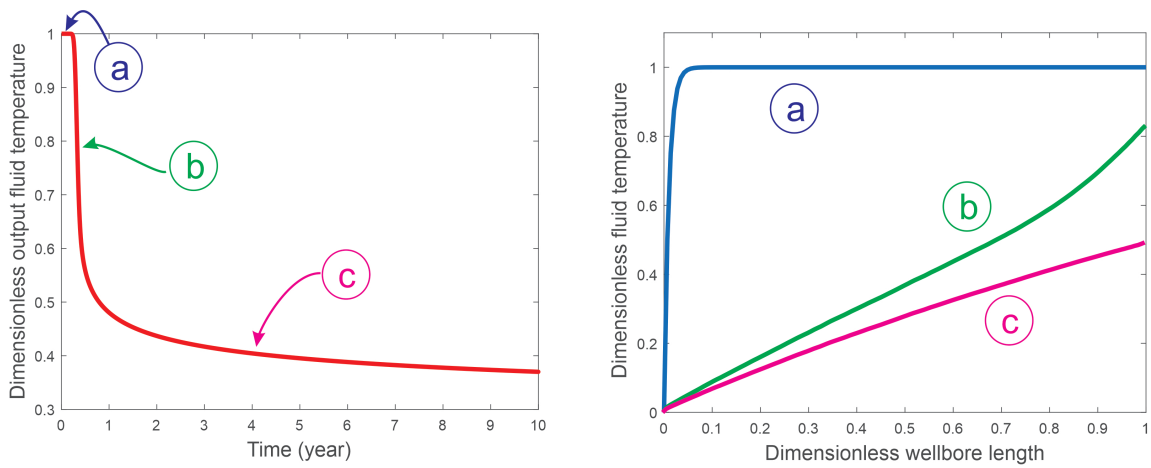

Figure 2.4: Left graph: the outlet fluid temperature over time. Right graph: the fluid temperature along the wellbore at three different times: (a) the first month, (b) the third month, and (c) the fourth year.

A sensitivity analysis is conducted to determine the dimensionless parameters' effects on the output fluid temperature. Figure 2.5 shows the output fluid temperature for three dimensionless parameters, separately, considering the two others to be constant. As can be seen, β has a negligible impact on the output temperature because β is relevant only to conductive heat transfer in the fluid. The impacts of α and γ on the output fluid temperature, unlike β, are considerable. α is associated with the magnitude of the rock mass temperature that provides heat along the wellbore; a higher value of α results in a higher output fluid temperature over time. γ acts on the horizontal wellbore wall as a coefficient related to the heat depletion rate from the rock mass; i.e., increasing γ accelerates the depletion rate, which leads to the output fluid temperature dropping more rapidly with time.

Considering negligible effects of β, the heat transfer process is a function of dimensionless parameters (α, γ) and horizontal well geometry (D, L). Depending on wellbore diameter and length, the range of dimensionless parameters will change in the given range in Table 2.2.

To be able to easily estimate the outlet fluid temperature at a given time, a Response Surface (RS) can be delineated to represent the output fluid temperature at specific times

as a function of α, γ, D, and L. Although this function does not include time directly, it can be calibrated for different times, D and L. A power law response surface is defined as

$$\hat{T}_{out} = c_0 \alpha^{c_1} \gamma^{c_2} = c_0 (4\frac{L}{D}St)^{c_1} (2\frac{L}{D}Bi)^{c_2} \tag{2.16}$$

in which $\hat{T}_{out}$ is the dimensionless output fluid temperature, and c_0, c_1, and c_2 are the coefficients dependent on α, γ, D and L. Tables 2.3 illustrates the coefficients and the goodness of fit for the power law fitted at different times for the first four years at different D and L. In this table R^2, SSE, and RMSE stand for R-square, Sum of Square Errors, and the Root Mean Square Error, respectively.

In practical applications, large values of α will not coincide with small values of γ, nor vice versa. For instance, increasing h increases both dimensionless parameters. Therefore, combinations of associated small α and large γ (and vice versa) were excluded from data used to fit the response surface. The upper and lower bounds of data points can be defined based on the minimum and maximum rock mass and fluid properties as

$$\gamma - 1.37 \times 10^6 \alpha < 0 \qquad \text{upper bound} \tag{2.17}$$

$$\gamma - 2.1 \times 10^4 \alpha > 0 \qquad \text{lower bound} \tag{2.18}$$

To be able to present unique coefficients for the power law in a general form, which are valid for all D, L, α, and γ, the power law coefficients can be expressed as a function of D and L. The coefficients of general form for the power law (C_0, C_1, and C_2), can be calculated using linear interpolation as follows (Table 2.4)

$$C = a_0 + a_1 D + a_3 L \tag{2.19}$$

To graphically demonstrate the output fluid temperature dependency on the dimensionless parameters, contours of dimensionless temperature for $D = 0.4m, L = 1000m$, as an example, are plotted for each of the first four years of production in Figure 2.6. Higher α and lower γ values result in higher output fluid temperature. In other words, to produce fluid at the production well with a higher temperature, α and γ must be as high and as low as possible, respectively.

The temperature of the produced fluid which feeds a geothermal power plant is a key parameter for power generation. Keeping the output fluid temperature as high as

Table 2.3: The power-law fit coefficients and goodness of fit table at given years for different D and L.

Year	$D(m)$	$L(m)$	c_0	c_1	c_2	R^2	SSE	RSME
1	0.2	2000	1842	0.971	-0.878	0.997	3×10^{-3}	3×10^{-3}
	0.3	1500	2342	0.982	-0.935	0.999	3×10^{-4}	1×10^{-3}
	0.4	1000	2391	0.969	-0.940	0.999	1×10^{-4}	8×10^{-4}
2	0.2	2000	2527	0.925	-0.891	0.999	3×10^{-3}	2×10^{-3}
	0.3	1500	2500	0.962	-0.940	0.999	1×10^{-4}	8×10^{-4}
	0.4	1000	2374	0.963	-0.945	0.999	8×10^{-5}	6×10^{-4}
3	0.2	2000	2648	0.921	-0.896	0.999	2×10^{-3}	2×10^{-3}
	0.3	1500	2509	0.959	-0.943	0.999	9×10^{-5}	7×10^{-4}
	0.4	1000	2337	0.962	-0.948	0.999	7×10^{-5}	6×10^{-4}
4	0.2	2000	2699	0.920	-0.899	0.999	2×10^{-3}	2×10^{-3}
	0.3	1500	2501	0.958	-0.944	0.999	8×10^{-5}	6×10^{-4}
	0.4	1000	2306	0.962	-0.949	0.999	6×10^{-5}	5×10^{-4}

possible (preferably higher than 0.7) over the geothermal project lifetime can assure the project viability. Fluid production temperatures less than 0.4 have little interest in power generation as they represent a 60% decrease from the maximum rock temperature (T_s^0) and the input fluid temperature (T_f^{inj}) (assumed constant). Figure 2.7 presents contour plots for the time required for the production temperature to decrease to temperatures 0.9 to 0.4 as a function of both α and γ at the same well diameter and length of the previous case ($D = 0.4m$ and $L = 1000m$). In other words, at different production temperatures, the associated times can be determined for specific α and γ (i.e., specific rock mass and fluid). To keep the output fluid temperature at a certain temperature for a longer time, high α and low γ are needed.

Times at specific temperatures can be found using a response surface model as a function of α and γ. The functional relationship between times and temperature higher than 0.4 in α and γ space can be defined by a power law expression:

$$Time = p_0 \alpha^{p_1} \gamma^{p_2} \tag{2.20}$$

Table 2.5 illustrates the power-law coefficients and the goodness of fit information for $D = 0.4m$ and $L = 1000m$.

The response surface model results are compared with the reference model results at

Table 2.4: The general power-law fit coefficients at given years, valid for all range of D, L, and dimensionless parameters (α and γ).

Coefficient	Year	a_0	a_1	a_2
C_0	1	3.0×10^{18}	-5.1×10^{18}	1.0×10^{15}
	2	6.8×10^{17}	-1.1×10^{18}	-2.2×10^{14}
	3	2.2×10^{17}	-3.7×10^{17}	-7.5×10^{13}
	4	-2.0×10^{16}	3.4×10^{16}	-6.8×10^{12}
C_1	1	1.6×10^{14}	-2.7×10^{14}	5.5×10^{10}
	2	2.7×10^{14}	-4.1×10^{14}	-8.2×10^{10}
	3	2.4×10^{14}	-4.0×10^{14}	8.0×10^{10}
	4	2.3×10^{14}	-3.9×10^{14}	-7.7×10^{10}
C_2	1	-3.5×10^{14}	5.9×10^{14}	1.2×10^{11}
	2	-3.0×10^{14}	5.0×10^{14}	1.0×10^{11}
	3	-2.8×10^{14}	4.8×10^{14}	9.6×10^{10}
	4	-2.7×10^{14}	4.5×10^{14}	9.1×10^{10}

Table 2.5: The power-law fit coefficients and goodness of fit table at given temperatures ($D = 0.4m, L = 1000m$).

Temperature	p_0	p_1	p_2	R^2	SSE	RMSE
0.4	0.0141	0.9903	-0.0958	0.997	5×10^{-4}	1×10^{-3}
0.5	0.0099	0.9987	-0.0780	0.998	2×10^{-4}	1×10^{-3}
0.6	0.0078	1.010	-0.0680	0.999	1×10^{-4}	8×10^{-4}
0.7	0.0063	1.024	-0.0610	0.999	1×10^{-4}	7×10^{-4}
0.8	0.0051	1.043	-0.0552	0.999	8×10^{-5}	6×10^{-4}
0.9	0.00387	1.071	-0.0496	0.999	6×10^{-5}	5×10^{-4}

different α and γ in Figure 2.8. Points refer to the response surface results, and continuous lines are the reference model results. Points are calculated using power-law Equations 2.16 and 2.20 with coefficients from Tables 2.3 and 2.5 for given temperatures and times. The computationally efficient response surface model provides sufficiently accurate results for engineering design and optimization. The response surface models can be viewed as an approximate analytical solution for geothermal energy production using conductive heat transfer to a single horizontal wellbore.

The temperature of the fluid produced can be readily calculated for a geothermal project using the response surface model (Equations 2.16 and 2.20). Two potential geothermal projects are assessed as examples to demonstrate the calculation process using the FEM and response surface models. The geothermal cases' characteristics are presented in Tables 2.6 and 2.7 with the same fluid and rock mass properties, but different injection flow rates (Q), wellbore lengths (L) and diameters (D). The rock mass and injection fluid temperatures for the two cases are the same ($T_s^0 = 150^oC$, $T_f^{inj} = 50^oC$). Case 1 consists of two parallel non-interacting wellbores in which the volumetric injection flow rate is subdivided equally between two wells. Figure 2.9 shows the reference model and response surface model results for two cases.

Employing optimization techniques in geothermal projects is challenging due to unavailable analytical solutions and expensive numerical simulations. Using response surface models, similar to the above models, optimization techniques can be more readily deployed. For instance, at a specific geothermal site (i.e., specific rock mass and fluid properties), different configurations of Q, L, and D can be readily examined using response surface models to determine the best configurations for optimum/maximum heat production while minimizing cost. Furthermore, these empirical solutions can be used to estimate the time required to recover initial project costs.

2.4 Conclusion

This chapter presented the solution to the problem of transient heat production from hot dry rocks in geothermal systems using a horizontal well. The outlet fluid temperature over time is the key quantity of interest for commercial viability of a project. The heat transfer process includes conduction in the rock, convection between the wellbore rock and the fluid, and advection and conduction in the fluid along the well.

Dimensionless forms of the governing equations were derived and depend on three dimensionless parameters: the ratio of the rate of heat storage in the fluid to the rate the

heat convection to the fluid from the rock ($\alpha = 4\frac{L}{D}St$); the ratio of the rate of conductive versus advective heat transfer in the fluid ($\beta = \frac{1}{Pe}$); and the ratio of heat convection to the rock from the fluid to the rate of heat depletion in the rock ($\gamma = 2\frac{L}{D}Bi$). The ranges of the dimensionless parameters were identified based on realistic bounds of the material properties (the rock and fluid), geometric parameters (the wellbore length and diameter), and injection flow rates. The solution to the governing equations was acquired using a custom FEM program.

The sensitivity analysis indicates that the impact of β is negligible on the output fluid temperature since the conductive heat transfer rate is much smaller than the advective heat transfer rate in the fluid. Contour plots of system response at different times and dimensionless output fluid temperatures were presented for practical values of α and γ. The results demonstrate that increasing α or decreasing γ leads to higher output fluid temperatures over time. However, based on practical meaningful inputs and dimensionless parameter definitions, combinations of very large α and very low γ (or vice versa) cannot coincide. Finally, power law response surface models were fitted using FEM analysis results; functional relationships between dimensionless output fluid temperatures and times were defined as a function of α and γ. The power law models provide the opportunity to accurately and quickly compute the temperature-time histories and can be deployed in the optimization of geothermal systems.

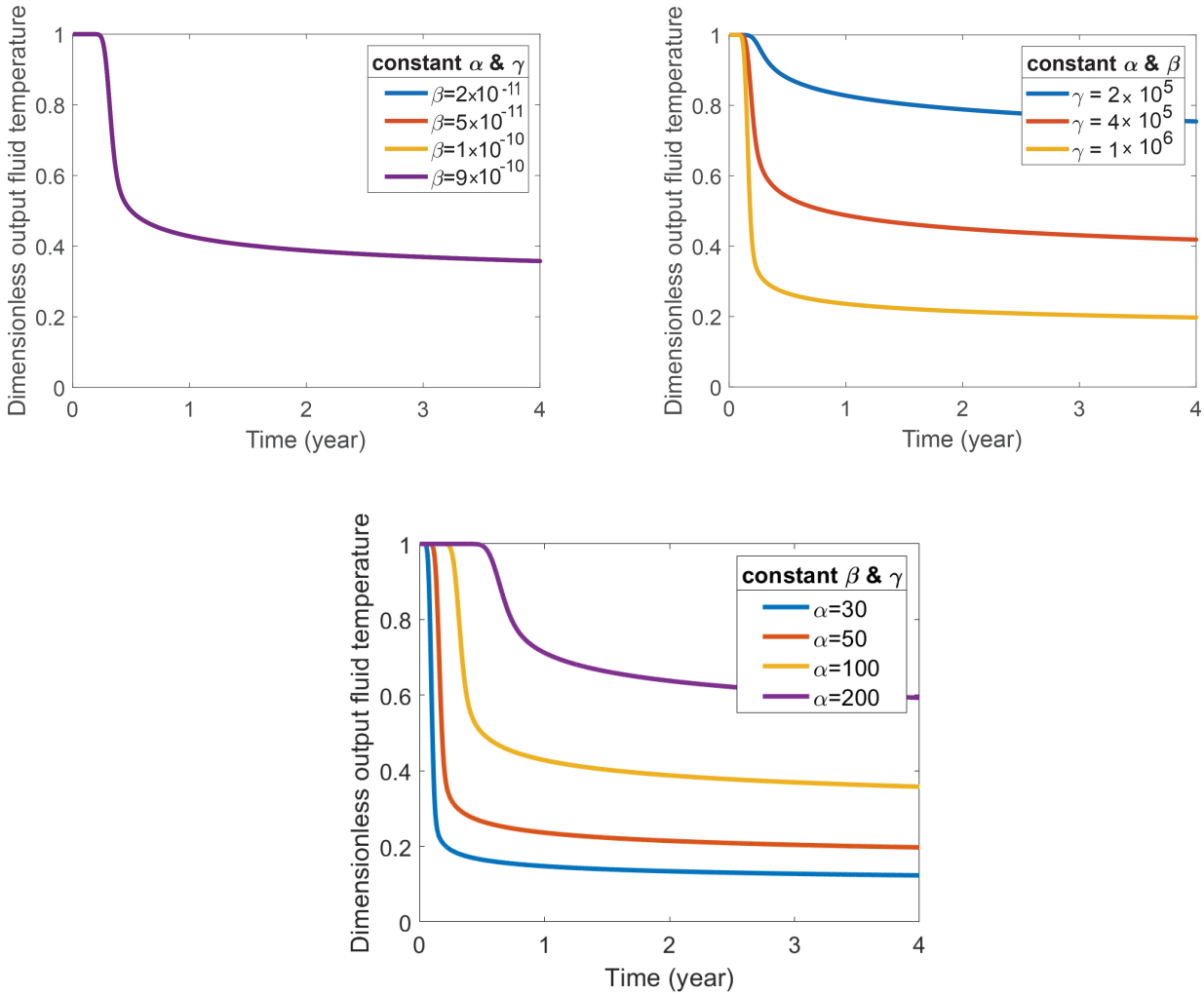

Figure 2.5: Sensitivity study of the effects of dimensionless parameters (α, β, γ) on the outlet fluid temperature over time.

Table 2.6: The rock mass and fluid properties of two potential geothermal cases' characteristics.

Case	$\rho_s(\frac{kg}{m^3})$	$c_s(\frac{J}{kgK})$	$k_s(\frac{W}{mK})$	$\rho_f(\frac{kg}{m^3})$	$c_f(\frac{J}{kgK})$	$\mu_f(Pa.s)$
1&2	2900	950	3.62	960	3250	3×10^{-4}

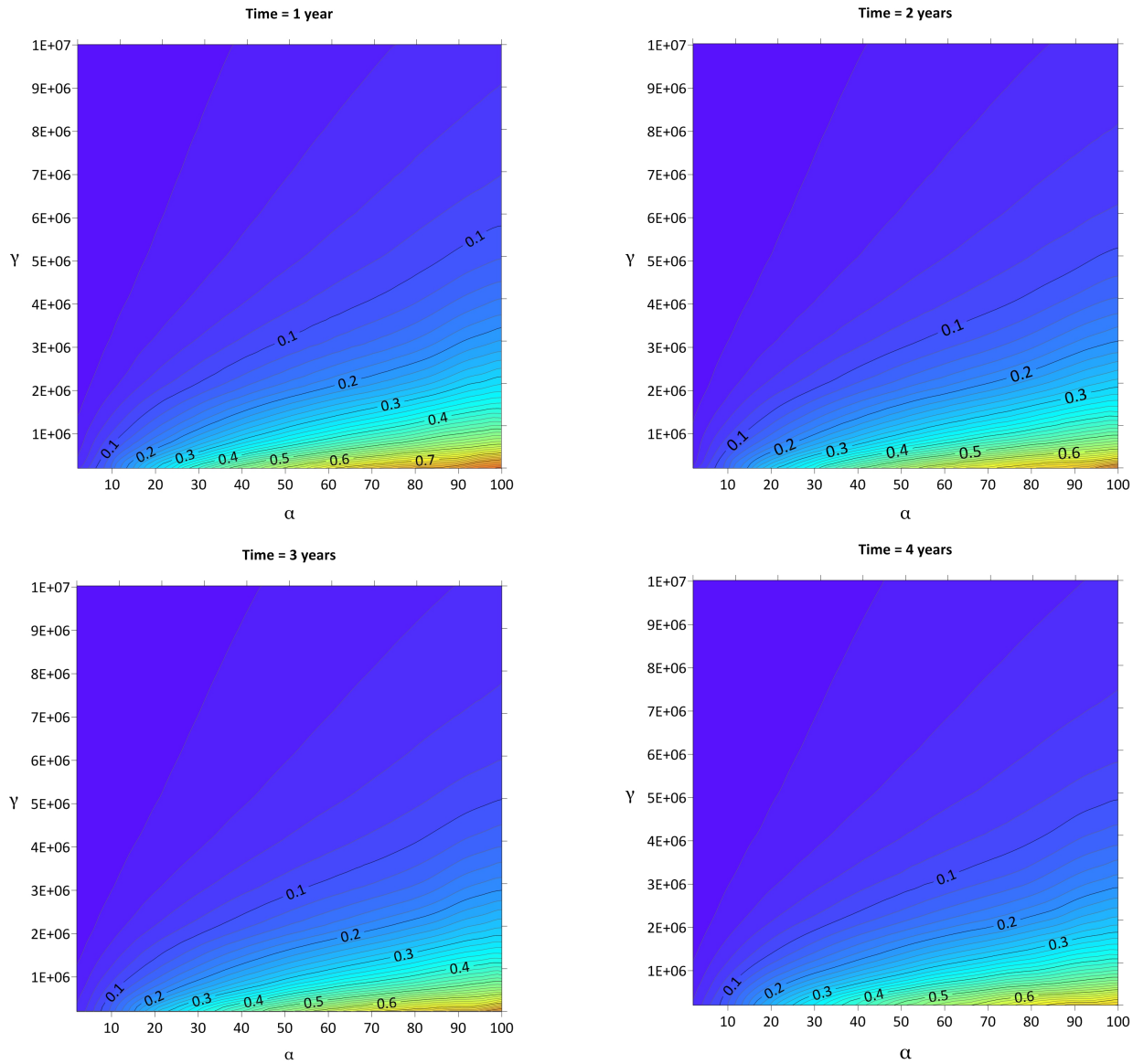

Figure 2.6: Contour plots of the dimensionless output fluid temperature at different times (years 1, 2, 3, 4) in α and γ space ($D = 0.4m, L = 1000m$).

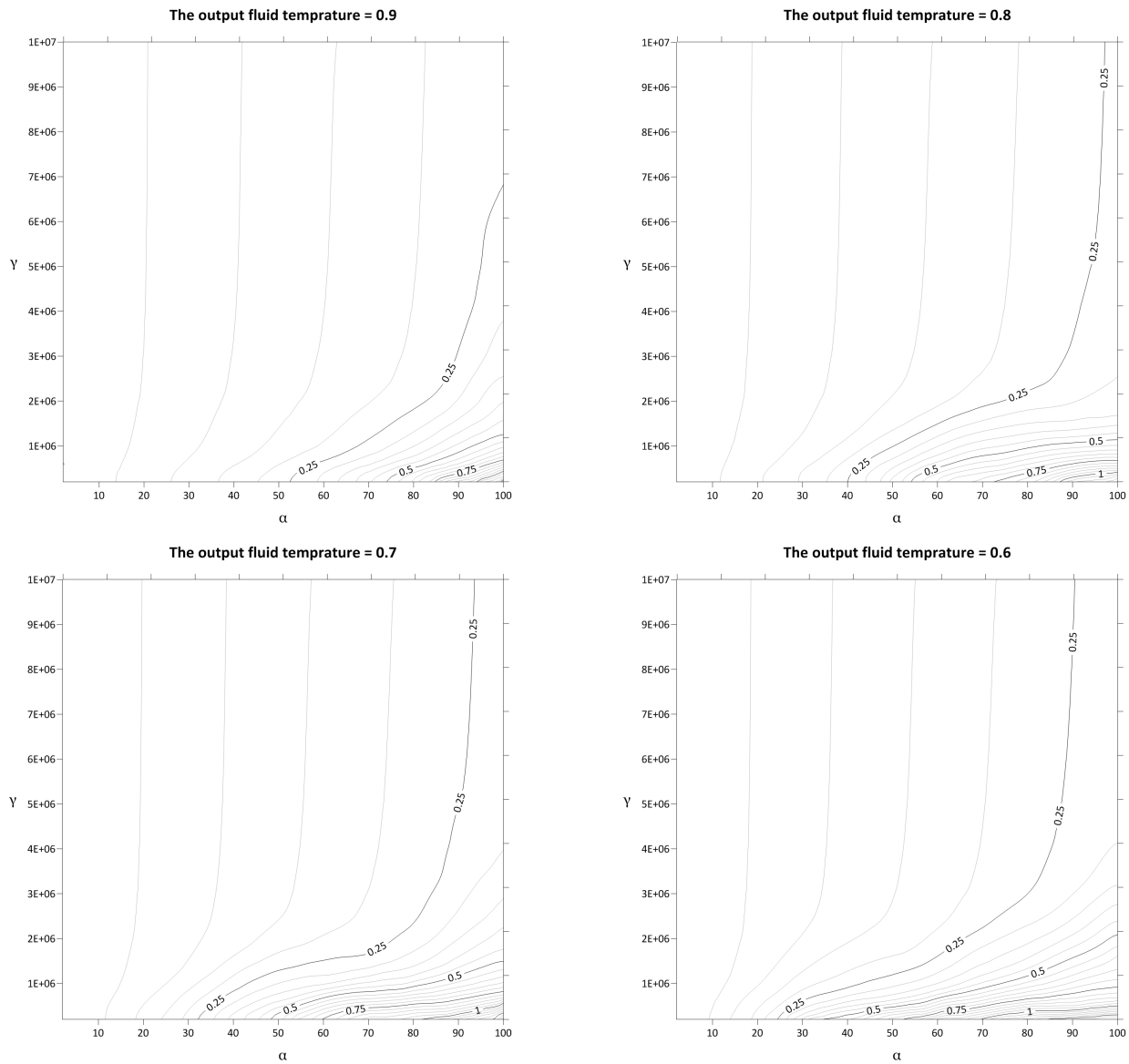

Table 2.7: Two potential geothermal cases' characteristics.

Case	$L(m)$	$D(mm)$	$Q(L/s)$	$\alpha = \frac{4L}{D}St$	$\gamma = \frac{2L}{D}Bi$
1	2(legs)×2000	200	33	60	1.37×10^6
2	2000	400	125	22	2.07×10^6

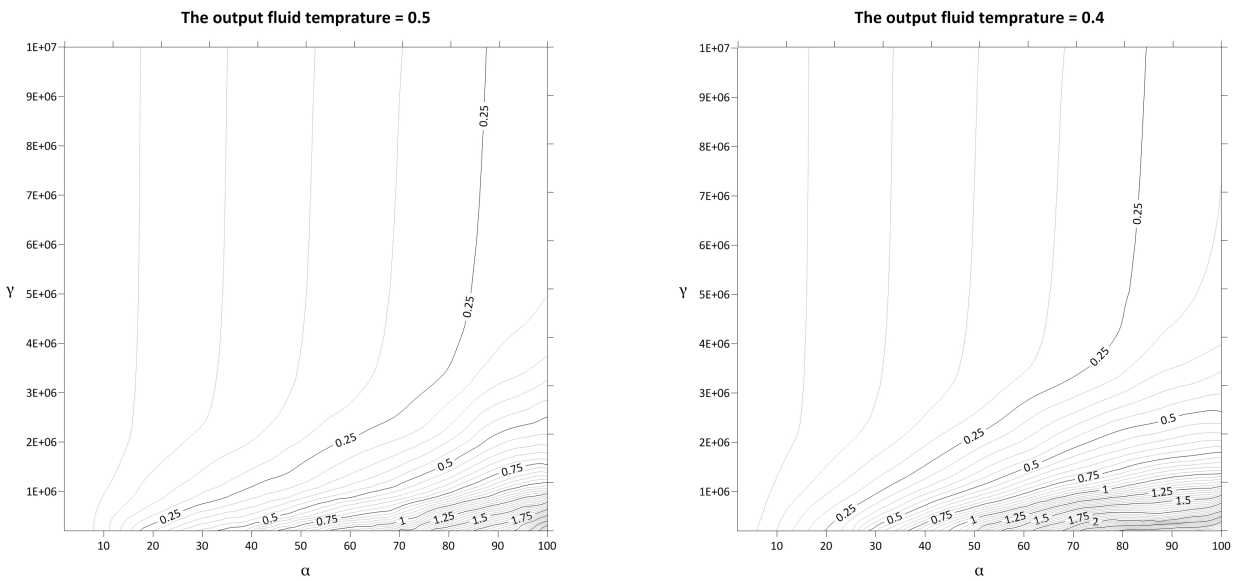

Figure 2.7: Contour plots of times (years) at different given dimensionless output fluid temperatures in α and γ space ($D = 0.4m, L = 1000m$).

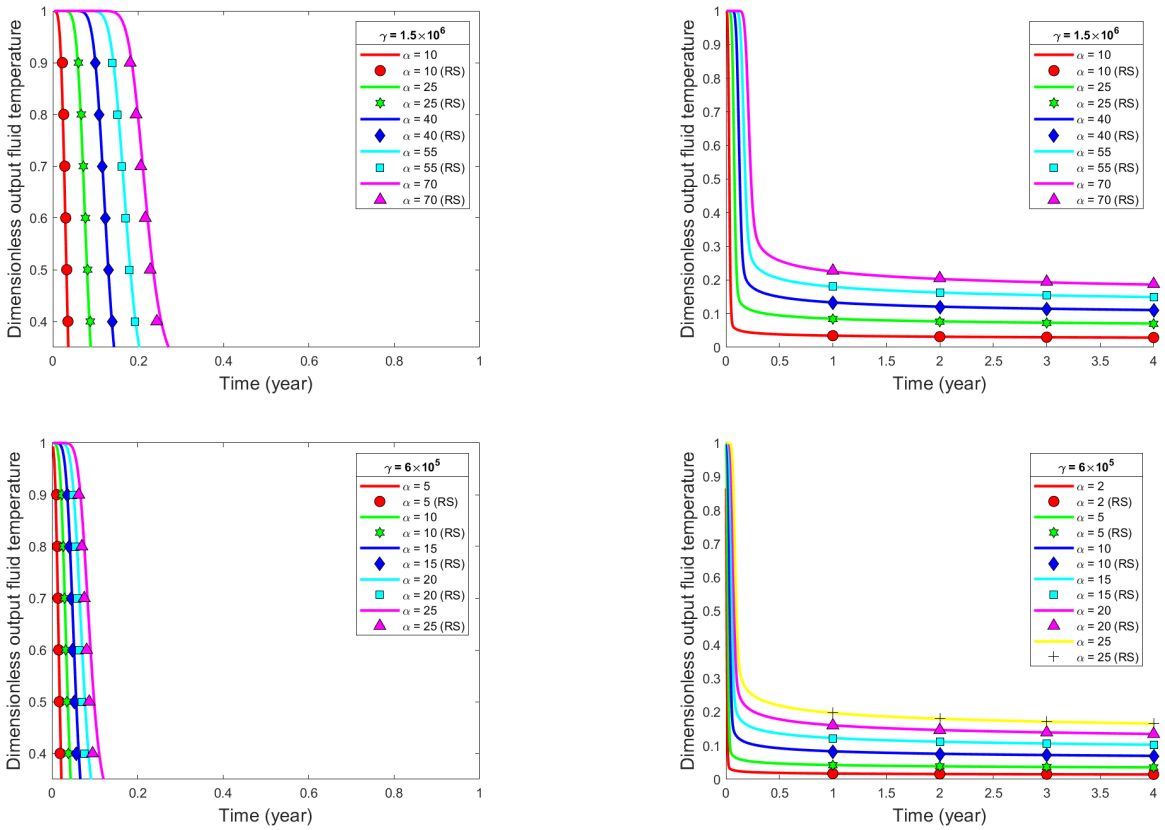

Figure 2.8: Power law fit results versus numerical results for different α and γ.

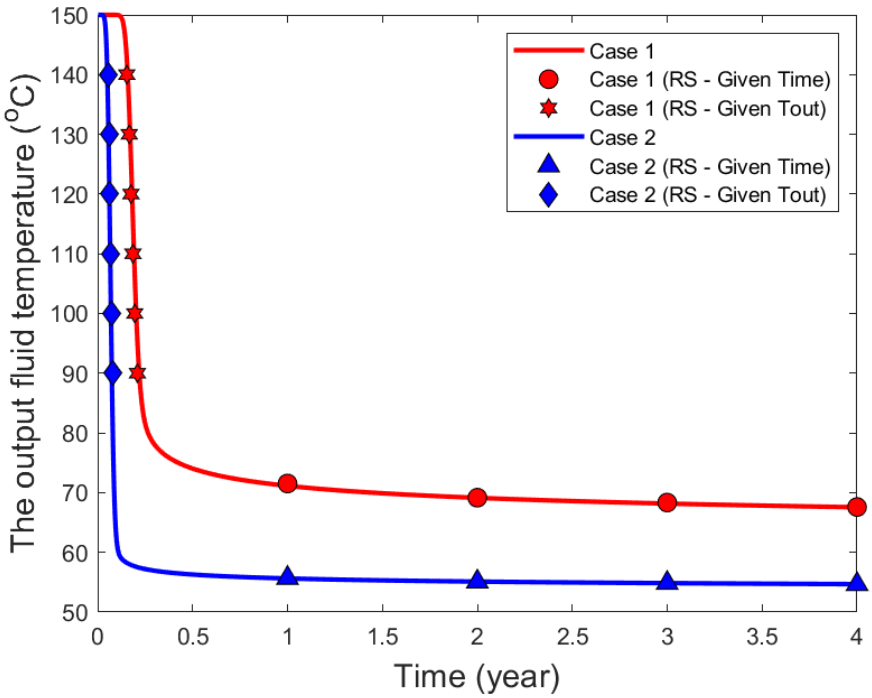

Figure 2.9: Assessment of two potential geothermal cases using FEM and RS models; case 1 (2 legs with low flow rate and small diameter) versus case 2 (single leg with high flow rate and large diameter).

Chapter 3

Design Parameters Impacting Electricity Generation From Horizontal Multilateral Closed-Loop Geothermal Systems in Hot Dry Rock

This chapter is based on the following journal article:

Ghavidel, A., Gracie, R., & Dusseault, M. (2022). Design Parameter Impacting Electricity Generation From Horizontal Multilateral Closed-Loop Geothermal Systems in Hot Dry Rock. *Geothermics*.

In this journal paper I was the first author and was responsible for the writing of the article. The paper was edited by Dr. Gracie and Dr. Dusseault. I also developed the mathematical and computational formulation and the numerical code.

3.1 Introduction

This chapter presents a parametric study of Closed-Loop Geothermal System (CLGS) design with multiple lateral horizontal wells, drilled in Hot Dry Rocks (HDRs), by developing a coupled finite element method (FEM) model for the problem of transient heat production in the reservoir and an Organic Rankine Cycle (ORC) model for electricity generation evaluation at the surface. The design parameters are well spacing and geometry, the number of wells, injection flow rate, energy losses along the well, and ORC working and cooling fluid mass flow rates. The study evaluates how these parameters affect the evolution of the spatial distribution of the temperature of the rock mass, the circulation fluid temperature leaving the reservoir, and the rate of electrical power generation with seasonal variations in surface air temperature. Hot Dry Rocks (HDRs), without fluids and flow paths, are widely available at depth, and could be a reliable source of energy in the future [11]. Areas with high thermal gradient can be found in many HDR regions; however, the absence of fluid, the low permeability, and the great depth present challenges to the extraction of heat [106].

An Enhanced Geothermal System (EGS) is a relatively well-known method for heat extraction from HDRs. In this method, the rock mass properties are enhanced by hydraulic stimulation (hydrofracturing or hydroshearing), creating pathways through which a fluid can be circulated to extract heat. The heat exchange volume and area may be further enhanced by multiple long wellbores, including inclined or horizontal wellbores. Heat extraction using EGS methods have been widely studied [13, 14, 15, 18, 16, 17]. Issues of concern in EGS development include heat transfer rate and efficiency, short-circuiting, well stimulation and integrity, and induced seismicity.

An Open Loop Geothermal System (OLGS) is an alternative method for heat extraction from HDRs, in which a closed-end horizontal well is drilled into HDR [20, 21, 22]. Injection and production pathways for the fluid flow are in the same well but in separate tubes and in different directions. The concept of this system is similar to Ground Heat Exchangers (GHEs). However, no commercial project is yet built or tested based on this system.

A new approach, known as a Closed Loop Geothermal System (CLGS), was recently introduced for heat production from HDRs using horizontal wells [23]. This approach is currently being tested at full-scale in Canada [107]; however, the economic feasibility remains to be more clearly demonstrated in practice. Beckers *et al.*, 2022, [62] have conducted an economic analysis where they have found that overall system costs are heavily dependent on drilling costs and estimated levelized cost of electricity between \$83 to \$2,200 per MWh. However, as will be demonstrated here, deployment in northern (cold) climates offer additional electricity and heat production opportunities.

In CLGS approach, an injection well is connected to a production well using long horizontal wells (1-5 km), forming a U-shape, closed loop system. The horizontal wells must be long enough to give sufficient time for the injected fluid to be heated up to an appropriate temperature. Since this system works in a closed-loop, it has the advantage of significantly reducing risks of water loss and aquifer contamination. It also helps to conserve heat by circulating warm fluids back into the reservoir.

CLGS may be established in sedimentary basin resources, where low to mid-temperature sedimentary layers (e.g., limestone, sandstone, shale) exist at great depth (>1 km) [108, 109]. The natural geothermal fluid in these resources is commonly minimal and not pressurized. These systems are conductive in nature; however, some convective systems may exist due to natural permeability, fractures, and faults. Therefore, heat flow in these resources differs widely. Establishing a CLGS in sedimentary basins, especially where natural fluid and permeability exist, will be useful for higher heat extraction rate because the geothermal fluid can play an important role in convective heat transfer in the rock. However, drilling, loss circulation, and casing in these areas may present challenges [110].

There have been several CLGS studies [61, 23], and a transient heat transfer analysis in CLGS through a horizontal well was recently conducted by [1]. This chapter presents a semi-analytical solution to quickly calculate the outlet fluid temperature for a wide range of system properties (e.g., rock and fluid properties, injection rate, and well geometry) over time. Analysis shows that the produced fluid temperature from a single well declines rapidly after the first few months. Commercializable heat production from this approach is challenging due to the small contact surface between the circulating fluid and rock (the horizontal well wall), and thus multiple lateral horizontal wells are required to increase total heat production rate. The outlet fluid temperature from CLGS was assessed by [61], where it was shown that fluid temperature changes along vertical wells segments (injection and production) are negligible compared to that from the horizontal well. However, previous studies evaluated only the outlet fluid temperature from the production well and do not assess impact of the time-varying produced fluid temperature on electricity generations and so are not sufficient on their own to assess the feasibility of CLGS projects.

Useful energy production (electricity, heat) from geothermal systems is needed for commercialization. This chapter provides a comprehensive parametric study of CLGS for reservoir design and electricity generation. The study couples a FEM reservoir model [1] and a surface Organic Rankine Cycle (ORC) model, evaluating the effects of a wide range of system and operations parameters on the amount of electricity generation from CLGSs. The analysis provides guidance on how to achieve electricity generation in the 5 MW range from CLGS in the Utah FORGE-like site over time. These parameters include the distance between the horizontal wells (for a wide range of reservoir properties), the number of wells,

flow rate in wells, well length and diameter, working and cooling fluid mass flow rates, and energy losses due to the friction. In addition, the impacts of climate specific non-constant ambient air surface temperature and non-constant fluid temperature are assessed - two variables not previously well studied together, but having significant impact on system performance.

3.2 CLGS Configuration, Models, and Governing Equations

3.2.1 CLGS Configuration

CLGS energy production using horizontal wells is similar to a U-shape buried-pipe system, in which long horizontal wells connect an injection well to a production well, and a binary power plant is used for electricity generation at the surface. A circulating fluid is pumped into the injection well, heating up during passage through the horizontal well. The horizontal well has to be long enough to provide sufficient time for the circulating fluid to absorb heat from hot rock. The hot fluid is extracted at the production well, providing thermal energy at the surface to a secondary circuit (i.e., ORC) for power production. The output fluid from the heat exchanger then moves through a surface pipeline, connecting the power plant to the injection well, and is recirculated through the primary circuit to minimize heat wastage [107].

A rapid decline in the outlet fluid temperature is one of the concerns and characteristics in CLGSs. Drilling multiple lateral horizontal wells is one of the solutions to mitigate this problem (Figure 3.1). Two separate cycles of multilateral wells can be employed, as shown in Figure 3.2, to further increase the system efficiency in comparison to a single cycle. Fluid flow in two cycles are in opposite directions, and two power plants are built at the surface close to the two production wells. The circulating fluid is reinjected into the second cycle, eliminating the need for the surface pipeline.

In this chapter, two models are developed to evaluate the whole CLGS over time: a subsurface reservoir FEM model to evaluate heat transfer and the outlet fluid temperature; and a surface ORC power plant model, fed by the extracted hot fluid in the evaporator, to evaluate electricity generation.

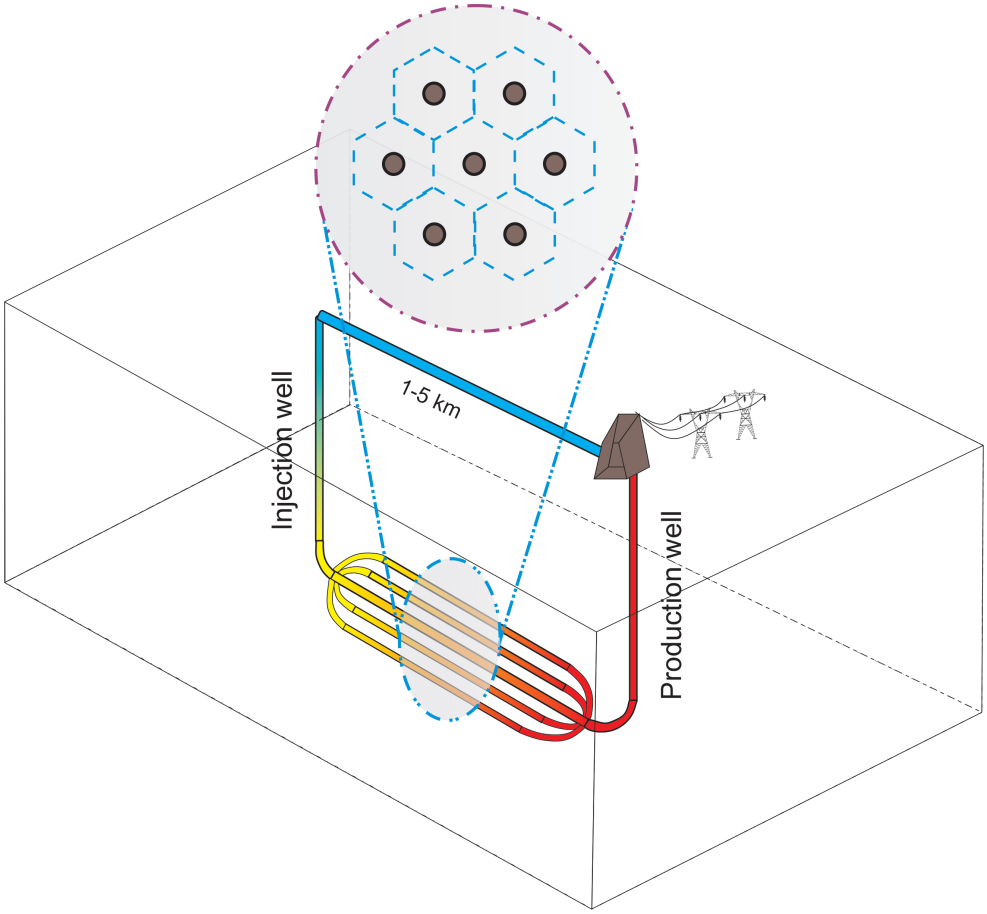

Figure 3.1: The closed loop geothermal system (CLGS) with multiple horizontal wells.

3.2.2 Reservoir FEM Model and Governing Equations

An axisymmetric FEM model was previously developed to evaluate the transient heat transfer between the rock and fluid flowing though horizontal wells in CLGS [1]. The main output of the FEM model is the production well outlet fluid temperature over time. Since the majority of the heat transfer from the rock to the fluid occurs through the horizontal wells [61], heat transfer in the vertical injection and production wells is not considered in the analysis. In this chapter, the horizontal wells are assumed be open hole wells and chemically sealed against water loss. Therefore, the role of the casing in heat transfer analysis is ignored.

Transient conductive heat transfer in HDRs like granite, which are assumed to be homo-

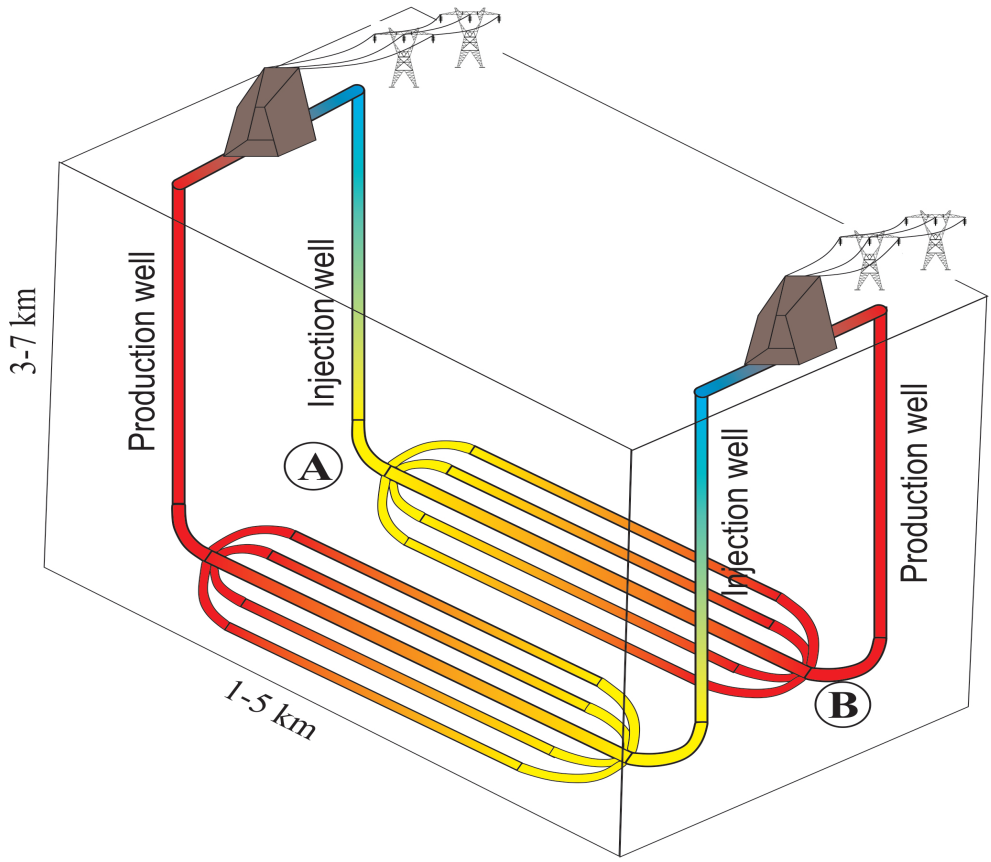

Figure 3.2: The CLGS with two sets of multilateral wells for increasing the system's efficiency.

geneous, isotropic, impermeable, and rigid because of very low porosity and permeability, is governed by conservation of energy [111]

$$\rho_s c_s \frac{\partial T_s}{\partial t} = k_s \nabla^2 T_s \tag{3.1}$$

in which ρ_s is the bulk density, c_s is the specific heat capacity, k_s is the thermal conductivity, T_s is the rock temperature, and t is time. The rock domain is subject to the initial temperature of T_s^0 and to convective heat flux boundary conditions due to heat transfer between the fluid and the rock, along the wellbore wall.

Heat transfer in the fluid in a horizontal well includes advection, diffusion, and heat convection between the rock and the fluid and is governed by [112, 113]

$$-\rho_f c_f u A \frac{\partial T_f}{\partial s} + A k_f \frac{\partial^2 T_f}{\partial s^2} + \pi D h (T_s - T_f) = 0, s \in [0, L] \tag{3.2}$$

in which h is the convective heat transfer coefficient between the circulating fluid and the well wall, k_f, ρ_f, c_f, u, and T_f are thermal conductivity, bulk density, specific heat capacity, velocity, and temperature of the fluid, respectively. The horizontal well has the area of $A = \frac{1}{4}\pi D^2$ with the diameter of D and length of L in s direction. The fluid is injected into the well at a constant temperature of T_f^{inj}.

Analytical solution of (3.1) and (3.2) for the evolution of both the rock and fluid temperatures have not been presented in the literature. Analytical solution for the evolution of the rock temperature do exist; however, only for the case where either the fluid temperature (or temperature at the wellbore) is known, or the heat flux from the rock at the wellbore is known. Similarly, solutions for the evolution of the fluid temperature are known only for the cases where the rock temperature or heat flux are prescribed [111, 114, 115]. However, in the general case evaluated here, neither the fluid/rock temperature nor the heat flux along the wellbore are known a prior- both vary in time and space and must be determined by the solution of the coupled system of partial differential equations. Beckers *et al.*, 2015, [116] have developed a solution to the coupled problem based on Green's functions, which they call a Slender Body Model; while the solution is analytical in form, computer and numerical implementation is still required to evaluate the integrals. In this chapter we have sought approximate solution to the coupled problem via Finite Element Analysis.

3.2.3 ORC Model and Governing Equations

Binary power plants are widely used for power production at the surface from low-temperature geothermal sources [64]. These power plants have two separate cycles: the primary cycle and secondary cycles. In the primary cycle, the circulating fluid passes through a heat exchanger, where it heats the working fluid; the fluid is then reinjected into the geothermal reservoir. In the secondary cycle, a low-boiling-point working fluid is circulated through the components of the power plant to generate electricity.

An Organic Rankine Cycle (ORC) model is developed in this chapter to evaluate electricity generation from CLGS. Figure 3.3 illustrates an ideal Rankine cycle (i.e., ORC), along with its components and the temperature-entropy (T-s) diagram. The components include a turbine, condenser, pump, and evaporator. The high temperature and pressure working fluid (after leaving the evaporator) enters the turbine as saturated vapor (or superheated vapor) and produces mechanical work by rotating the turbine, connected to a generator to produce electricity [47].

Following a standard ORC model [47], conservation of mass and energy, based on the first and second laws of thermodynamics, are applied to each ORC components. The turbine and the pump are assumed to operate in irreversible adiabatic processes. The heat exchangers (evaporator and condenser) are assumed to do no work and to be well insulated; no heat transfer occurs with the surrounding area. The kinetic and potential energy changes are ignored in the analysis because they are small compared to the work and heat transfer terms. It is also assumed that all components work under steady-state conditions.

Propane is commonly used as a working fluid in the ORC. Unlike many power plant simulations, in which the ambient and inlet (in the evaporator) temperatures are presumed to be constant (e.g., a constant heat source like gas power plants), this analysis assumes both inlet and ambient temperatures as non-constant parameters. The primary cycle fluid temperature from the CLGS declines with time. The cooling fluid, with non-constant temperature over time as a function of ambient temperature, is circulated through the the condenser, where extra heat is rejected to the environment. As a result, the evaporator and condenser working pressures change based on the fluid and ambient temperatures.

3.3 CLGS Design

Performance of closed loop geothermal systems (CLGSs) depends on both subsurface reservoir and surface equipment parameters, including reservoir rock and fluid properties, well

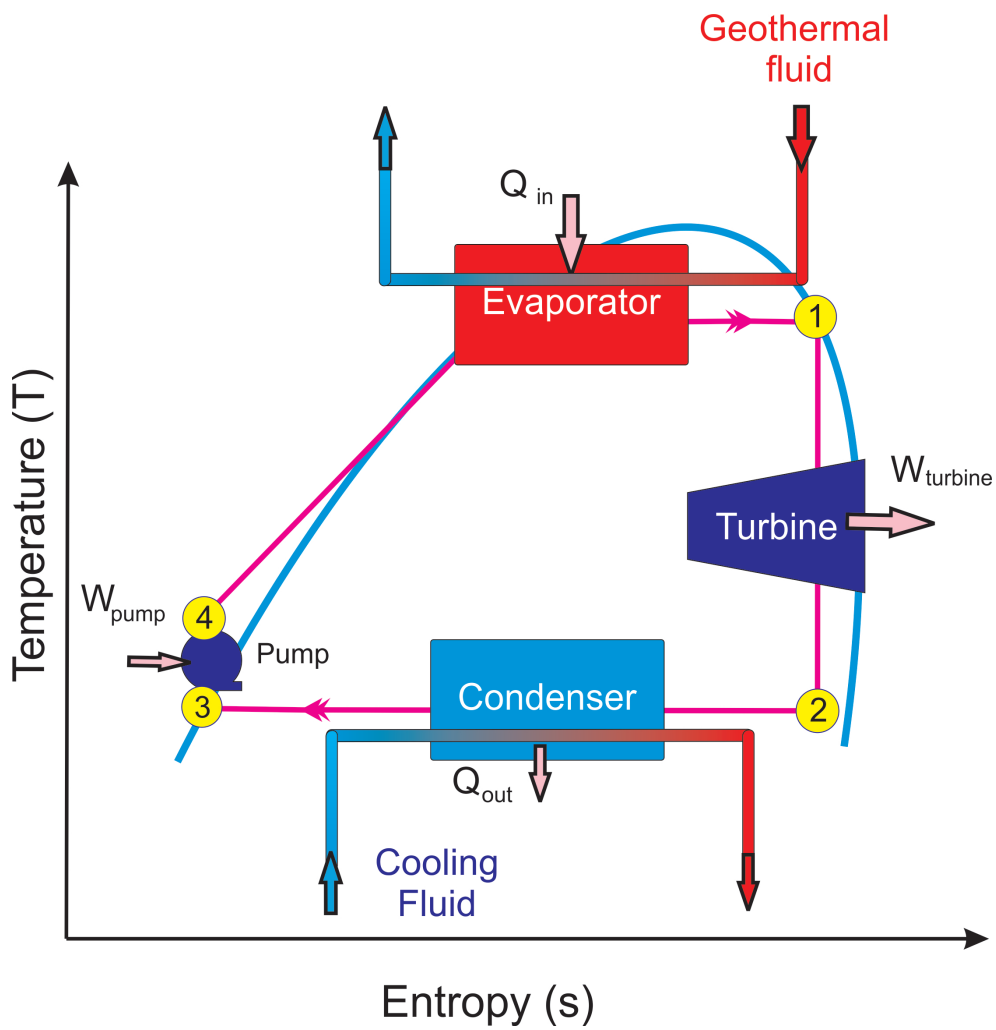

Figure 3.3: Schematic diagram of an ideal Rankine cycle (T-s diagram and components).

geometry characteristics (length and diameter), injection flow rate, well arrangements, ORC parameters (working fluid, turbine, pump, heat exchangers), and ambient conditions. Assessing all subsurface and surface parameters for CLGS design is beyond the scope of the current chapter; therefore, the reservoir rock (granite) and fluid (water) properties are assumed to be known in most of the analyses conducted. The ambient temperature is assumed to be a non-constant parameter over time, emulating seasonal changes in a temperate to cool climate. The analysis determines the distance between horizontal wells, number of wells, fluid injection flow rate, well length and diameter, and the working and cooling fluid mass flow rates for electricity generation.

3.3.1 Reservoir Design (Distance Between Horizontal Wells)

Multiple lateral horizontal wells (as illustrated in Figures 3.1 and 3.2) is one way to increase and sustain heat production from a CLGS, mitigating the rapid decline in the produced fluid temperature of a single well. The distance between the horizontal wells ($2R$) is a key factor impacting the outlet fluid temperature. If wells are drilled too close, the outlet fluid temperature drops faster in each well because of the effects of heat extraction from neighboring wells, reducing the commercial viability and lifetime of the project. On the other hand, if wells are placed too far apart, the drilling cost, the most expensive part of the project, will significantly increase because all lateral horizontal wells are deviated from the injection well and rejoin at the production well. The recent economic analysis from [62] for a wide range of system and reservoir properties has found that the total capital investment for a CLGS will be significantly dependent on drilling costs, and as a result, CLGS has relatively high levelized costs, compared to other geothermal systems.

To study the role of well spacing on fluid production temperature, it is helpful to consider the response of two systems: (1) a single isolated well in an infinite rock mass (Figure 3.4); (2) an infinite hexagonal array of wells, in which the wells are separated by a distance of $2R$ (Figure 3.5). Hexagonal array has the advantages of maximizing heat production from an available volume of rocks [117]. Let the safe distance ($2R_{safe}$) be defined as the distance between wells beyond which the performance of a single isolated well is practically indistinguishable from that of an array of wells. Let the optimum distance ($2R_{opt}$) be some distance $R_{opt} < R_{safe}$.

In this subsection, we study the impact of the distance between wells for the range of practical material and system properties given in Table 3.1. The reservoir rock is assumed to be granite, as a common HDR, and the fluid is assumed to be water.

Ghavidel *et al.*, 2021, [1] demonstrated that solutions of equations 3.1 and 3.2 in di-

mensionless form for a CLGS, comprised of a single horizontal well in an infinite rock, can be defined in terms of the ratio of well length to diameter (L/D) and just three other dimensionless parameters:

$$\alpha = 4\frac{L}{D}St; \qquad \beta = \frac{1}{Pe}; \qquad \gamma = 2\frac{L}{D}Bi \tag{3.3}$$

$$\hat{T}_f = \frac{T_f - T_f^{inj}}{T_s^0 - T_f^{inj}}, \hat{T}_s = \frac{T_s - T_f^{inj}}{T_s^0 - T_f^{inj}} \tag{3.4}$$

where St is the Stanton number, Pe is the Peclet number, and Bi is the Biot number. α represents the ratio of the rate of heat storage in the fluid to the rate of heat convection to the fluid from the rock. β, which has negligible impact for systems of interest [1], expresses the ratio of the rate of conductive versus advective heat transfer in the fluid. γ is the ratio of the rate of heat convection to the rock from the fluid to the rate of heat depletion in the rock. Based on a realistic range of material properties of granite and water and for a range of reasonable CLGS reservoir characteristics given in Table 3.1, the corresponding practical ranges of dimensionless parameters are presented in Table 3.2.

Heat transfer from an array of hexagonally organized wells can be approximated by a finite sized axisymmetric model with an outer insulated boundary at a fixed radial distance of $R + D/2$. The rock temperature is evaluated in terms of L, D, and three dimensionless parameters (α, β, γ).

Figure 3.6 summaries the rock temperature in the radial direction, near the injection well, for different values of parameters given in Table 3.1 and 3.2 at given times. The evaluation of the temperature in the rock mass is similar along the well; however, temperature changes are greatest near the injection point since the fluid temperature is lowest there. Each thick line (identified for a given year) in the figure comprises more than 100 thinner lines, as shown in a smaller rectangular. These thin lines represent the rock temperature in the radial direction for different combinations of dimensionless parameters, and well length and diameter (e.g., $D = 0.4\,m$, $L = 2000\,m$, $\alpha = 100$, $\beta = 1 \times 10^{-10}$, $\gamma = 6 \times 10^6$). As can be seen, temperature of the rock for different values of L, D, and dimensionless parameters (thin lines) are very close to each other at a given time. This means that the variation in the change in the rock temperature in the radial direction is negligible for different values of reservoir parameters at a given time.

Variation of system parameters (rock and fluid properties and well geometry) within the practical ranges presented in Table 3.1, do not significantly influence the evolution of the

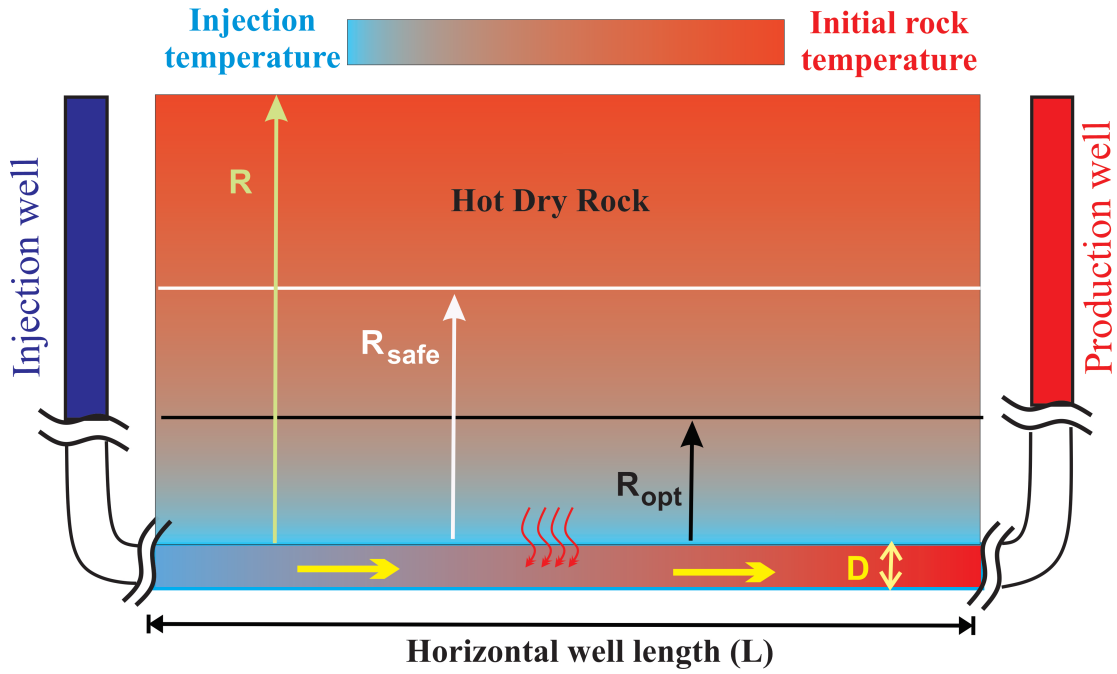

Figure 3.4: Schematic presentation of R_{safe} and R_{opt} in two dimensional view for a single horizontal well.

rock temperature in the radial direction. This is because the process is mainly controlled by the geometry of the system and the rate of conductive heat transfer to the well, which both have a narrow range. Regardless of the reservoir properties, R_{safe} is about 100 m. Placing an array of wells 200 m apart (or farther) results in an outlet fluid production temperature that is maximum and practically indistinguishable from that of the single isolated well.

The system behavior observed in Figure 3.6 is similar to the boundary layer behavior described with respect to the simple radial heat transfer models of heat extraction by convection from a hollow cylinder of infinite extent [115]. For a fixed fluid temperature of 50 ^oC, rock temperature of 150 ^oC, thermal diffusivity of 10^{-6} $[m^2/s]$, thermal conductivity of 3 $[W/mK]$, and convective heat transfer coefficient of 1000 $[W/m^2K]$, the bounds for the radial thermal penetration depth are 50 m and 116 m after 30 years. However, this same simple model predicts a much more rapid decrease in the well wall temperature, down to less than 51 ^oC in less than 1 month, which can be contrasted with much higher longer term production temperatures (Figure 3.8). So, while the model of [115] shares characteristics with the more complex analysis conducted here, the more complex analysis is needed to

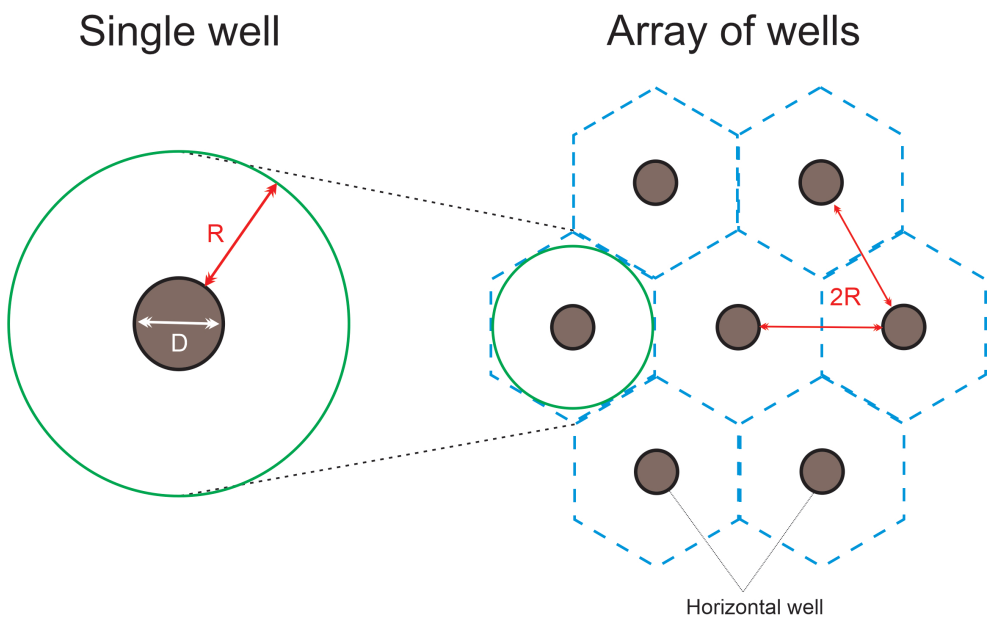

Figure 3.5: Cross-section view of a single isolated horizontal well and a hexagonally distributed array of horizontal wells of CLGS.

Table 3.1: Typical range of physical properties of granite and water and potential ranges of CLGS design and operation parameters [1].

Properties	**Variable**	**Units**	**Value**	**Reference**
Rock density	ρ_s	kg/m^3	2500–3010	[93, 94]
Specific heat capacity of rock	c_s	J/kgK	790–950	[95, 96, 97, 98]
Rock thermal conductivity	k_s	W/mK	0.96–3.62	[93, 95, 99, 100, 101]
Fluid density	ρ_f	kg/m^3	950-1200	[102, 103]
Specific heat capacity of fluid	c_f	J/kgK	3200–4180	[103, 104]
Fluid thermal conductivity	k_f	W/mK	0.6–0.7	[105, 103]
Fluid dynamic viscosity	μ_f	$Pa.s$	2.8×10^{-4}–8×10^{-4}	[105]
Horizontal wellbore diameter	D	m	0.2–0.4	
Horizontal wellbore length	L	m	500–2000	
Fluid velocity	u	m/s	0.5-2	
Convective heat transfer coefficient	h	W/m^2K	1200–13000	[92, 91]

Table 3.2: Dimensionless parameters ranges based on practical ranges of reservoir properties.

Parameter	Minimum	Maximum
$\alpha = 4\frac{L}{D}St$	1	3×10^{2}
$\beta = \frac{1}{Pe}$	2×10^{-11}	9×10^{-10}
$\gamma = 2\frac{L}{D}Bi$	7×10^{4}	3×10^{7}

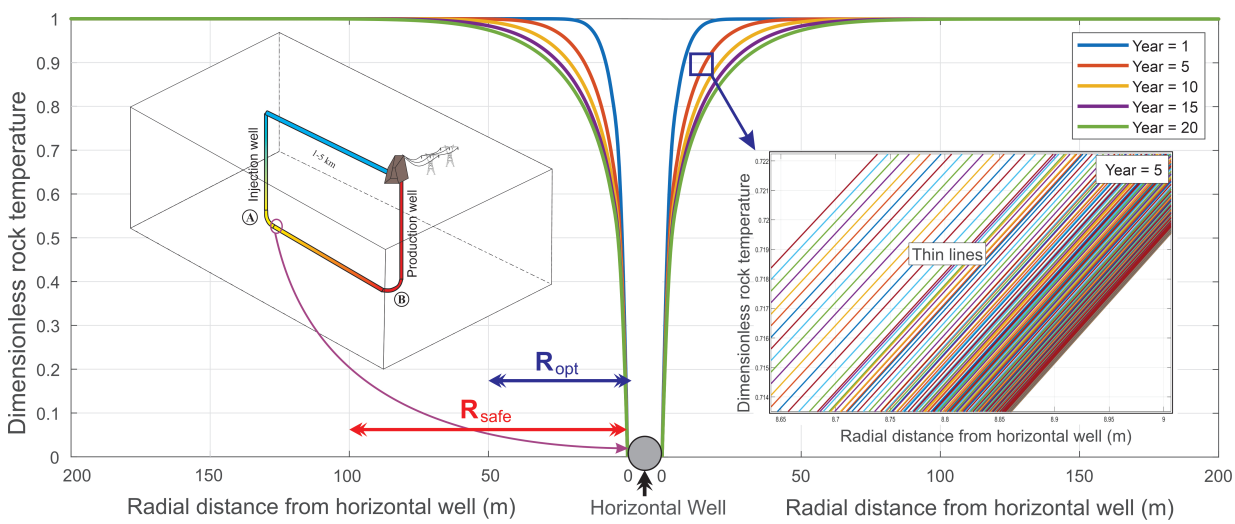

Figure 3.6: The rock temperature changes in the radial direction from horizontal well (near the injection well) for a wide practical range of geometric, rock and fluid properties (dimensionless numbers α and γ) over time.

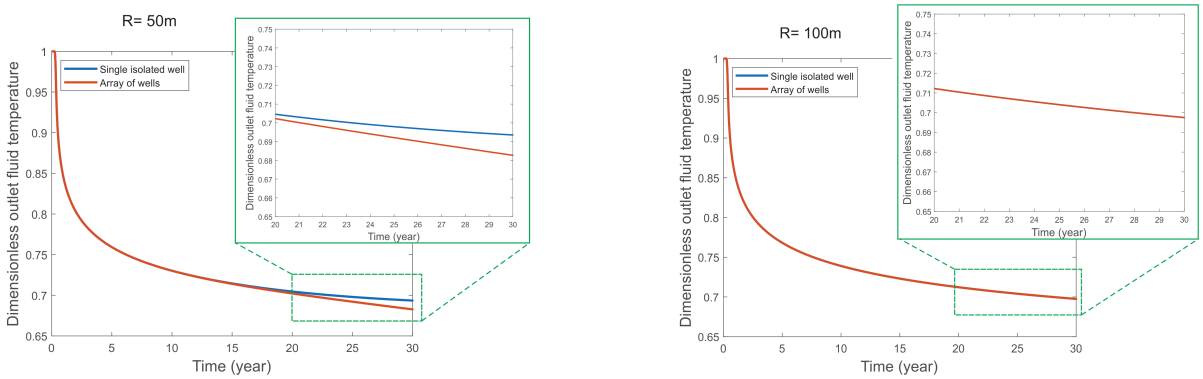

Figure 3.7: The outlet fluid temperature of a single isolated well and an array of wells for $R = 50\ m$ and $R = 100\ m$, indicating $100\ m$ is a reasonable distance between wells ($R_{opt} = 50\ m$).

accurately compute electricity and heat generation.

Since drilling costs increase with the distance between horizontal wells, it is best to decrease the distance as long as the deviation of the outlet fluid temperature is acceptably small. This distance is defined as optimum distance ($2R_{opt} < 2R_{safe}$). To gain insight into R_{opt}, the outlet fluid temperatures from two systems (single well and array of wells) are compared for different values of R.

For wells more than $200\ m$ apart, the outlet fluid temperatures of two cases are almost the same over time (with a difference $< 0.001\%$), confirming conclusions from the previous subsection, in which the rock temperature (Figure 3.6) does not change significantly over the project's lifetime (30 years). The importance of this conclusion in the schedule of the project is that wells can be switched on or off at any time without impacting the outlet temperature from other wells.

Figure 3.7 illustrates how the distance between wells can be reduced from $200\ m$ to $100\ m$ with a negligible effect on the outlet fluid temperature in the first 15 years and only a small impact after 30 years ($\sim$1%). If the injection and initial rock temperatures are assumed to be $50\ ^oC$ and $200\ ^oC$, the temperature difference in the outlet fluid will be about $1\ ^oC$ after 30 years. Therefore, it seems likely that in many practical applications the optimal spacing ($2R_{opt}$) of wells will be significantly less than safe distance ($2R_{safe}$). The specific spacing used in a particular project will depend on additional variables affecting drilling costs.

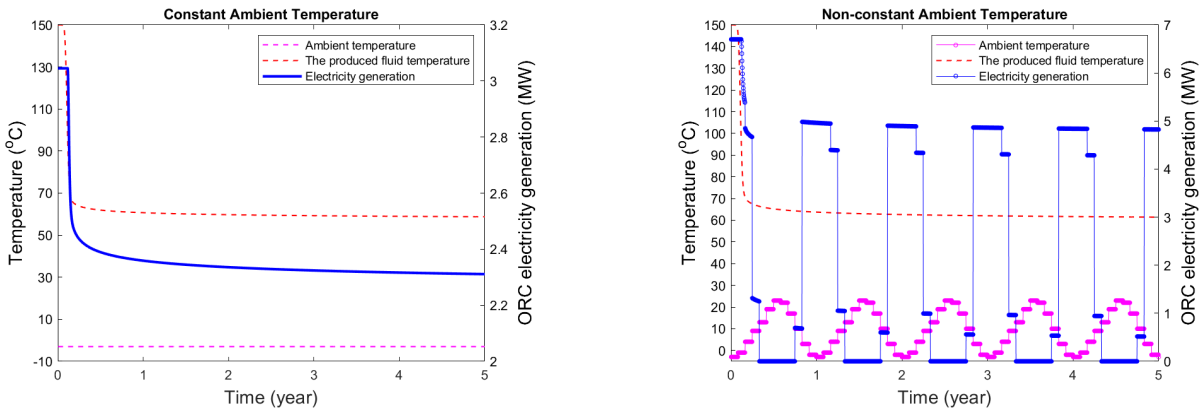

Figure 3.8: Electricity generation from a closed loop geothermal system (CLGS), assuming constant (the first graph) and non-constant ambient temperature (the second graph).

3.3.2 The Impacts of Ambient Temperature on Electricity Production

Non-constant ambient temperature can significantly affect the output electricity from CLGS, and assuming it as a constant input, like many power plant models, underestimates or overestimates the output electrical power. The impacts can be more noticeable if the temperature difference between summer and winter is high, in as Canada.

To show the effect of assuming a non-constant ambient temperature on outlet electricity from a CLGS, the results of two systems with the same properties but with constant and non-constant ambient temperatures are compared. Figure 3.8 shows electricity generation from a CLGS with four 1 km horizontal wells and injection flow rate of 2 $m^3/min/well$, operating in an environment with variable ambient temperature over the year. Ambient temperatures shown in the figure are monthly and annually averages of surface temperatures of the Utah FORGE site.

Reservoir and climate information of the Utah FORGE site is used for analysis in the following sections, and water is assumed to be the circulation fluid. The Utah FORGE site is located in central Utah (350 km south of Salt Lake City) and has been extensively explored in support of geothermal development. The FORGE site has more than 100 wells (3.8 km the deepest) with geologic mapping and three-dimensional seismic reflection, gravity, hydrologic and soil gas surveys. A bottom hole temperature of 197 ^oC was measured in Tertiary granite rocks, and more than 2000 natural fractures were measured in the well; however, the permeability is low (<30 microdarcies) [3]. The Utah FORCE site

Table 3.3: The reservoir rock of the Utah FORGE site, fluid (water), and ORC properties used in the analysis.

Properties	Variable	Units	Value
Reservoir rock (granite)			
Reservoir Depth	–	m	2000
Rock density	ρ_s	kg/m^3	2800
Specific heat capacity of rock	c_s	J/kgK	900
Rock thermal conductivity	k_s	W/mK	3
Rock initial temperature	T_s^o	^oC	150
Circulating fluid (water)			
Fluid injection temperature	T_f^{inj}	^oC	50
Fluid density	ρ_f	kg/m^3	1000
Specific heat capacity of fluid	c_f	J/kgK	4180
Fluid thermal conductivity	k_f	W/mK	0.6
Fluid dynamic viscosity	μ_f	$Pa.s$	3×10^{-4}
Organic Rankine Cycle			
Working fluid	wf	–	Pentane
Working fluid mass flow rate	$\dot{m}_{wf}$	kg/s	55
Cooling fluid	cf	–	Water
Cooling fluid mass flow rate	$\dot{m}_{cf}$	kg/s	150
Pump efficiency	η_p	–	0.75
Turbine efficiency	η_t	–	0.85
Evaporator pinch point	ΔT_{pp}	^oC	5
Ambient/Cooling fluid/Circulating fluid temperatures			Non-constant
Evaporator/Condenser pressures			Non-constant

is currently being developed using an Enhanced Geothermal System (EGS) and not using a CLGS. Table 3.3 illustrates the reservoir and ORC properties used in this study. The monthly averages of surface temperatures of the Utah FORGE site [2], as non-constant ambient temperature, is shown in Table 3.4.

If the ambient temperature is assumed to be constant, electrical power generation follows the inlet fluid temperature pattern over time. However, if the ambient temperature is non-constant, in the first few months, the output electricity is mainly affected by the fluid temperature (falling over time). Thereafter, electricity generation is mainly dominated by the ambient temperature.

Electricity generation changes significantly during hot months (summer) and cold months

Table 3.4: Monthly average surface air temperature of the region of the Utah FORGE site [2].

Month	**Surface Temperature (^oC)**	**Month**	**Surface Temperature (^oC)**
January	-3	July	23
February	-1	August	22
March	4	September	17
April	9	October	10
May	13	November	3
June	19	December	-2

(winter), highlighting the impacts of temperature difference between the ambient and inlet fluid (ΔT) on electricity generation. For a higher ambient temperature, the condenser has to work at a higher pressure (if all other parameters are assumed to be constant), which in turn causes lower electrical power generation. During winter, since the ambient temperature is low, the condenser can work at the lowest possible pressure, at which the ORC produces the highest electrical power output. Fortunately, this leads to better performance when needed - during the cold months. In general, ORC efficiency is $\sim$25% for the inlet and ambient temperature differences of 100-120 ^oC and drops to less than 20% when the temperature difference is less than 60 ^oC.

In addition to higher amounts of electricity generation in cold regions/seasons than in hot areas/seasons, CLGS provides valuable direct heat in cold regions/seasons. In northern regions, heat is valuable during most of the year. In Canada, for example, a considerable amount of electricity is used for home heating purposes [118]. Direct heating can also be achieved using Ground Heat Exchanger (GHE) and Ground Heat Pump (GHP). In the future, it would be valuable to conduct a comparative techno-economic analysis of individual and hybrid CLGS-GHE-GHP systems. The value of low-grade heat in cold regions become more important when the energy wasted through electricity generation processes (low efficiency power plants, transportation, etc.) and the high cost of fossil fuel delivery to remote areas are taken into account [119, 120, 118]. In addition to available heat in the produced fluid, there is considerable heat in the output fluids from the ORC evaporator and condenser. The temperature of the output fluid from an ORC system is still high enough to provide a valuable source of low-grade heat for residential, industrial and agricultural sectors. For example, for the system with 5 wells with the length of 2 km and diameter of 20 cm, the output fluid temperature from ORC varies between 15 ^oC (January) to 50 ^oC (August) during the third year. Available rejected heat in the condenser varies between about 10 and 20 MW, depending on injection and ORC flow rates. If the heat in the output fluid from the evaporator and heat rejected from the condenser is used,

the overall efficiency of the system would be greatly improved. Therefore, higher amounts of electricity generation along with use of the low-grade heat output from an ORC in cold regions/seasons makes geothermal systems attractive options for more sustainable energy in remote northern communities.

3.3.3 ORC Properties (Working and Cooling Fluid Mass Flow Rates)

ORC has several parameters that impact the outlet power production in different ways. The effects of working and cooling fluid mass flow rates, as two important parameters affecting the outlet power in an ORC configuration, are evaluated to determine an acceptable range for mass flow rates for 5 MW power production from CLGS. The same model and properties of the previous section for the available data from Utah FORGE site are used in this section.

Generally, small mass flow rates for working and cooling fluids are preferred in ORC because they require small amounts of energy for circulation. However, this leads to a small amount of output power from the ORC. When other parameters are held constant, mass flow rates need to be increased if a higher level of electricity generation is desired.

Sensitivity analysis shows that for a constant cooling fluid mass flow rate, increasing working mass flow rate decreases the amount of electricity generation. On the other hand, increasing the cooling mass flow rate, with a constant working fluid mass flow rate, increases the electricity generation level but to some limit. Working and cooling mass rates need to be in proper ratio for optimum electricity generation.

A response surface model is used to obtain the relation between the working and cooling fluid mass flow rates and electricity production. Figure 3.9 shows the results of the response surface model, in which black straight lines represent the turbine outlet electrical power for different amounts of working and cooling fluid flow rates. The relation between working and cooling fluid mass flow rates shows a linear behavior for constant electricity generation levels. Areas with no data on the graph represent flow rates in which the proposed model generates no electricity.

The minimum amount of mass flow rates on the graph (green highlighted area, where the black straight lines start) represents the optimum values of mass flow rates in terms of minimum energy consumption for circulation. To obtain the relation between optimum cooling and working fluid mass flow rates, valid for the whole presented ranges of mass flow rates, a linear equation can be fitted for flow rates in the green highlighted area as follows

$$\dot{m}_{cf} = 3\dot{m}_{wf} + 30 \ , \qquad \dot{m}_{wf} \in [10, 60] \tag{3.5}$$

in which $\dot{m}_{cf}$ is cooling fluid mass flow rate and $\dot{m}_{wf}$ is working fluid mass flow rate. To be able to present a general relation, which includes associated amounts of electricity generation in addition to $\dot{m}_{cf}$ and $\dot{m}_{wf}$ (valid for green highlighted area), a curve can be fitted on available data using a linear regression as follows

$$\begin{gathered} E_{tur} = -0.10 + 0.12\dot{m}_{wf} - 0.0037\dot{m}_{cf} \\ \dot{m}_{wf} \in [10, 60] \qquad and \qquad \dot{m}_{cf} \in [30, 160] \end{gathered} \tag{3.6}$$

in which E_{tur} is electricity generated by the turbine in the ORC. Equations 3.5 and 3.6 can be used to estimate the amount of electricity generation for different values of mass flow rates.

The results presented in Figure 3.9 span the first month of operation and are based on a coupled reservoir-ORC model. At start-up, 5 MW of electricity generation can be achieved with mass flow rates $\dot{m}_{wf}$ and $\dot{m}_{cf}$ are 45 kg/s and 130 kg/s, respectively. Since the temperature of produced fluid varies in time, optimal values of $\dot{m}_{wf}$ and $\dot{m}_{cf}$ will also vary in time. Using the initial optimal mass flow rates, electricity generation decreases by about 1 MW in the first 4-5 months of operation. After the first year the produced fluid temperature stabilizes, as seen in Figure 3.8. The optimal working and cooling fluid mass flow rates are 55 kg/s and 150 kg/s for 5 MW and remain fairly constant there after.

3.3.4 Number of Wells and Geometry

Optimum horizontal well spacing ($2R_{opt} = 100\ m$) and working and cooling mass flow rates ($\dot{m}_{wf} = 150\ kg/s$, $\dot{m}_{cf} = 55\ kg/s$), determined in the previous sections, are used in the following analysis to evaluate the role of well diameter and length, the number of wells, and injection flow rates in terms of the amount of electricity generation.

To determine the well diameter for CLGS, the outlet fluid temperature from the reservoir and outlet electrical power from ORC are calculated for the same system. Figure 3.10 shows the output fluid temperature (blue lines) along with electricity generation (red lines) from CLGS for three practical well diameters (20, 30, and 40 cm). The effects of well diameters on the outlet fluid temperature from the reservoir and outlet electricity from ORC are negligible because of slow conductive heat transfer in the rock mass and the small

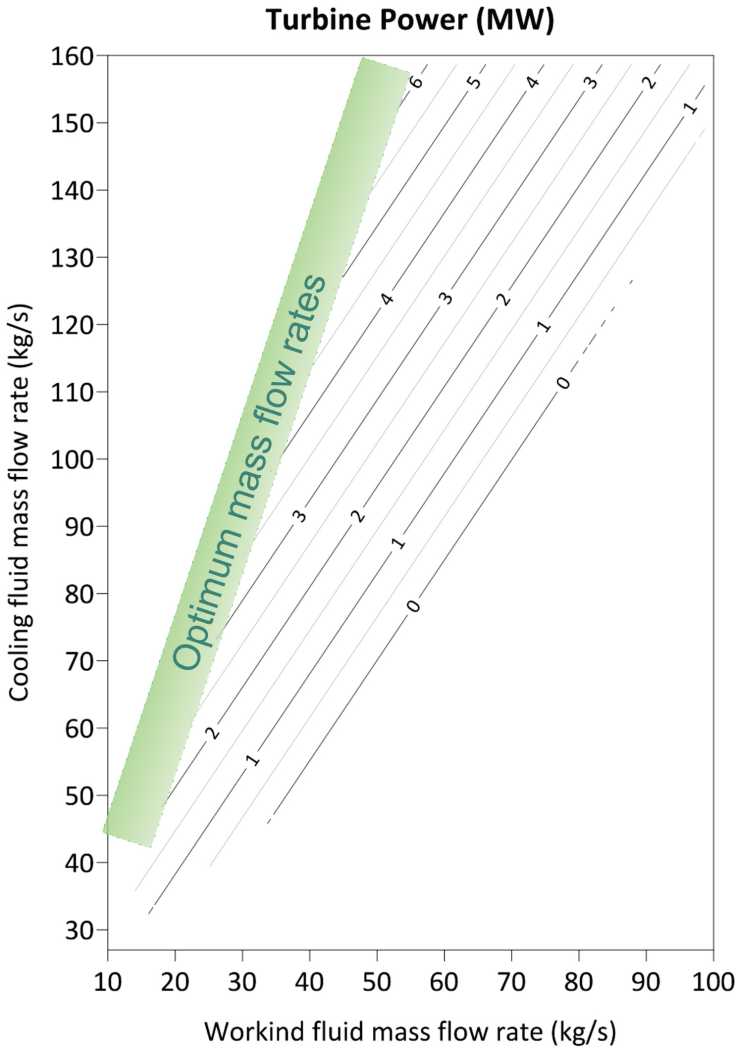

Figure 3.9: Electricity generation for different amounts of working and cooling mass flow rates, assuming ORC parameters as constant values (highlighted green area represents the optimum mass flow rates).

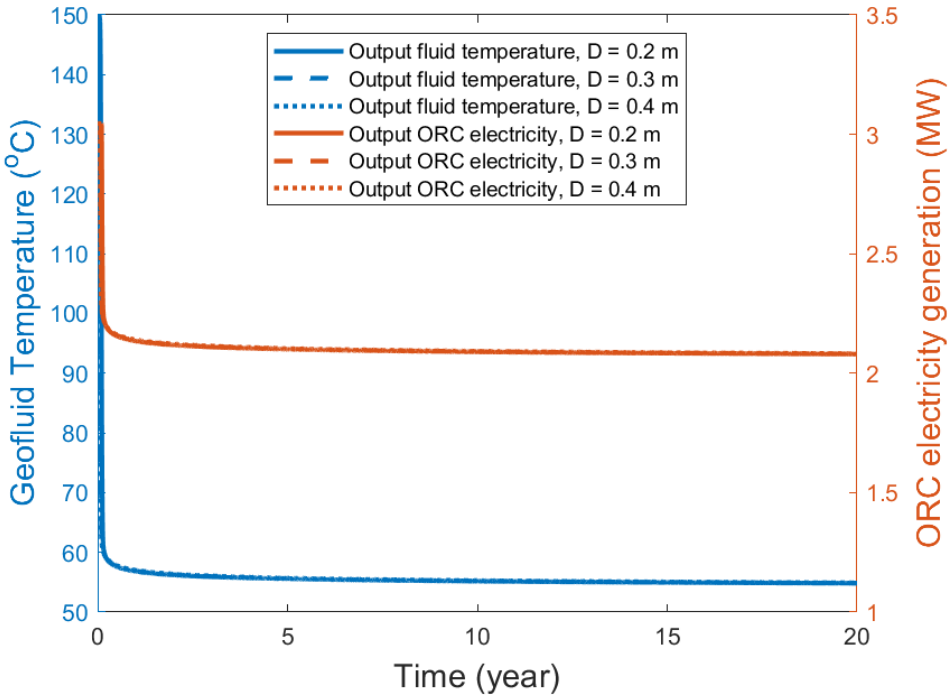

Figure 3.10: Negligible effects of different well diameters on the outlet fluid temperature and outlet electricity from a closed loop geothermal system, over time.

contact surface between the fluid flow and rock mass (i.e., horizontal well wall). Since the change in the well diameter has a negligible impact on the output electrical power, the smallest practical diameter (i.e., 20 cm) is preferred to decrease the drilling cost - the major expenditure in CLGSs.

The effects of different numbers of wells, well lengths, and injection flow rates (in the reservoir) on the output electricity are assessed in the following. The analysis considers practical ranges of well length of $1 - 2$ km, injection flow rates per well of $0.01 - 6$ m^3/s, and the number of wells of $1 - 10$. The analysis is presented for different months of the second year. Electricity production for the same months after the first year declines a negligible amount (Figure 3.8) because the level of electrical power production depends on the fluid temperature.

Figure 3.11 illustrates the output electricity from CLGS with 1 and 2 km wells in cold months (November, December, January, and February). As shown in the graphs, 4-5 horizontal wells with the injection flow rate of 2 $m^3/min/well$ are sufficient to generation

$\sim$5 MW electricity using proposed CLGS for available data in the Utah FORGE reservoir in cold months. Adding more horizontal wells or increasing injection flow rates does not increase the amount of electricity generation.

Based on the analysis here, one 1-2 km well with the injection flow rates below 3 m^3/min produces no electricity over a year. Drilling more than five wells and operating with injection flow rates above 2 $m^3/min/well$ is irrational because they produce almost the same level of electricity ($\sim$5 MW) as three to five wells. Increasing injection flow rates above 2 $m^3/min/well$ for more than five wells has a negligible effect on the electrical power outlet from a fixed ORC system; it will only increases fluid circulation energy consumption.

Horizontal wells with a length of 2 km deliver higher electrical power than 1 km wells because they provide a bigger volume of heat source (rock) for the fluid to interact with; however, the outlet electrical power difference between two cases is not considerable. Plus, longer wells impose a higher energy loss due to the friction. Therefore, wells with a length of 1 km may be preferred because doubling the length significantly increases the drilling cost.

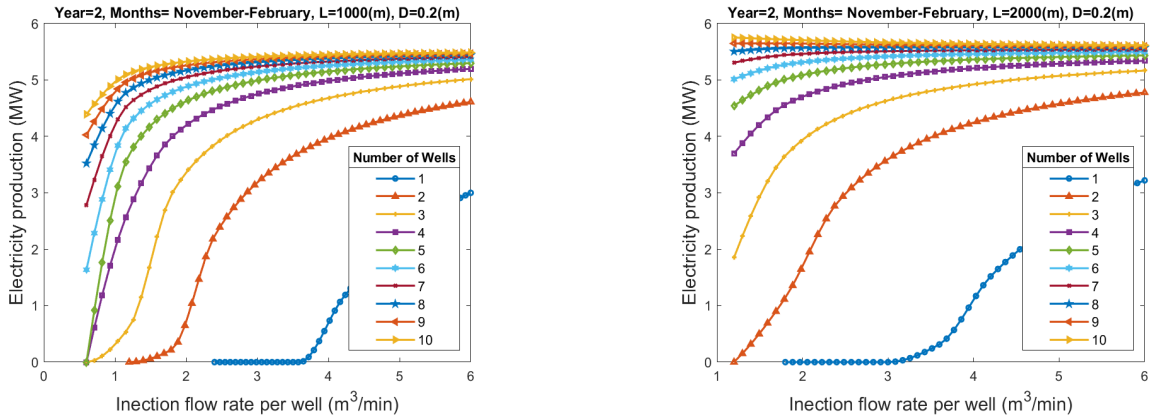

Figure 3.11: Electricity generation from CLGS with 1 and 2 km horizontal wells during cold months (November, December, January, and February) of the second year for different amounts of injection flow rates and the number of wells.

The same system in April and October produces almost 2MW electricity, as shown in Figure 3.12. The system produces almost zero electricity during hot months (May to September) because the condenser has to work at higher pressures, hence the amount of electricity generated decreases. However, retuning the ORC for these months, the system might produce a higher amount of electricity; an analysis, which is out of the scope of the current study, is needed.

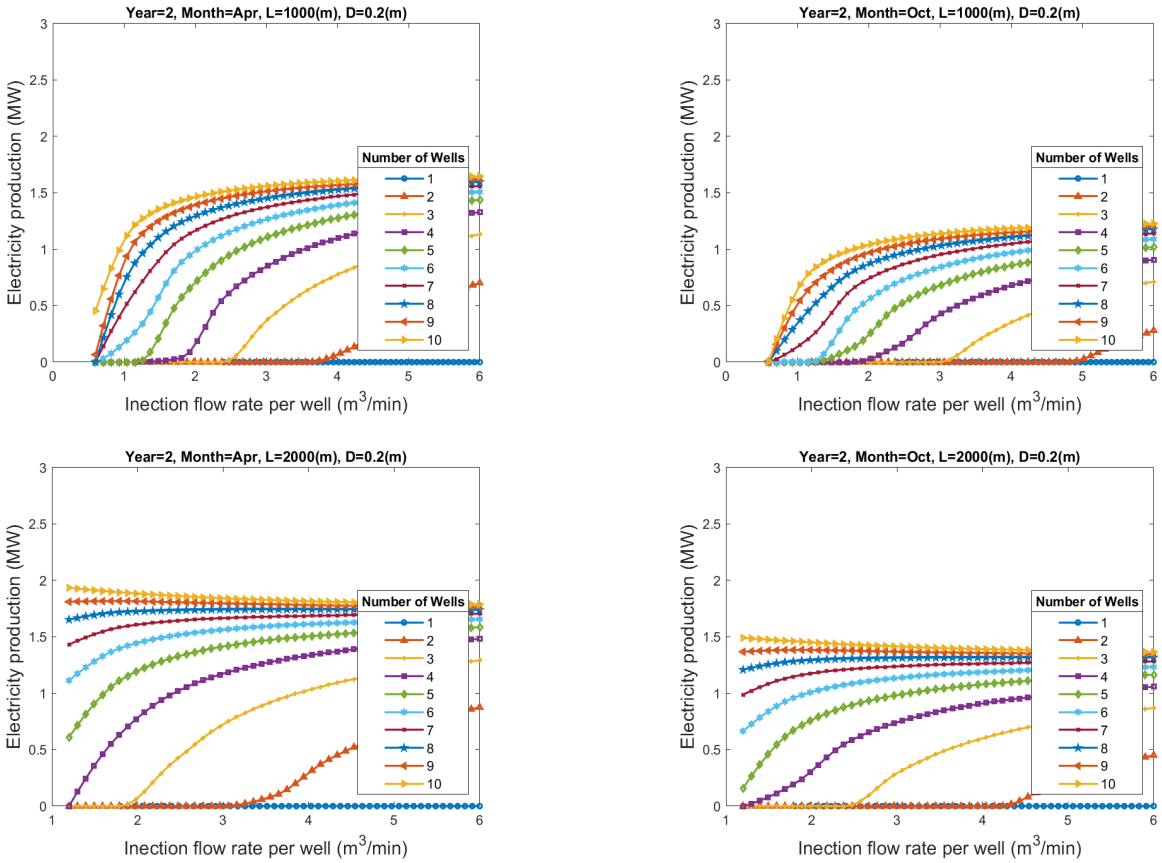

Figure 3.12: Electricity generation from CLGS with 1 and 2 km horizontal wells during April and October of the second year for different amounts of injection flow rates and the number of wells.

3.3.5 Energy/Head Loss

Energy loss due to the friction in horizontal wells is another factor that needs to be taken into account for CLGS design. Energy loss results in a pressure drop along the well and requires more pumping power to sustain the flow rate. If energy loss is too high, net output energy from the system might be inadequate. Therefore, energy loss imposes some limits on parameters, such as injection flow rate, well length and diameter, and so need to be taken into account in the CLGS design process.

Head losses due to friction in a straight pipe can be calculated using the Darcy-Weisbach empirical equation [121]

$$h_L = f\frac{L}{D}\frac{u^2}{2g} \tag{3.7}$$

in which $h_L$is head loss, f is Darcy friction factor, L is well length, D is well diameter, u is the fluid velocity, and g is the local acceleration due to gravity. Darcy friction factor (f) can be estimated using different methods depending on the fluid flow regime (laminar or turbulent). Practical ranges of parameters assumed in this study yield turbulent fluid flow through the wells (i.e., Reynolds number (Re) greater than 4000); therefore, f is calculated using the Colebrook equation [122] as

$$\frac{1}{\sqrt{f}} = 2log_{10}\left(\frac{\epsilon/D}{3.7} + \frac{2.51}{Re\sqrt{f}}\right) \tag{3.8}$$

in which ϵ is the absolute roughness of the well wall surface. Absolute roughness (ϵ) for a concrete-cased well is 1-3 mm [123, 124] and for open-hole wall well in igneous rocks with very low fracture (e.g., granite) is 3-6 mm [125]. In this study, ϵ is considered to be 1-5 mm, covering the range for cased wells and open-hole wells in many HDRs.

Figure 3.13 illustrates energy loss per kilometer due to friction for different injection flow rates, well diameters, and absolute roughness. For instance, loss for a CLGS with five 2 km horizontal wells with a diameter of 20 cm and a circulation rate of 5 $m^3/min/well$ would be about 0.1 $MW/km/well$ or about 1 MW for the whole system. Such large losses may justify the drilling of large diameter or shorter wells. Small losses are preferred to decrease energy consumption, i.e., low injection flow rates, short wells, and big well diameters. In the 5 MW system considered in the previous section based on the Utah FORGE site characteristics, the suggested D=20 cm, L=1 km, number of wells=5, and flow rate 2 $m^3/min/well$ leads to a small head loss. Thermosiphon effects are negligible

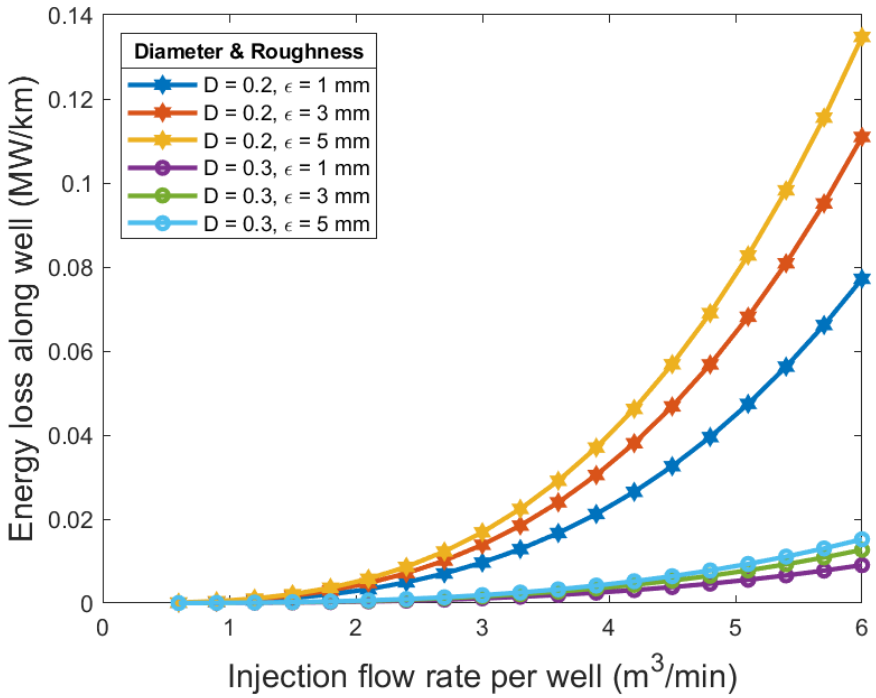

Figure 3.13: Energy loss per kilometer along a horizontal well for different well diameters, injection flow rates, and absolute roughness.

in the CLGS model considered here, since the circulating fluid in the wells is assumed to be water, which is nearly incompressible. However, thermosiphon effects are important in CLGS when the circulating fluid is compressible (e.g., with CO_2).

Although bigger D results in smaller energy loss due to friction along the well, a smaller diameter is still preferred because of two reasons; first, the output fluid temperature and output electrical power from ORC are practically the same for different D, and second, since drilling cost dominates the capital expenditures in CLGSs, bigger D significantly increases the total project cost. In realistic scenarios, the rate of penetration for a hole is proportional to the area of the hole, and drilling costs are exponential with depth.

3.4 Conclusion

This chapter presents a study of design parameters for electricity generation in a deep closed-loop geothermal system in hot dry rock. The study design parameters are: well spacing and geometry, the number of horizontal wells, injection flow rate in wells, and working and cooling mass flow rates of the ORC power generation plant. The effects of these parameters are assessed based on produced fluid temperature, rock mass temperature, electricity production, and friction losses. Analysis is based on granite properties granite reservoirs with water as the circulating fluid by developing a coupled axisymmetric FEM model for reservoir evaluation (transient heat transfer between the rock and fluid) and an Organic Rankine Cycle (ORC) model for electricity generation evaluation. The vertical segments are ignored in the study. The analysis yields the following observations and design guidance:

- The fluid temperature can decrease rapidly in the first months of production, but approximately stabilizes after about 1 year.
- Optimal parameters for the ORC system depend on the fluid temperature and seasonal surface temperature. Values for a particular season vary little after the first year.
- The change in the temperature of the reservoir rock in time and in radial direction is not greatly influenced by the reservoir, well, and fluid properties; however, it is influenced by the difference of the initial temperature of the reservoir and the temperature of the injected fluid.
- The distance between the horizontal wells, beyond which the performance of a single isolated well is practically indistinguishable from that of an array of wells, and consequently the produced fluid temperature is practically unaffected by heat extraction from neighboring wells, is 200 m over 30 years.
- Wells placed 100 m apart show practically negligible interaction in the first 15 years and only a small impact during the next 15 years of production ($\sim$1%). Thus, CLGS may be configured with well spacing less than 200 m to reduce drilling costs.
- Well diameter (20-40 cm) has a negligible impact on electricity generation regardless of the number of wells and injection flow rates. Therefore, drilling wells with a small diameter is recommended to decrease the drilling cost.

- Low injection flow rates, short wells, and big well diameters result in small energy losses in horizontal wells. For using wells with a diameter of 20 cm, the injection flow rate should be below 2 m^3/min to avoid huge losses.

- Seasonal variation in ambient air temperature can lead to significant seasonal differences in electricity generation. For the reservoir temperature less than 150 ^oC and ambient air temperature variations from -3 to 23 ^oC, electricity generation using CLGS in summer is near to zero, while in winter, the system produces more electricity ($\sim$5 MW).

- A CLGS using reservoir characteristics similar to the Utah FORGE site (rock temperature of 150 ^oC) with four to five operational 1 km horizontal wells with a diameter of 20 cm and injection flow rates of 2 $m^3/min/well$ can produce $\sim$5 MW electrical power during cold months. Increasing the number of wells (resulting in increasing total injection flow rate) or injection flow rate (with a fixed number of wells) does not increase the amount of electricity generation, but increases energy losses.

- Using wells with a length of 2 km increases the amount of electricity production compared to 1 km wells (e.g., 0.1-0.5 MW increase for 4 wells with injection flow rate of 2 $m^3/min/well$), but it might not be considerable in comparison to the drilling cost. Furthermore, energy losses due to the friction for longer wells are higher.

- While a 5 MW system operating 6 months of the year may not be economically feasible in many regions, the very high cost of electricity combined in the large demand for heat in northern communities (e.g., Yukon, Canada) motivates the need for more details economic analysis of CLGS in the future.

Chapter 4

Energy From Horizontal Multilateral Closed Loop Geothermal Systems Using Supercritical CO_2 or Water

This chapter is based on the following journal article:

Ghavidel, A., Dusseault, M. & Gracie, R. (2022). Energy From Horizontal Multilateral Closed Loop Geothermal Systems Using Supercritical CO_2 or Water. *Geothermics*.

In this journal paper I was the first author and was responsible for the writing of the article. The paper was edited by Dr. Dusseault and Dr. Gracie. I also developed the mathematical and computational formulation and the numerical code.

4.1 Introduction

Heat and electrical power production are evaluated from a Closed-Loop Geothermal System (CLGS) with supercritical CO_2 (SCO_2) or water circulating in a hexagonal array of horizontal wells in Hot Dry Rock (HDR). The analysis is based on a coupled numerical model, evaluating compressible temperature-dependent pipe flow of water and SCO_2 in the wells and transient conductive-convective heat transfer within and between the rock and fluid, and electricity generation at a non-constant ambient air temperature.

The world is experiencing consequences of extreme fossil fuel use for primary energy. Switching to carbon-free energy sources is needed to meet climate change challenges, as two thirds of anthropogenic CO_2 emissions are related to fossil fuels. However, renewable energy sources struggle with technical and economical uncertainties [126, 127]; for instance, without massive storage capacity, wind and solar cannot operate as a base-load source since they are seasonal (latitude), variable (daily), and intermittent (cloud cover). Geothermal energy from Hot Dry Rocks (HDRs) can provide a clean, carbon-free, reliable, steady and sustainable source of energy; it is gradually becoming more competitive through technological innovation, falling costs, and improved social acceptance.

HDRs (i.e., granite, basalt, low-porosity and low-permeability sedimentary rocks) are widely available at depth and could provide a great deal of energy. However, the absence of natural fluids, the low permeability, and the great depths needed to access sufficient temperatures in low geothermal gradient regions present challenges to the extraction of useful energy from HDRs.

Various methods have been proposed for heat extraction from HDRs, each requiring the creation of circulation pathways. In an Enhanced Geothermal System (EGS) rock mass properties are "enhanced" by hydraulic stimulation (hydrofracturing and hydroshearing), creating pathways through which a fluid can be circulated [14, 12]. Short-circuiting mechanisms in deep EGSs have been identified which may requires more complex operational requirements (zoning) [16]. In an Open-Loop Geothermal System (OLGS) a closed-end well is drilled into the HDR. Injection and production pathways for the fluid flow are in the same well but in separate tubes (or annuli) [21, 22]. A Closed-Loop Geothermal System (CLGS) is a relatively new approach for heat extraction from HDRs, currently being tested at full-scale in Canada with different configurations [1, 23, 63]. In most configurations, a CLGS is a U-shaped subsurface circulation system that comprises two vertical segments (injection and production wells) and one horizontal section, which may include multiple horizontal wells (1-5 km). The horizontal wells can be implemented with or without casing, depending on *in situ* conditions. Since the system operates as a closed loop, CLGS reduces

water needs and environmental risk [63]. Compared to an OLGS drilled to the same depth, the horizontal section of a CLGS allows it to access a larger volume of the hottest rocks; however, at the cost of significantly more drilling in hard rock.

The production fluid temperature from an CLGS generally drops rapidly and significantly during the first few months of production, before entering into a prolonged period of slow decline. This behaviour leads to questions about commercial viability [61, 1, 128, 129]. Most studies have focused on rock mass heat flux and production temperatures only. Electricity generation is an important aspect of geothermal energy use, and Ghavidel *et al.,* 2021, [129] recently provided a parametric study of CLGS with water as the circulation fluid in terms of electricity generation by coupling a reservoir model to an Organic Rankine Cycle (ORC) model. They identified the appropriate ranges of system parameters for an acceptable level of electrical power generation, including number of horizontal wells, flow rates in the reservoir and ORC, well spacing, and well lengths and diameter. Nevertheless, in realistic scenarios the production temperature and electrical power output of the system is low, particularly where the reservoir temperature is modest (e.g. 150 $°C$) and the ambient temperature is high (e.g., 20-35 $°C$), challenging the commercial viability of CLGS because of the high drilling costs to develop a multi-well array [62, 129].

Most geothermal systems and analyses presume brine/water as a circulating fluid to extract heat from HDRs. The production fluid temperature and electrical power from the system can be enhanced by using a circulating fluid with a higher capacity of heat absorption. Recently, supercritical CO_2 (SCO_2), as an alternative to water, has attracted attention because of its unique thermodynamic properties and a potentially higher produced SCO_2 temperature [130, 131, 132, 133, 128]. Compared to water, SCO_2 has i) a lower kinematic viscosity, allowing for more efficient advection [134]; ii) a significant buoyancy drive produced by the difference in density between the low-temperature SCO_2 in the injection well and the high-temperature SCO_2 in the production well, which can reduce or eliminate the need for circulation pumps [135, 136]; and, iii) reduced fluid-mineral reactions and casing problems [137]. To fully understand the potential advantages of SCO_2 based CLGS, the amount of electric power generation should be quantified; however, to date, there is no study which compares the electricity production for a SCO_2 CLGS with that of a water-based CLGS.

We present a comprehensive study of heat and electrical power generation from a CLGS model with vertical and horizontal segments (injection, production, and multiple lateral horizontal wells) using SCO_2 and water as circulating fluids. First, a Finite Volume Method (FVM)/Finite Element Method (FEM) program is developed to evaluate the compressible/incompressible fluid flow and transient heat transfer within and between the rock and circulating SCO_2/water in the wells. The FVM/FEM CLGS heat transfer simulator

is linked to an Organic Rankine Cycle (ORC) to evaluate electrical and thermal power produced. The produced SCO_2/water temperature, thermal power and electrical power in non-constant ambient temperature conditions are presented for different numbers of wells and injection flow rates. A comparison of SCO_2 and water-based CLGS and natural circulation due to thermosyphon effects of SCO_2 are also discussed.

4.2 CLGS Configuration and Model Description

A closed loop geothermal system (CLGS) is comprised of an injection well(s) and a production well(s), connected by multiple lateral horizontal wells in the subsurface reservoir, and a binary power plant for electricity generation at the surface (Figure 4.1). In the primary cycle, a circulating fluid enters the injection well, heating up during passage through vertical and horizontal segments. Then, the hot fluid is extracted at the production well at the surface to feed the ORC and returned into the reservoir after leaving the ORC and passing through another heat exchanger, in which the circulating fluid temperature is returned to a constant injection temperature.

Within the ORC the hot circulating fluid in the primary cycle heats up a low-boiling-point secondary cycle working fluid (e.g., propane, pentane) through heat exchangers. The working fluid circulates through the power plant components (turbine, condenser, pump, and evaporator) shown in Figure 4.1. The high temperature and pressure working fluid, after leaving the evaporator, enters the turbine as saturated or superheated vapor and produces mechanical work by rotating a turbine connected to a generator to produce electricity. The pressure of the working fluid drops after leaving the turbine. The low-pressure working fluid loses heat through the condenser in indirect contact with a cooling fluid like water or air. Then, the working fluid is pressurized to the evaporator working pressure using a pump and returned to the evaporator, completing the secondary closed loop cycle [64].

The CLGS reservoir can be designed in different configurations for higher performance. Figure 4.1 shows a schematic view of the system used in this chapter. The horizontal wells are assumed to be organized in a hexagonal array, which has the advantages of maximizing heat production from an available volume of rocks [117].

A coupled FEM/FVM/ORC model is developed to evaluate heat and electrical power generation. The FEM model evaluates the transient heat transfer within and between the rock mass and compressible fluid flow in the injection, production, and horizontal wells. The heat transfer process includes conductive heat transfer in the rock mass and convective

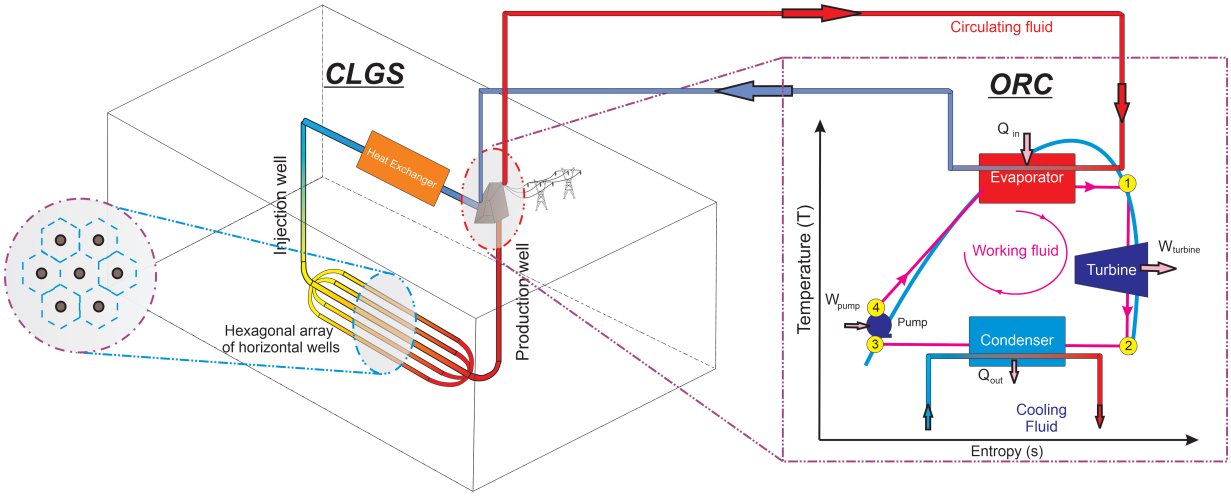

Figure 4.1: Schematic diagram of the CLGS with multiple horizontal wells in an hexagonal array and an ideal Rankine cycle (T-s diagram and its components).

and conductive heat transfer in the fluid. The FVM model solves compressible pipe flow (conservation of mass and momentum) in wells for pressure and velocity fields, exposed to temperature and pressure changes along the well. The ORC model evaluates the electricity generation for non-constant inlet fluid and ambient temperature. The mathematics of the proposed model is discussed in the next session.

4.3 Governing Equations

4.3.1 Heat transfer in the rock mass

HDRs (e.g., granite and basalt) have very low porosity and permeability and can be assumed to be homogeneous, isotropic, impermeable, and rigid rocks. Transient heat transfer in the rock mass is governed by conservation of energy, which can be expressed in axisymmetric form (each segment of the CLGS is approximately axisymmetric) as [111]

$$\rho_s c_s \frac{\partial T_s}{\partial t} = \frac{1}{r} k_s \frac{\partial}{\partial r}(r \frac{\partial T_s}{\partial r}) + k_s \frac{\partial^2 T_s}{\partial z^2} \tag{4.1}$$

in which r and z are the radial and axial directions in axisymmetric coordinates, t is time, ρ_s is the bulk density, c_s is the specific heat capacity, k_s is the thermal conductivity, and

T_s is the rock temperature. The rock domain is subject to an initial temperature of T_s^0 and to far-field boundary conditions of constant temperature, T_s^0, and convective heat flux on the well wall (between the circulating fluid and rock), $h(T_s - T_f)$, in which T_f is the fluid temperature and h is the non-constant convective heat transfer coefficient along the wells, which changes with fluid properties. In this chapter, the wells are assumed to be open hole wells and chemically sealed against water loss; therefore, the role of casing and cement can be omitted from the heat transfer analysis.

4.3.2 Pipe flow for compressible and incompressible fluids

The governing equations describing the general incompressible and compressible flow through a circular pipe in the direction of well axis (s) (Figure 4.2) are the conservation of mass, conservation of momentum and an equation of state for the circulating fluid relating pressure, temperature, and density [138, 139, 140, 141].

Incompressible fluid (water)

$$\frac{\partial u}{\partial s} = 0 \tag{4.2}$$

$$\frac{\partial u}{\partial t} + \frac{\partial u^2}{\partial s} + \frac{\partial p}{\partial s} - \mu_f \frac{\partial^2 u}{\partial s^2} + \rho_f g sin\alpha = 0 \tag{4.3}$$

Assuming a laminar and fully developed flow along the pipe results in defining an average velocity ($u_{s,ave}$) for a parabolic velocity profile as

$$u_{s,ave} = \frac{D^2}{32\mu_f}\frac{\partial p}{\partial s} - \frac{D^2}{32\mu_f}\rho_f g sin\alpha \tag{4.4}$$

Compressible fluid (SCO_2)

$$\frac{\partial \rho}{\partial t} + \frac{\partial}{\partial s}(\rho_f u) = 0 \tag{4.5}$$

$$\frac{\partial}{\partial t}(\rho_f u) + \frac{\partial}{\partial s}(\rho_f u^2) + \frac{\partial p}{\partial s} + \frac{2f\rho_f u|u|}{D} - \mu_f \frac{\partial^2 u}{\partial s^2} + \rho_f g sin\alpha = 0 \tag{4.6}$$

$$P = Z\rho_f RT \tag{4.7}$$

in which ρ_f, μ_f, Z, and R are the density, the dynamic viscosity, the compressibility factor and constant of the compressible fluid (gas), respectively, u is the average of the fluid velocity profile in the pipe, D is the well diameter, g is the local gravitational acceleration in vertical direction, f is the Darcy friction factor, α is the angle of well inclination with respect to the horizontal plane, and P is the pressure.

In the equations above, $\mu_f \frac{\partial^2 u}{\partial s^2} - \frac{f \rho_f u|u|}{2D}$ is the experimental constitutive term that approximate the viscous force ($\nabla \cdot \boldsymbol{\tau}$), for flow in circular pipes [142]. The first term, $\mu_f \frac{\partial^2 u}{\partial s^2}$, is derived from Newton's law of viscosity (or normal stress, τ_{xx}) and represents the axial viscous term, which operates as a diffusion of momentum along the pipe axis [143]. The second term, $\frac{f \rho_f u|u|}{2D}$, represents a friction term due to shear stresses (τ_{xy}). In most viscous flows, normal stress components are much smaller than shear stresses. Normal stress components become important when the normal velocity gradients ($\frac{\partial u}{\partial s}$) are very large, such as inside a shock wave.

The velocity profile and the friction factor for compressible flow are different than well-known solutions in incompressible pipe flow. In incompressible and fully-developed pipe flow, the average axial velocity gradient ($\frac{\partial u}{\partial s} = 0$) and radial velocity component (v) are assumed to be zero, resulting in a parabolic velocity profile and a constant pressure gradient along the pipe axis.

For compressible flow, the gas compressibility leads to a change both in the magnitude and the shape of the velocity along the pipe; i.e., the fully developed velocity profile can never be established for compressible pipe flow, even if the pipe is extremely long [144, 139, 145, 146]. The former leads to additional pressure drop along the pipe, and the latter increases the departure of the friction factor from its conventional correlation. To evaluate the compressibility effects of gas flow on the velocity profile shape, one-dimensional analysis is insufficient. Guo *et al.,* [144, 147] carried out two-dimensional analysis and presented the relation between the friction factor (f) and the Mach number (M), concluding that velocity profile and friction factor are functions only of the Mach number for $M > 0.1$. They demonstrated that higher Mach numbers lead to more deviation from a parabolic velocity profile (toward plug flow) and consequently larger friction factors. This is because the Mach number itself represents the magnitude of gas compressibility. The Mach number is defined as

$$M = \frac{u}{a} = \frac{u}{\sqrt{\gamma Z R T}} \tag{4.8}$$

in which a is the speed of sound and γ is the specific heat ratio.

In our study, the Mach number of the flow is low ($M < 0.1$) and the velocity profile is very close to that of fully developed flow (parabolic). Therefore, the well-known Colebrook equation can be used to estimate f [122, 148].

$$\text{Laminar } (Re < 2300) \quad f = 64/Re \tag{4.9}$$

$$\text{Turbulent } (Re > 4000) \quad \frac{1}{\sqrt{f}} = 2log_{10}\left(\frac{\epsilon/D}{3.7} + \frac{2.51}{Re\sqrt{f}}\right) \tag{4.10}$$

in which ϵ is the absolute roughness of the well wall surface. Absolute roughness (ϵ) for a steel-cased well is 1-3 mm [123, 124] and for open-hole wall well in igneous rocks with a very low number of natural fractures (e.g., granite) it is 3-6 mm [125].

4.3.3 Heat transfer for compressible and incompressible fluids

Heat transfer during compressible flow in a well due to advection-diffusion and convection between the rock and the compressible fluid is governed by [149, 150]

Incompressible fluid (water)

$$-\rho_f c_f u A \frac{\partial T_f}{\partial s} + A k_f \frac{\partial^2 T_f}{\partial s^2} + \pi D h (T_s - T_f) = 0 \tag{4.11}$$

Compressible fluid (SCO_2)

$$-\rho_f c_f u A \frac{\partial T_f}{\partial s} + A k_f \frac{\partial^2 T_f}{\partial s^2} + A \frac{f \rho_f |u| u^2}{2D} + \pi D h (T_s - T_f) = 0 \tag{4.12}$$

in which k_f, c_f are thermal conductivity and specific heat capacity of the gas inside the well, respectively. The third term in Equation 4.12 is the heat generated due to friction. The well has a cross-sectional of $A = \frac{1}{4}\pi D^2$ with the diameter of D and length of L in s direction. The injection temperature and volumetric flow rate (or velocity distribution) are assumed to be constant.

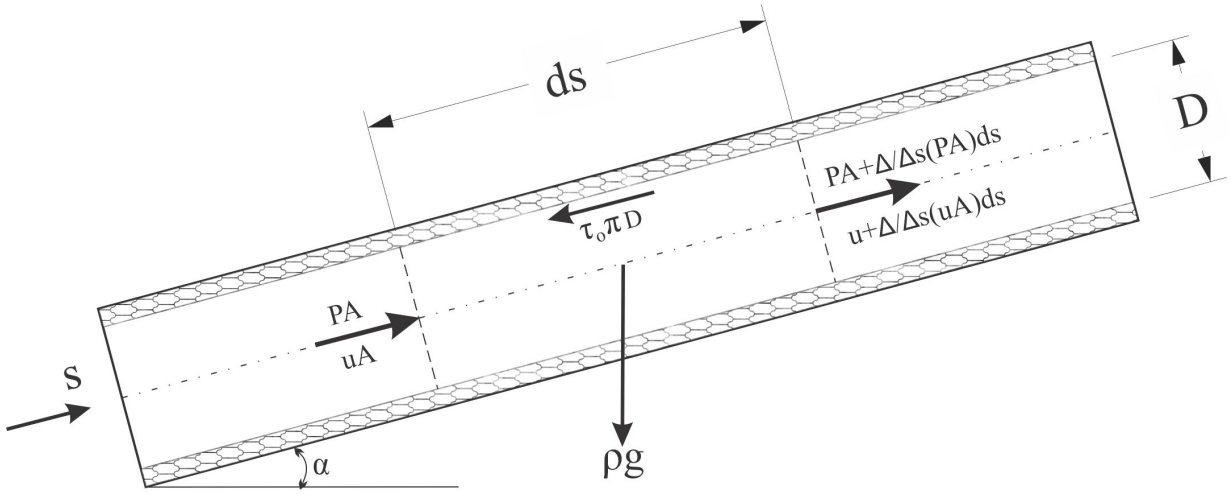

Figure 4.2: Circular inclined pipe flow components.

4.3.4 Organic Rankine Cycle (ORC)

The conservation of mass and energy are applied to ORC components based on the first and second laws of thermodynamics. The turbine and the pump are assumed to work as irreversible adiabatic processes. The heat exchangers are assumed to do no work and to be well insulated; no heat transfer occurs with the surrounding area (i.e., adiabatic processes). The kinetic and potential energy changes are ignored in the analysis due to their small magnitude compared to the work and heat transfer terms. It is also assumed that all components operate under steady-state conditions. Conservation of mass of the working fluid can be expressed at the inlet and outlet of each components as follows

$$\dot{m}_1 = \dot{m}_2 = \dot{m}_3 = \dot{m}_4 = \dot{m}_{wf} \tag{4.13}$$

Subscripts indicate different states of the working fluid at the inlet/outlet of each component, as shown in Figure 4.1. $\dot{m}_1$, $\dot{m}_2$, $\dot{m}_3$, $\dot{m}_4$ are the mass flow rates at the inlet/outlet of components of ORC, and $\dot{m}_{wf}$ is the working fluid mass flow rate. The conservation of energy for each component can be expressed as [47]

Turbine:

$$\eta_{tur} = \frac{h_1 - h_2}{h_1 - h_{2s}} \tag{4.14}$$

$$\dot{W}_{tur} = \dot{m}_{wf}(h_1 - h_2) \tag{4.15}$$

Condenser:

$$\dot{m}_{wf}(h_2 - h_3) = \dot{m}_{cf}(h_{out-cf} - h_{in-cf}) \tag{4.16}$$

Pump:

$$\eta_{pump} = \frac{h_{4s} - h_3}{h_4 - h_3} \tag{4.17}$$

Evaporator:

$$\dot{m}_{wf}(h_1 - h_4) = \dot{m}_f(h_{in-f} - h_{out-f}) \tag{4.18}$$

in which h_1, h_2, h_3, and h_4 are the real enthalpy (irreversibility assumption) at the inlet and outlet of the ORC components, h_{2s} and h_{4s} are the ideal enthalpy (isentropic assumption) of the turbine and pump outlets, respectively, η_{tur} is the turbine efficiency, η_{pump} is the pump efficiency, $\dot{W}_{tur}$ is the outlet work of the turbine, $\dot{m}_{cf}$ is the cooling fluid mass flow rate, h_{in-cf} and h_{out-cf} are enthalpy of the cooling fluid (circulating in the cooling tower) at condenser inlet and outlet, $\dot{m}_f$ is the mass flow rate of the produced fluid from the geothermal reservoir, and h_{in-f} and h_{out-f} are enthalpy of the produced fluid at the inlet and outlet of the evaporator.

4.4 Results and Discussions

The proposed coupled model is used to analyze the incompressible (water) and compressible fluids (SCO_2) temperature (from the reservoir) and the outlet electrical power (from the ORC) for the CLGS. In an earlier paper, the optimum values of well geometric characteristics (length, diameter, spacing) were determined for the CLGS (with a hexagonal array of horizontal wells) and water as the circulating fluid in granite rock [129]. That study indicated that horizontal wells with 100 m interwell spacing and 20 cm diameter could produce essentially the same circulating fluid temperature and ORC electrical power as a CLGS with a well array with greater interwell spacing and larger well diameters. The article also demonstrated that 1-km horizontal wells with a certain flow rate range produced

Table 4.1: Characteristics of the reservoir based on data from the Utah FORGE site data [3].

Properties	Variable	Value	Units
Reservoir depth	–	2000	m
Temperature gradient	–	0.07	$^oC/m$
Injection/Production well length	L	2000	m
Injection/Production well diameter	D	20	cm
Horizontal well length	L	1000	m
Horizontal well diameter	D	20	cm
Rock density	ρ_s	2800	kg/m^3
Specific heat capacity of rock	c_s	900	J/kgK
Rock thermal conductivity	k_s	3	W/mK
Initial reservoir rock temperature	T_s^o	150	^oC
Injection fluid temperature	T_f^o	35	^oC

almost the same electrical power as 2-km wells because of slow conductive heat transfer and small contact surface between the rock and fluid, and the ORC capacity; however, longer wells will clearly give a longer life span due to the larger effective volume of heat teservoir. Therefore, in the current chapter, the horizontal wells are assumed to have a length of 1 km, a diameter of 20 cm, and an interwell spacing of 100 m.

Table 4.1 summarizes the reservoir properties used in the analysis below. These properties and ground temperature gradient used in this study are based on those reported for the Utah FORGE site [3], which has been extensively explored in support of geothermal development in central Utah (350 km south of Salt Lake City).

4.4.1 Temperature, pressure, and density distribution of SCO_2 along the wells

A CLGS with the vertical injection/production wells and a single horizontal well is assumed for the analysis in this section. Figure 4.3 shows the temperature distribution of the circulating SCO_2 along the injection, horizontal, and production wells after two years. An injection temperature of 35 ^oC and a flow rate of 4 m^3/min are assumed. Heat transfer occurs from the formation to the circulating SCO_2 or vice versa during passage through the vertical injection and production wells, depending on the depth and temperature difference between the SCO_2 and formation.

At depths shallower than 200 m in the injection well, the circulating SCO_2 tempera-

ture is higher than the ground temperature; the SCO_2 temperature decreases due to the heat transfer from the SCO_2 to the formation. However, this temperature loss is negligible ($<1\ ^oC$). Beyond this depth, the SCO_2 temperature increases due to heat transfer from higher temperature formations to the SCO_2. In the horizontal well, the SCO_2 temperature increases nearly linearly (from 45^oC to $55\ ^oC$) through the horizontal well. The SCO_2 temperature continues to rise along the production well (from 2000-600 m). Then, a negligible temperature loss ($<2\ ^oC$) occurs in shallower depths ($< 600\ m$) due to heat transfer from the high-temperature SCO_2 to the low-temperature formation. The circulating fluid temperature evolution and distribution vary for different scenarios (different flow rates, well lengths, etc.).

In practical cases, the heat extraction from the reservoir is the greatest in the horizontal section for two reasons: first, the rock temperature is the highest; and second, the SCO_2 velocity in the horizontal section is generally lower than in the injection/production wells (due to the presence of multiple horizontal wells), providing more time for SCO_2 to absorb heat.

Figure 4.4 illustrates the produced SCO_2 temperature for the same CLGS conditions as in the above analysis over time. The temperature behaviour can be divided into four periods: ascend, descend, transition, and stable. During the first few months of the injection, in the ascend period, the produced SCO_2 temperature increases from a value close to the ground temperature (near the surface) to a maximum value below the reservoir temperature at 2 km, 150 ^oC. This ascending behaviour occurs due to initial cooling in the production well and lasts only a few months, until an equilibrium is approached between the average temperature of SCO_2 and the production well formation temperature. In practice, this could motivate insulating the upper portions of the injection and production wells. In descend period, there is a rapid decline in the produced SCO_2 temperature occurs over time. Then, the temperature versus time curve flattens to a stable period after a short transition period. If cooling in the production well is ignored, the produced SCO_2 temperature would be the same as the reservoir temperature at the beginning (dash-line in Figure 4.4).

The stable period is reached in less than a year, which is negligible compared to the CLGS project's lifetime ($>$ 30 years). The reason for rapid decline in the temperature of the produced SCO_2 over time is the small contact surface area between the rock and the circulating fluid and slow conductive heat transfer in the rock [62, 61]. Based on a desired project lifetime of +30 years, the stable period is the most important section for the analysis.

A density-forced convection circulation loop (thermosyphon) is induced when SCO_2

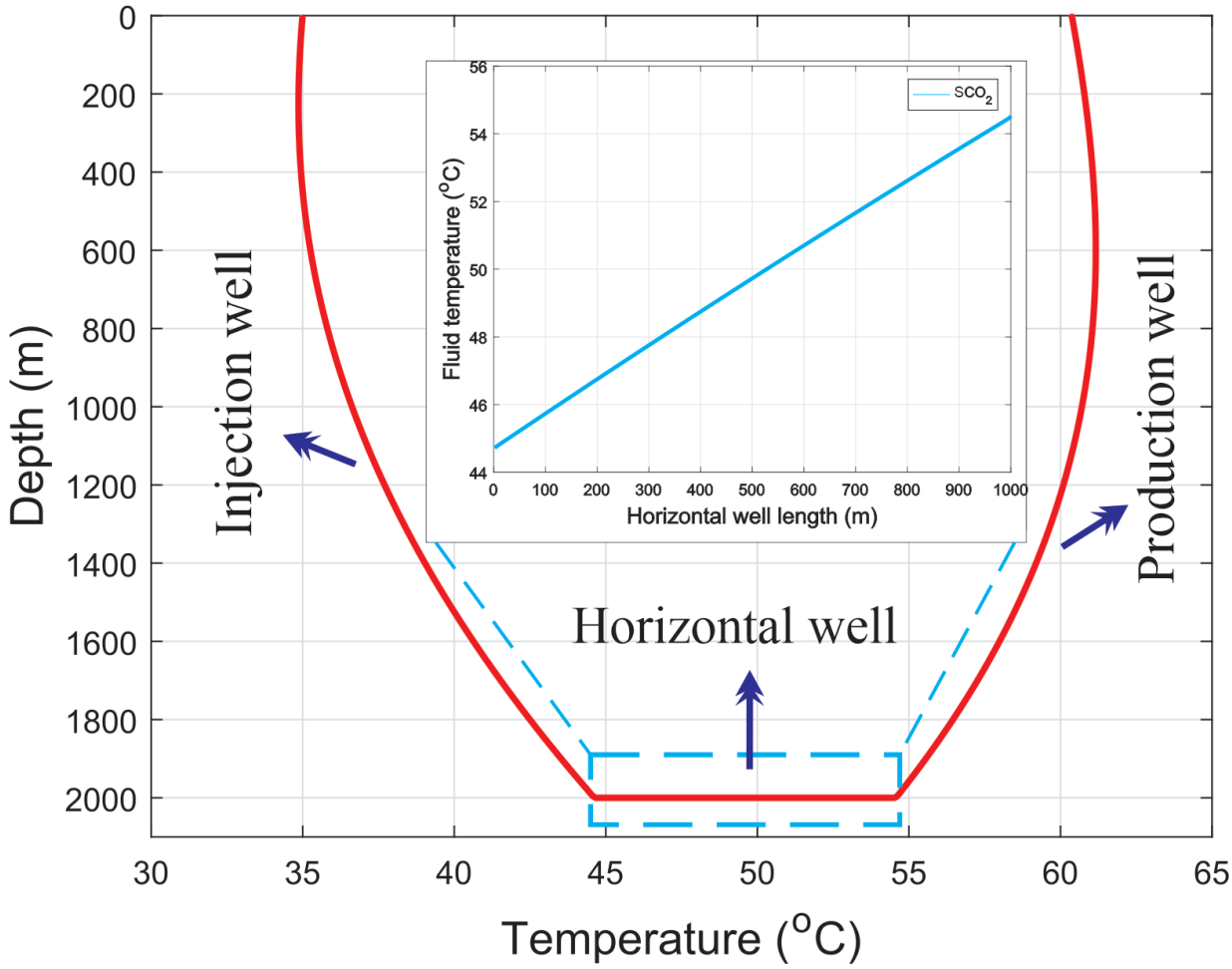

Figure 4.3: Temperature distribution of circulating SCO_2 along the wells for the CLGS with the injection temperature of 35 ^oC and flow rate of 4 m^3/min after 2 years.

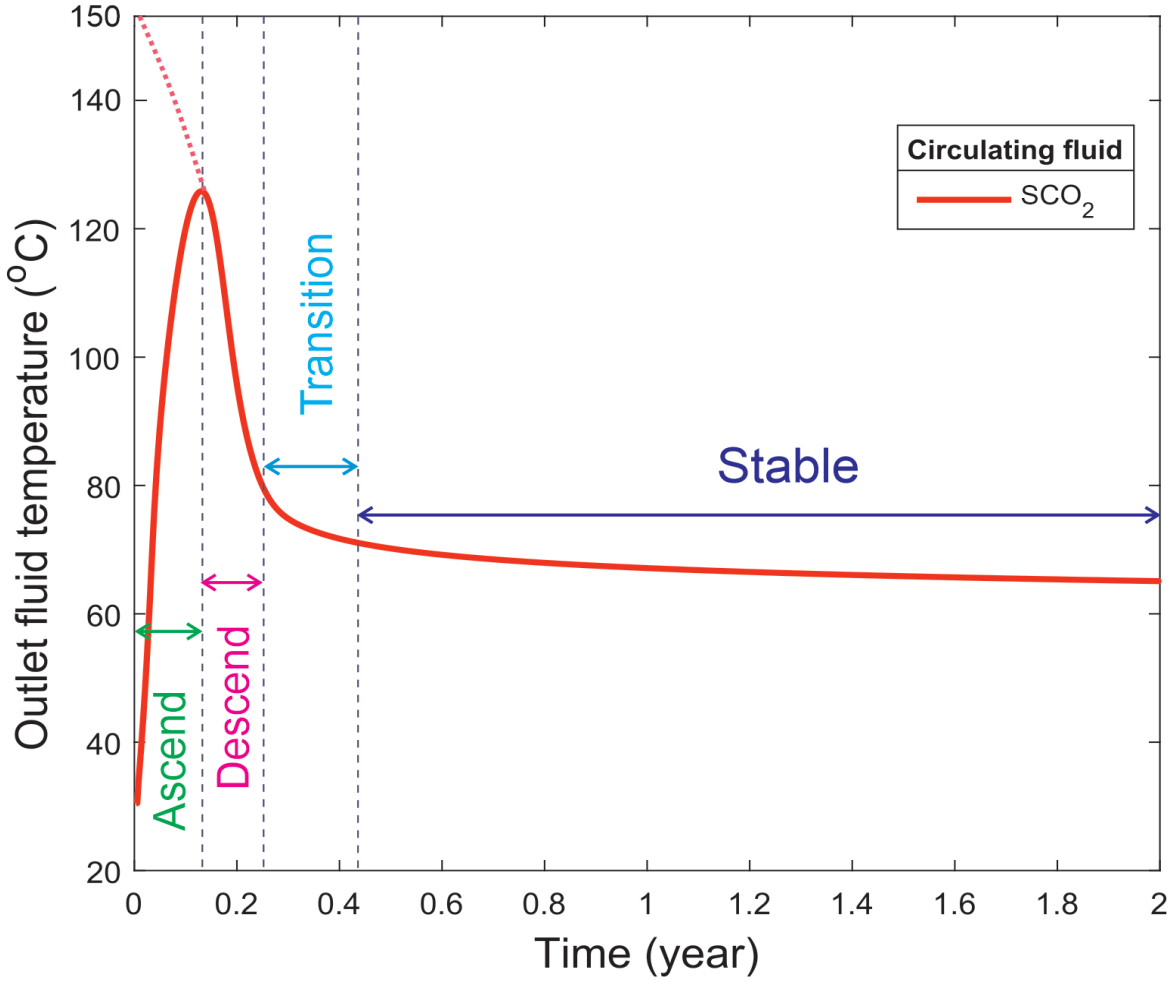

Figure 4.4: The temperature of the produced SCO_2 from the reservoir over time.

is used as the circulation fluid because the density difference induced by the temperature/pressure changes. Natural circulation systems present a great advantage due to lower energy consumption needed to pump the circulating fluid. Figure 4.5 shows SCO_2 density changes along the injection, horizontal, and production wells, caused by temperature and pressure changes. The density decreases along the injection well and increases along the horizontal and production wells. The total (net) change in the density along the wells is significant (from 0.7 to 0.36 g/cm^3), leading to a density-forced convection circulation through the wells, alleviating the need for additional mechanical work.

4.4.2 The CLGS performance using SCO_2 compared to water as circulating fluids

Temperature distribution along the wells

Incompressible water and compressible SCO_2 fluids behave significantly different in CLGS. Figure 4.6 illustrates the temperature distribution of SCO_2 compared to that of water, as they move along the injection, horizontal, and production wells after two years of production (during the stable period). The rate of temperature change of the SCO_2 along all wells is higher than that of water, expect at shallow depths. The net effect is that the output temperature for SCO_2 at the production well is $\sim$13 ^oC higher.

The results of the same analysis over time are shown in Figure 4.7. The difference between the temperature of the produced fluid ($\sim$13 ^oC) remains practically constant after the first half year. This temperature difference may be greater with a decrease in the injection flow rate or increase in the number of horizontal wells and the well lengths.

A higher temperature of the produced SCO_2 is the result of its unique thermodynamic properties. In addition, the rock properties, well length and diameter, and injection flow rate affect the circulating fluid temperature. To evaluate the effects of system parameters on the produced SCO_2 temperature, it is expedient to analyze the effects in terms of two dimensionless numbers: the Stanton number ($St = h/\rho_f c_f u$), and Biot number ($Bi = hD/2k_s$). The Stanton number relates the rate of convective heat transfer between the rock at the well and the circulating fluid to rate of advective heat transfer in the fluid. The Biot number relates the rate of convective heat transfer between the rock and the circulating fluid to the rate of conductive heat transfer in the rock. For a constant ratio of well length to diameter (L/D), increasing St or decreasing Bi leads to higher circulation temperatures.

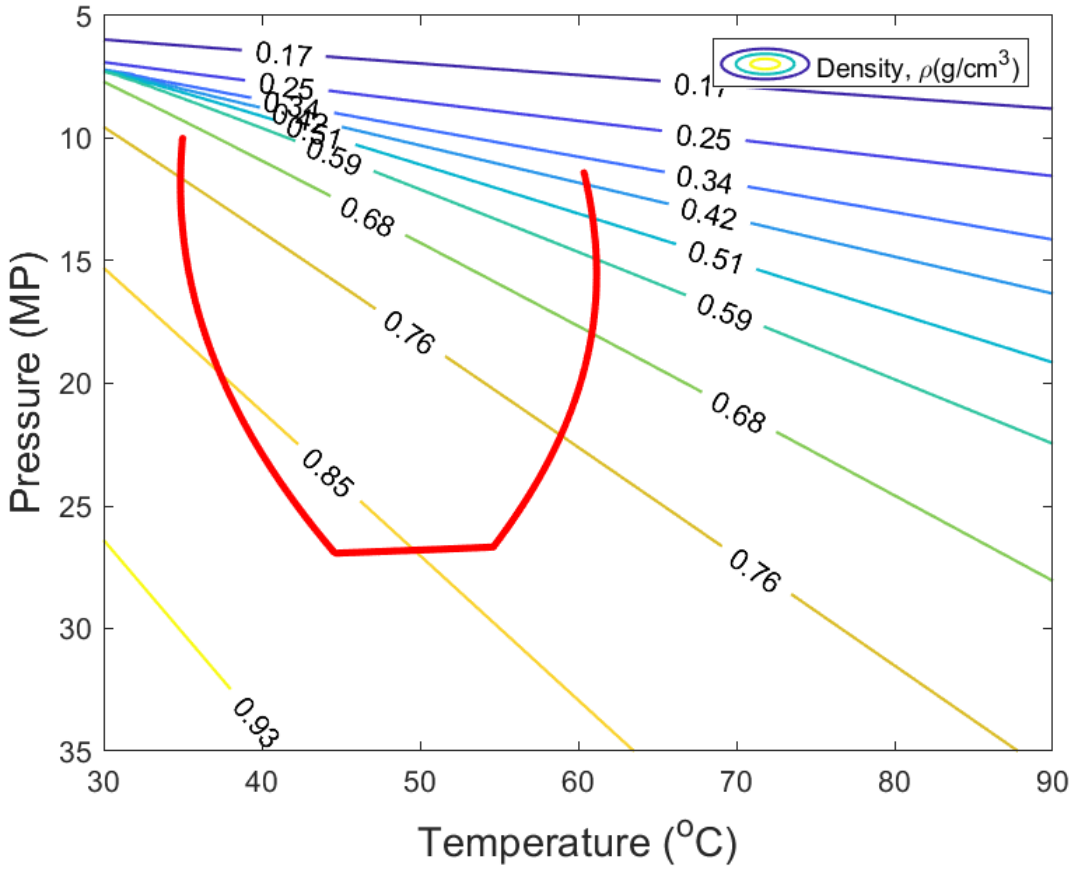

Figure 4.5: Density of SCO_2 at different temperatures and pressures along the injection, horizontal, and production well.

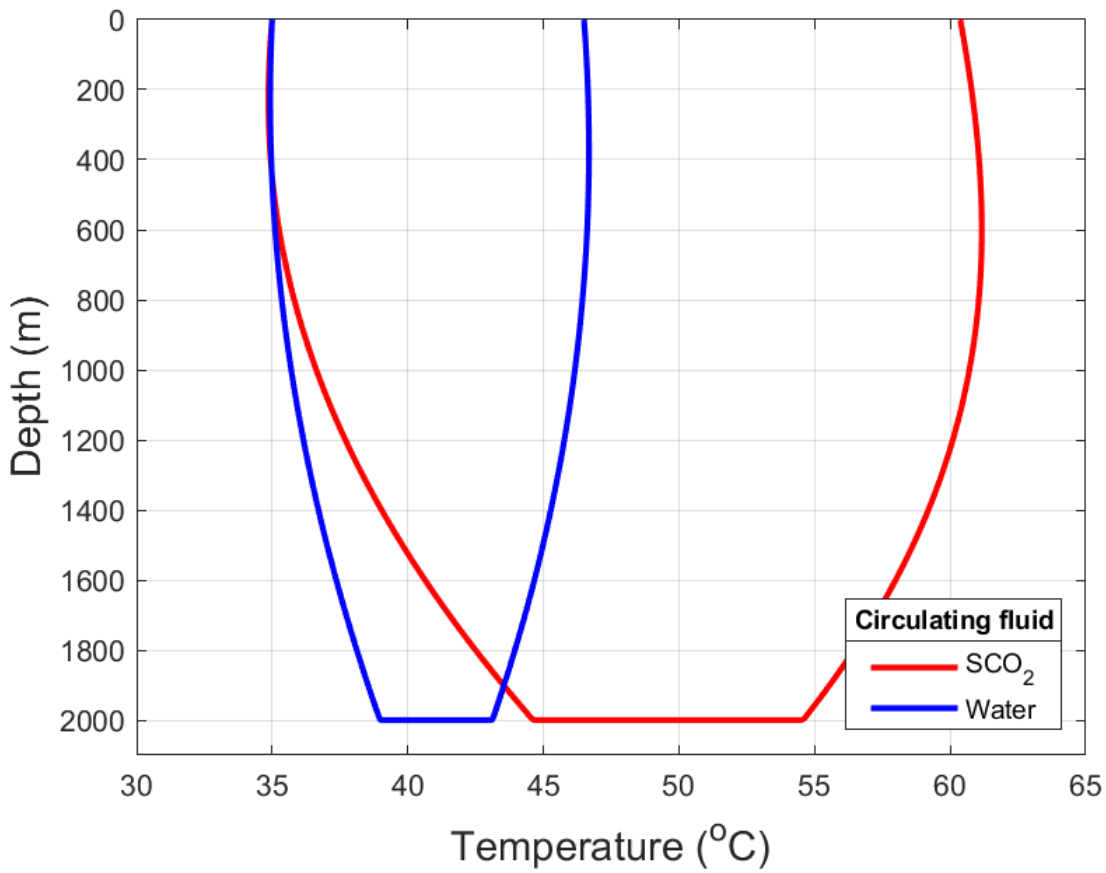

Figure 4.6: Temperature distribution of circulating SCO_2 along the wells compared to that of water for the same CLGS with the same injection and reservoir conditions after the second year.

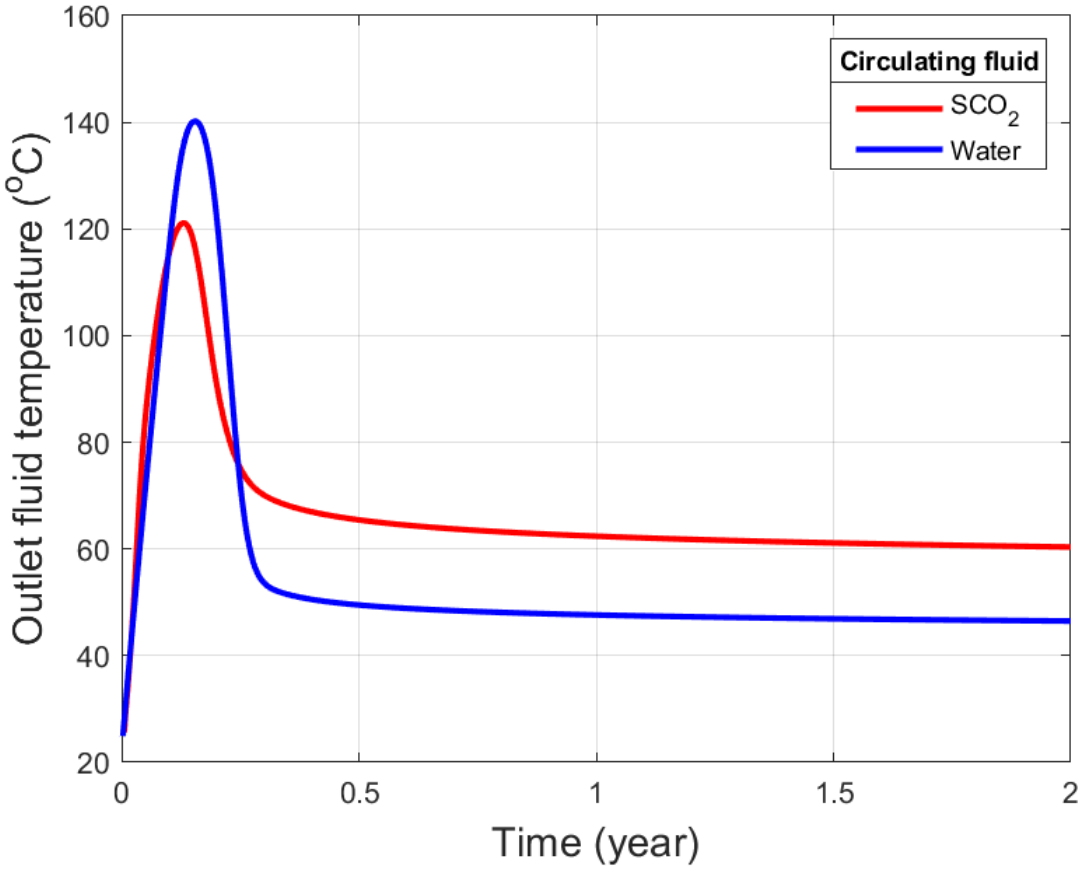

Figure 4.7: The difference between the production fluid temperature from the reservoir over time, assuming SCO_2 and water as circulating fluids.

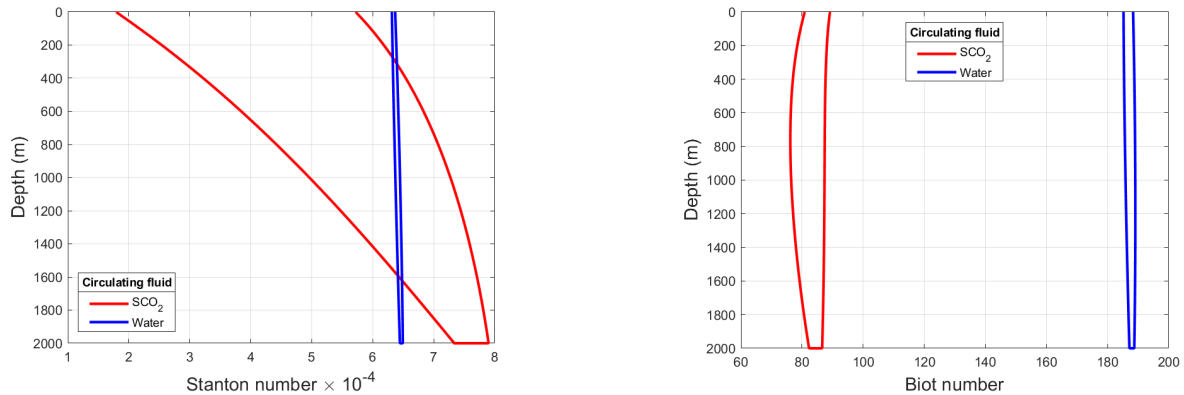

Figure 4.8: (First graph) The St number, and (Second graph) the Bi number of water and SCO_2 along the wells.

Figure 4.8 illustrates the St and Bi numbers for SCO_2 and water along the injection, horizontal, and production wells for the same CLGS, reservoir, and the injection properties of the previous section. The St and Bi are practically constant for water along the wells, whereas they vary for SCO_2. The accumulative effects of St and especially the significantly smaller Bi for SCO_2 leads to a higher SCO_2 temperature distribution along the wells (Figure 4.6), and consequently, a higher produced SCO_2 temperature over time (Figure 4.7).

The production fluid temperature and thermal power for different injection flow rates and number of wells

Assuming constant properties for the reservoir rock and well geometry (L and D), decreasing velocity (injection flow rate) is one way to increase the production fluid (SCO_2/water) temperature. Figure 4.9 illustrates the temperature distribution of the circulating SCO_2 along the wells for two different injection flow rates (2 and 4 m^3/min). A smaller flow rate in the wells provides more time for the fluid to heat up (Figure 4.10), leading to a higher fluid temperature along the wells and at the surface of the production well over time. However, a lower total flow rate can result in lower power production from the ORC.

One solution to keep the total injection flow rate high while decreasing the velocity is to drill multiple horizontal wells. Increasing the number of horizontal wells decreases the fluid velocity in the horizontal section for a constant total injection flow rate, providing more volume and time for the fluid to receive heat. As a result, the increase in the fluid

temperature for a higher number of horizontal wells is higher (Figure 4.11). Comparable behavior can be observed for water-based systems.

To understand the simultaneous effects of different numbers of horizontal wells and total flow rates on the produced fluid temperature, the results for these three parameters are shown in Figure 4.12 for SCO_2 and water after two years. The produced fluid temperatures for water (blue lines) are less than those for SCO_2 (red lines) in all scenarios. For example, five-horizontal-wells CLGS using water produces the same temperature as one-horizontal-well CLGS using SCO_2. This figure helps to readily find the total injection rate and the number of horizontal wells for a desired produced SCO_2/water temperature. The analysis assumes practical ranges for the number of wells of 1-6 and total injection flow rates of 4-10 m^3/min. A lower injection flow rate and a higher number of horizontal wells are preferred to sustain a higher produced fluid temperature; however, a higher number of horizontal wells increases the drilling cost, and lower injection flow rates decrease the total power (heat and electrical) generation.

To depict the difference between extracted heat using SCO_2 and water from the same CLGS, the produced thermal power (change in energy stored in the circulating fluid) in all scenarios of Figure 4.12 (i.e., different total injection flow rates and number of wells) are evaluated and presented in Figure 4.13. Although using SCO_2 provides a higher produced fluid temperature, the available thermal power in SCO_2 is less than that of water due to the lower volumetric heat capacity of SCO_2. A higher injection flow rate and a higher number of horizontal wells provide greater thermal power.

Electrical power generation for different injection flow rates and number of horizontal wells

Electricity generation is one of the main goals of geothermal projects. The outlet electrical power from the CLGS is assessed by coupling the proposed ORC model to the reservoir simulator. Circulating SCO_2 or water feeds the ORC in the evaporator, and propane and water are assumed as working and cooling fluids, respectively. A summary of ORC parameters used in the analysis for both water-based and SCO_2-based CLGSs is presented in Table 4.2.

The ORC performance can be affected by the ambient temperature. Therefore, a non-constant ambient temperature is taken into account. Table 4.3 summarizes the climate information (the monthly average ambient temperature) for the same location as the assumed reservoir used in the analysis (the Utah FORGE site).

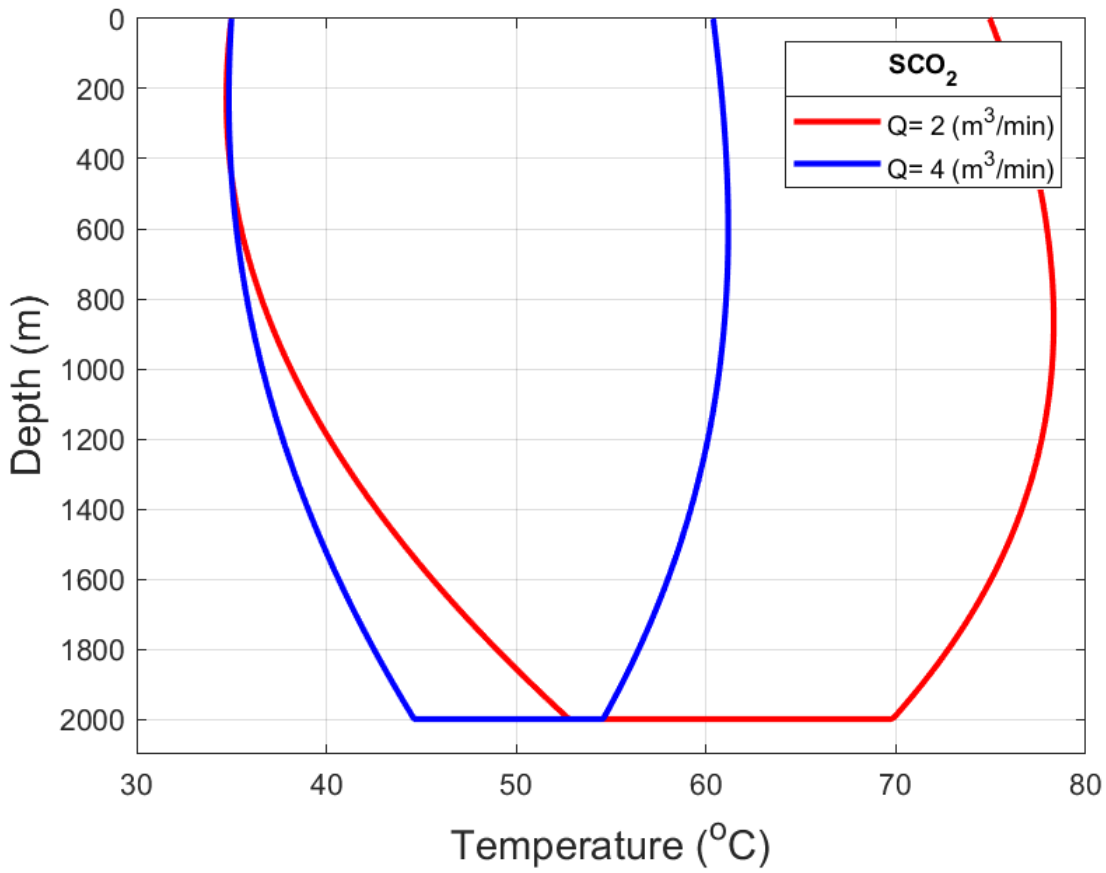

Figure 4.9: The temperature distribution of circulating SCO_2 along a single well at the second year for two different total injection flow rates (2 and 4 m^3/min).

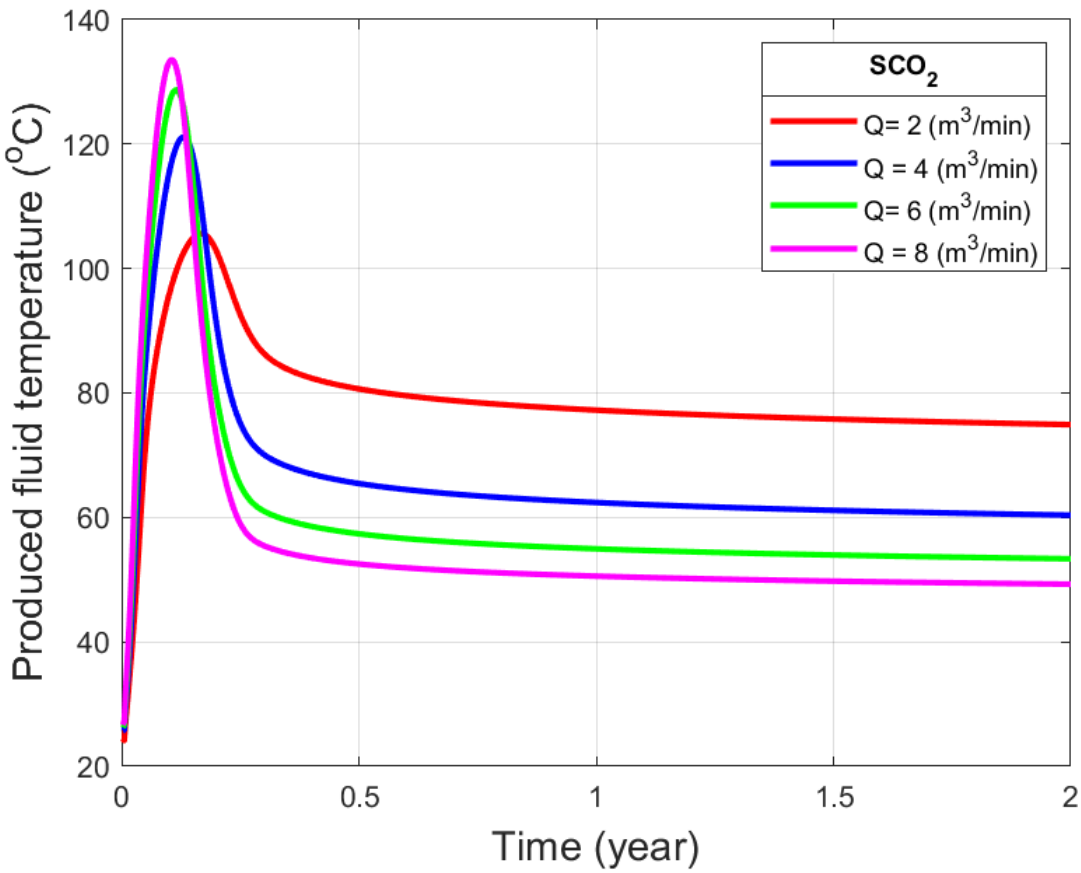

Figure 4.10: The production SCO_2 temperature at the production well at the surface for different injection flow rates over time.

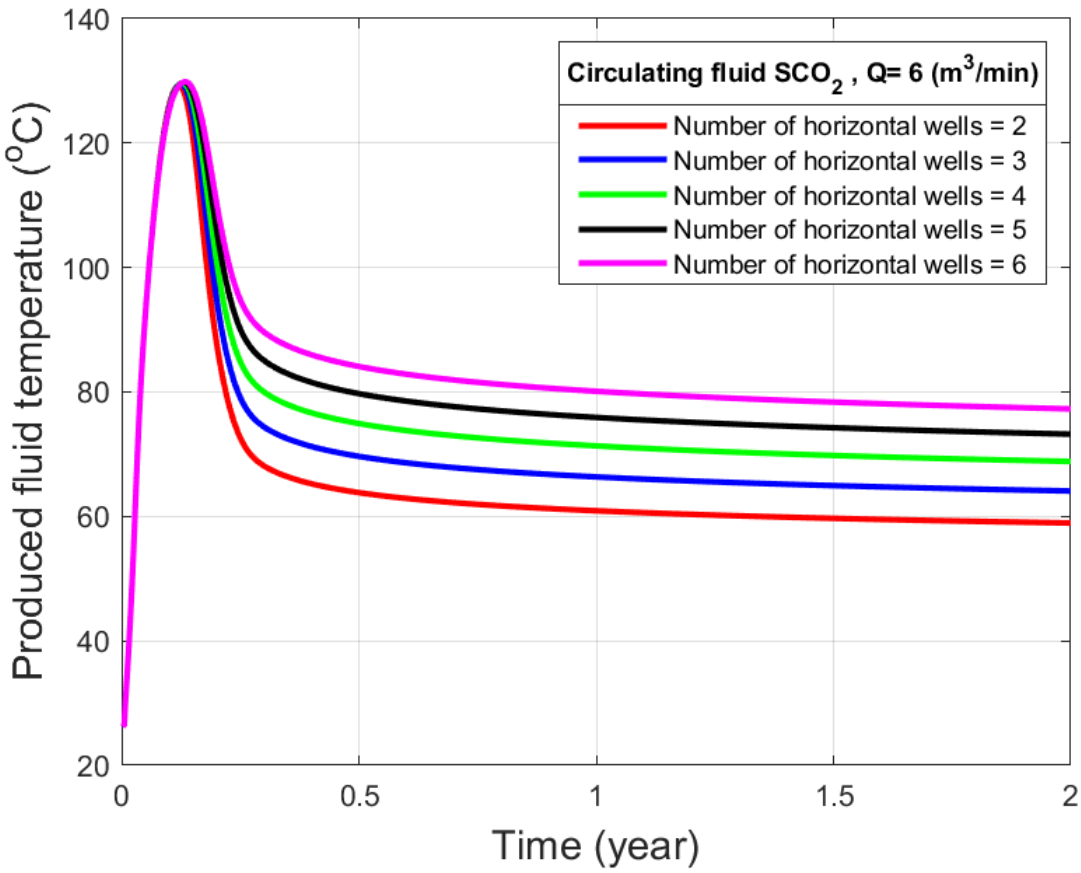

Figure 4.11: The production SCO_2 temperature for different number of horizontal wells (with a length of 1 km) at a constant total injection flow rate of 6 m^3/min.

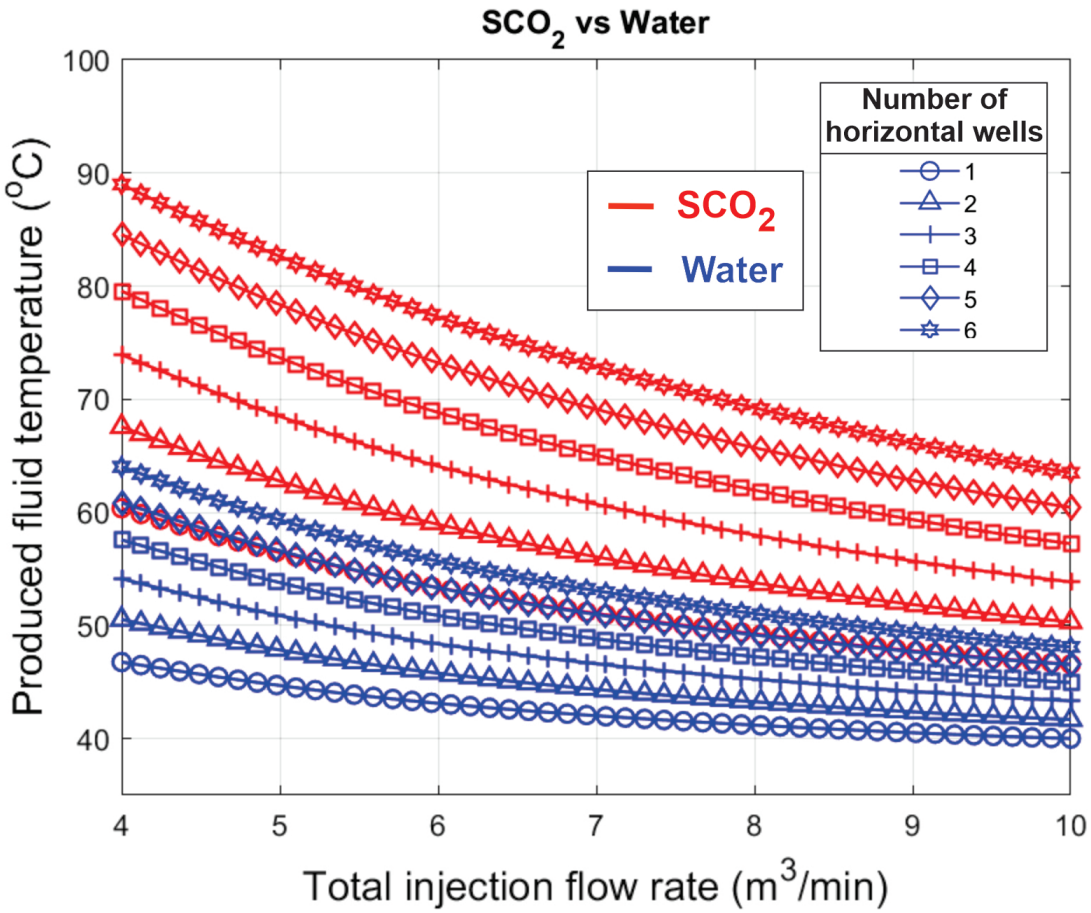

Figure 4.12: The produced SCO_2 and water temperature at the production well for different total injection flow rates and the number of horizontal wells at the second year (with characteristics used in Table 4.1).

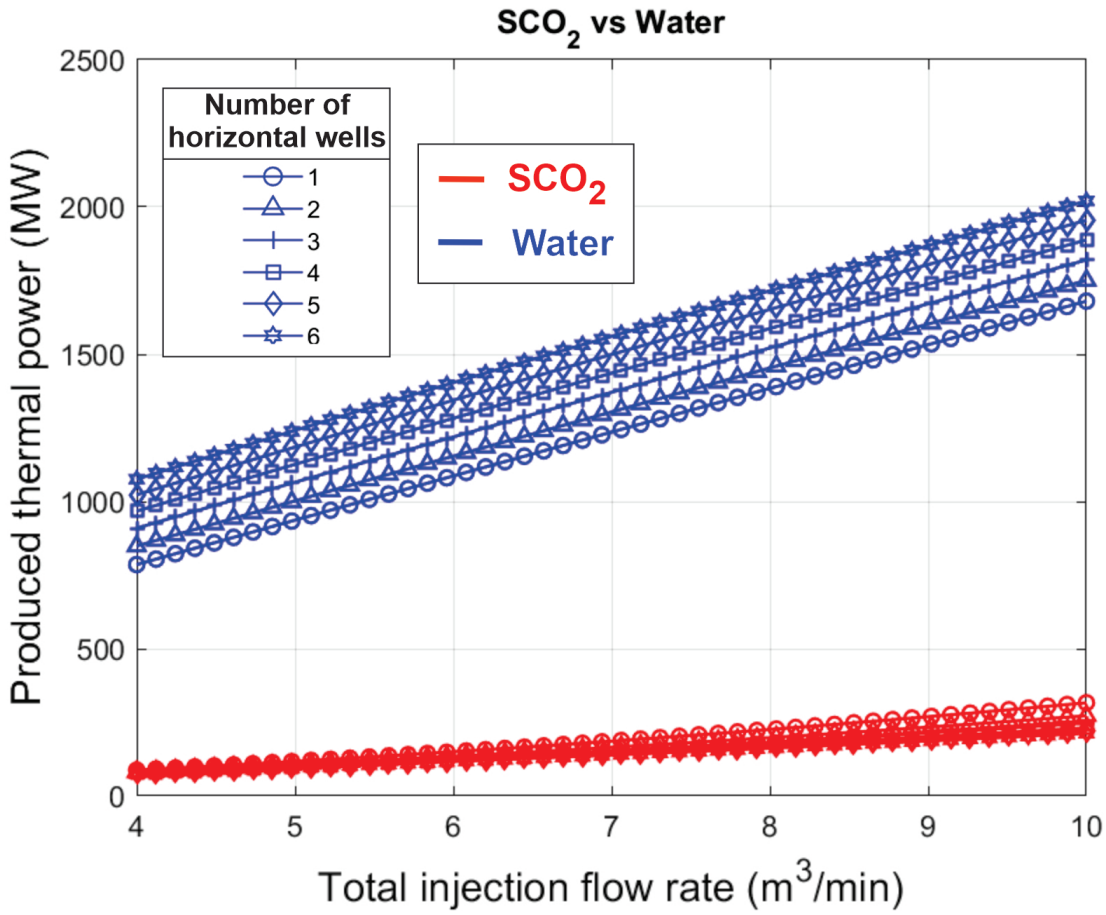

Figure 4.13: The rate of heat extraction from SCO_2-based and water-based CLGSs for different total injection flow rates and the number of horizontal wells after two years (Reservoir characteristics of Table 4.1 with the injection temperature of 35 ^oC and the initial reservoir temperature of 150 ^oC).

Table 4.2: ORC properties used in the analysis for SCO_2-based and water-based CLGSs.

Properties	**Variable**	**Value**
Working fluid	wf	Propane
Cooling fluid	cf	Water
Pump efficiency	η_p	0.75
Turbine efficiency	η_t	0.85
Working fluid mass flow rate	$\dot{m}_{wf}$	Variable
Cooling fluid mass flow rate	$\dot{m}_{cf}$	Variable
Ambient/Cooling fluid/Circulating fluid temperatures		Non-constant
Evaporator/Condenser pressures		Non-constant

Table 4.3: Monthly average surface air temperature used for electricity generation from ORC [2].

Month	**Surface Temperature (^oC)**	**Month**	**Surface Temperature (^oC)**
January	-3	July	23
February	-1	August	22
March	4	September	17
April	9	October	10
May	13	November	3
June	19	December	-2

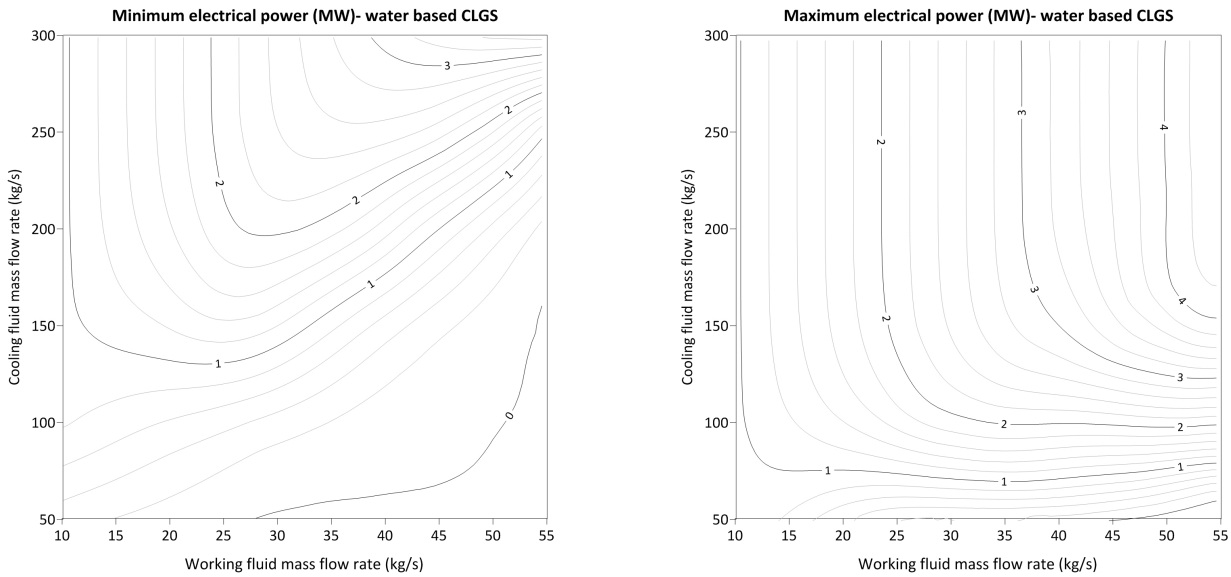

Figure 4.14: The outlet electrical power from a water-based CLGS with 6 horizontal wells and the total injection flow rate of 10 m^3/min for different values of working and cooling mass flow rates during warm seasons (minimum) and warm seasons (maximum) of the second year.

The electricity produced by a SCO_2-based CLGS depends in a different way, compared to a water-based system, on the working and cooling fluid mass flow rates of the ORC due to greater change in the properties of SCO_2 as it passes through the evaporator. Optimal ORC mass flow rates for water-based and SCO_2-based CLGSs (with 6 horizontal wells and 10 m^3/min total injection flow rate) are obtained in Figures 4.14 and 4.15, respectively, in terms of electrical power generation. The maximum and minimum periods of electricity production occur in cold months (October-April) and warm months (May-September), respectively. The optimal mass flow rates show a similar behavior for CLGSs with different injection flow rates and horizontal wells but in different level of electricity production.

As an example, Figures 4.16 illustrates the outlet electrical power and the inlet and outlet water temperatures to/from the ORC for water-based CLGS with 6 horizontal wells and total injection flow rate 10 m^3/min along with the monthly average ambient surface temperature (January to December). When the ambient temperature is high during the warm season, the condenser has to work at a higher pressure (if all other parameters are assumed to be constant), which leads to lower electrical power generation. In contrast, during cold seasons or in cold regions, since the ambient temperature is low, the condenser works

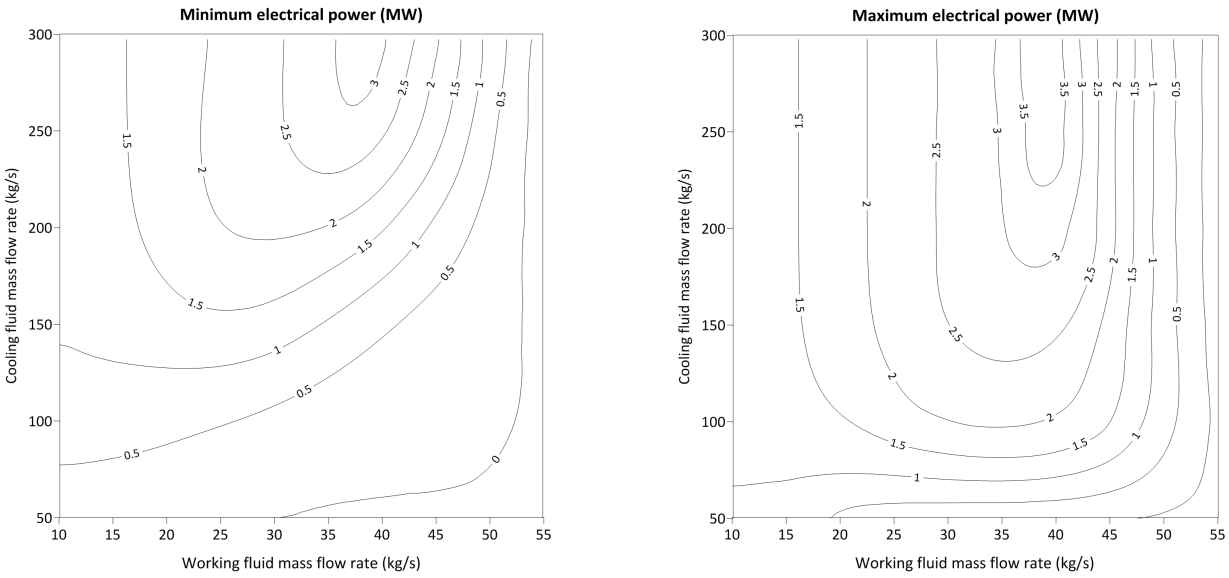

Figure 4.15: The outlet electrical power from a SCO_2-based CLGS with 6 horizontal wells and the total injection flow rate of 10 m^3/min for different values of working and cooling mass flow rates during warm seasons (minimum) and cold seasons (maximum) of the second year.

at lower pressures, at which the ORC produces a higher electrical power output. Therefore, the ORC requires to be "retuned" for a higher constant level of electricity generation during the whole year with lower energy consumption based on the ambient temperature, i.e., lower and higher mass flow rates during cold and warm seasons, respectively.

Within the range rates considered, for constant $\sim$4 MW electrical power production from water-based system, the approximate optimal working and cooling mass flow rates are 50 and 150 kg/s during October to April and 50 and 300 during May to September. An example for the above same water-based CLGS with 6 horizontal wells and the total injection flow rate of 10 m^3/min is shown in Figure 4.17. SCO_2-based system is less sensitive, compared to water-based system, to mass flow rates. For constant $\sim$3.5 MW of electricity generation from a SCO_2-based CLGS, the approximate optimal working and cooling mass flow rates are 40 and 150 kg/s during October to April and 40 and 250 kg/s during May to September. An example for the same water-based CLGS with 6 horizontal wells and the total injection flow rate of 10 m^3/min is shown in Figure 4.18. However, there may be practical limitation for high cooling mass flow rates.

With the above mentioned assumptions of different mass flow rates during cold months (October-April) and warm months (May-September), the produced electrical power from water-based and SCO_2-based CLGSs are evaluated for practical ranges of total injection flow rates (4-12 m^3/min) and the number of horizontal wells (1-6 wells with the length of 1 km), shown in Figures 4.19 and 4.20. The analysis is presented for the second year because electricity production after the first year declines slowly and is approximation cyclical year over year.

Based on the analysis, water-based CLGSs can be more efficient than SCO_2-based systems. For $\sim$3.5 MW electrical power generation, the water-based CLGS needs 2 horizontal well and total injection flow rate of 10 m^3/min (or alternatively 3 wells and flow rate of 9 m^3/min), whereas SCO_2-based system needs 4 wells and total flow rate of 12 m^3/min or (or alternatively 5 wells and flow rate of 10 m^3/min). In Figure 4.19, ORC mass flow rates in the water-based system are slightly higher than those of CLGS-based system. For the same flow rates, water-based system shows still a better performance, similar to Figure 4.19, with maximum $\sim$3.5 MW electrical power production. 3-4 MW electrical power generation using water-based CLGS with one or two horizontal well is reasonable for a moderate-size community with perhaps 500-1000 homes in remote areas (e.g., northern Canada), where the fuel or electricity delivery is highly expensive [119, 120, 118].

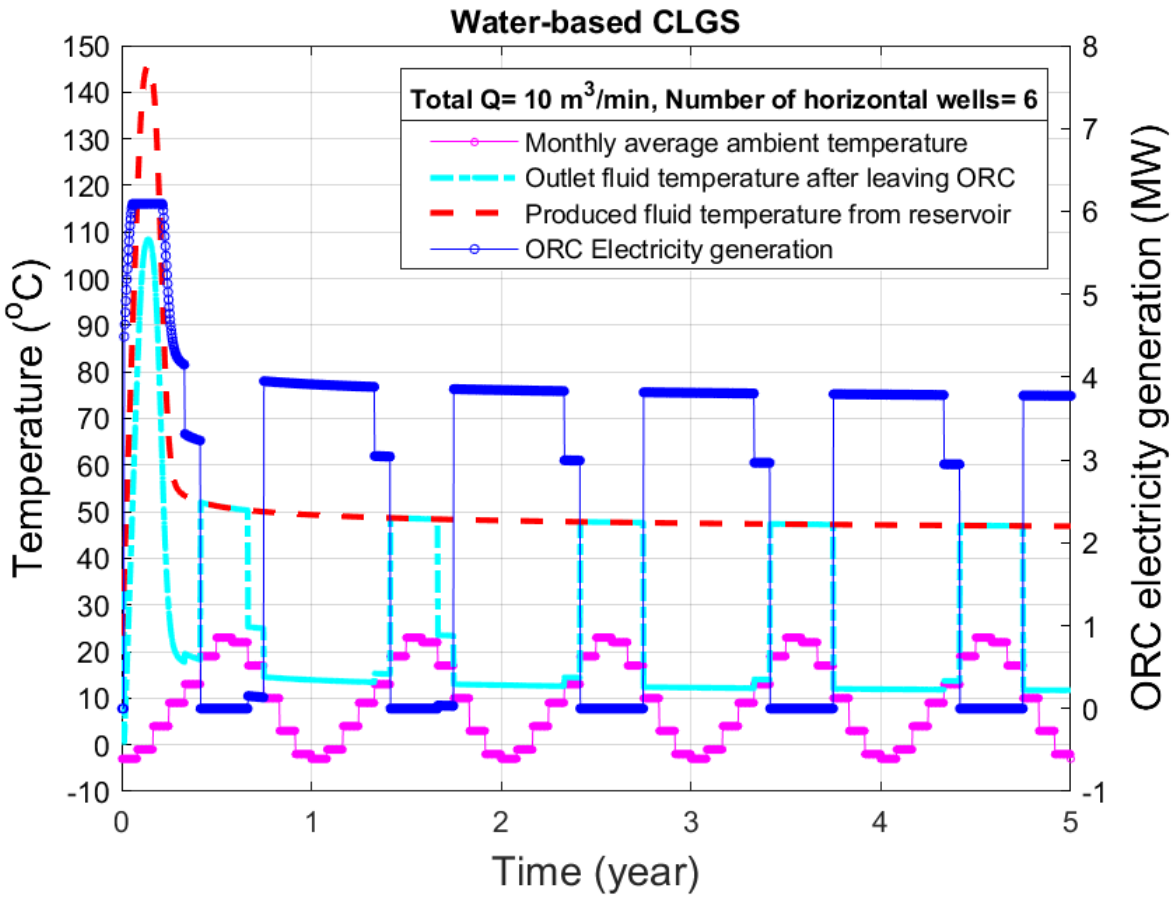

Figure 4.16: The produced electrical power from a water-based CLGS with a total injection flow rate of 10 m^3/min and 6 horizontal well under non-constant ambient temperature ($\dot{m}_{wf} = 50\ kg/s$, $\dot{m}_{cf} = 180\ kg/s$).

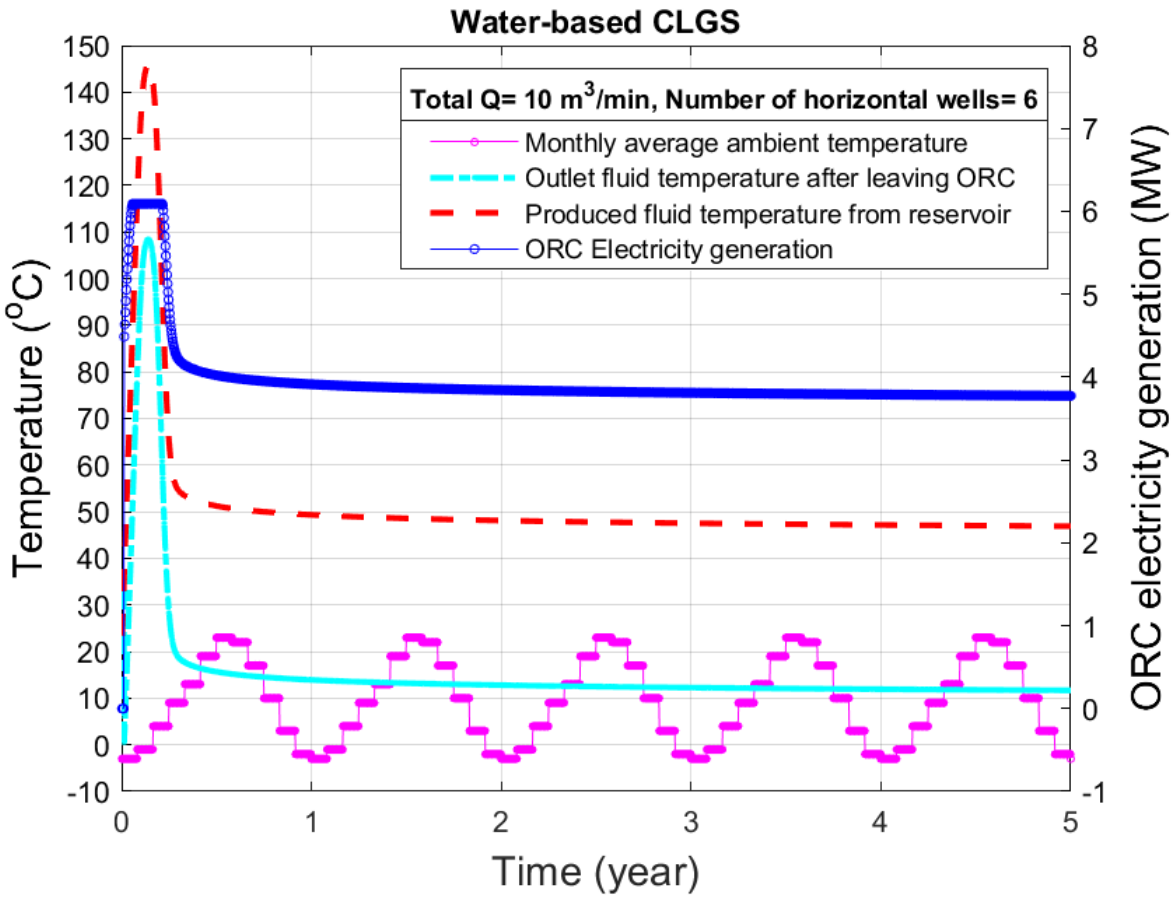

Figure 4.17: The produced electrical power from a water-based CLGS with a total injection flow rate of 10 m^3/min and 6 horizontal well under non-constant ambient temperature. ORC working fluid mass flow rate of 50 kg/s and cooling fluid mass flow rate of 150 kg/s during October to April and 300 kg/s during May to September.

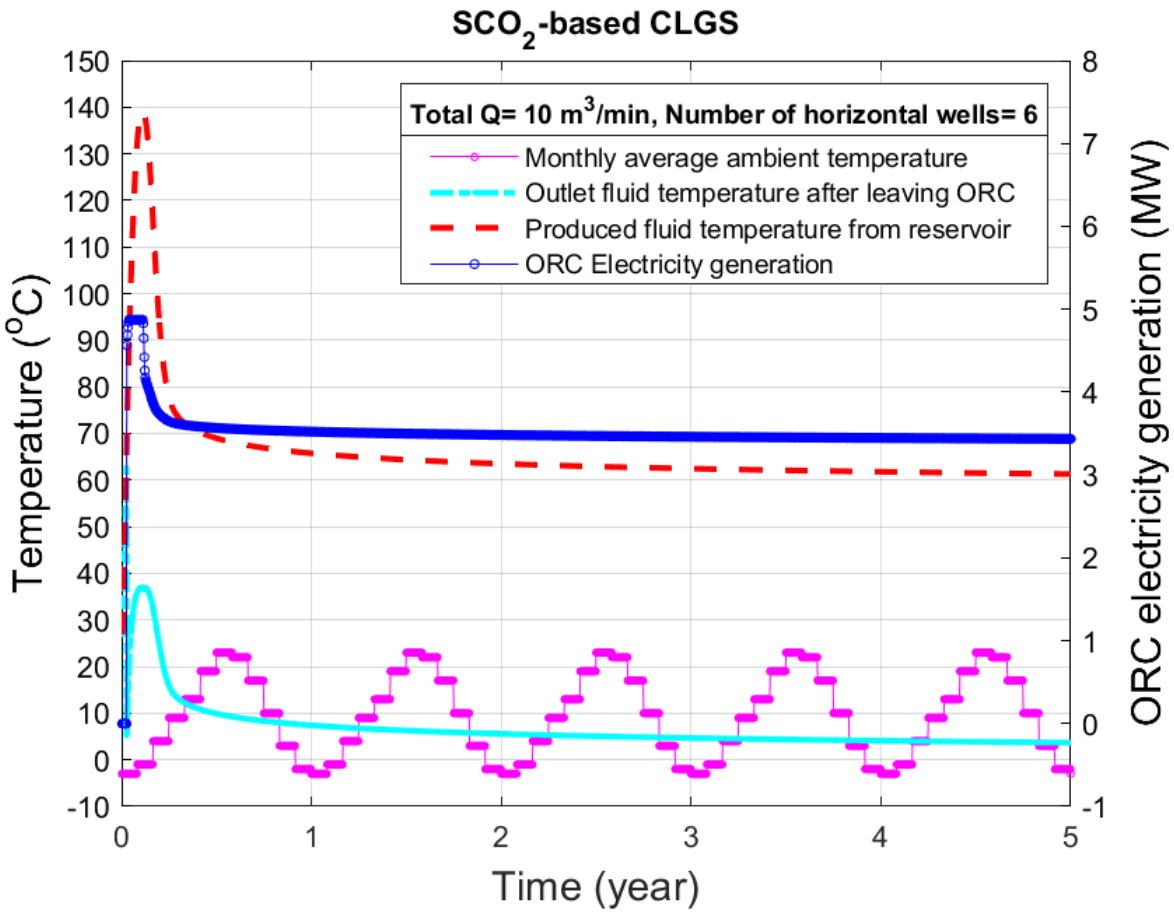

Figure 4.18: The produced electrical power from a SCO_2-based CLGS with a total injection flow rate of 10 m^3/min and 6 horizontal well under non-constant ambient temperature. ORC working fluid mass flow rate of 40 kg/s and cooling fluid mass flow rate of 150 kg/s during October to April and 250 kg/s during May to September.

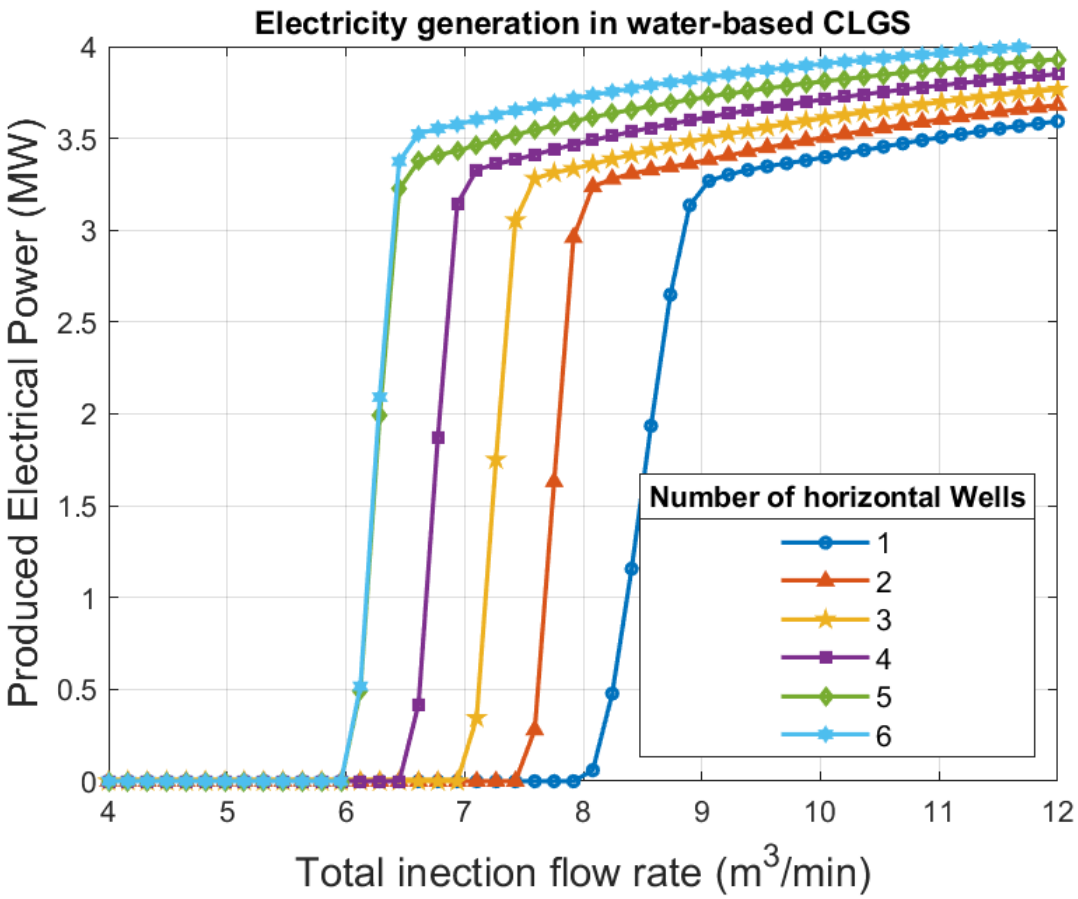

Figure 4.19: The outlet electrical power from water-based CLGS for different total injection flow rates and number of horizontal wells in the second year, with ORC working fluid mass flow rate of 50 kg/s and cooling fluid mass flow rate of 150 and 300 km/s during cold and warm months, respectively (reservoir properties from Table 4.1, injection temperature 35 ^oC, rock temperature 150 ^oC).

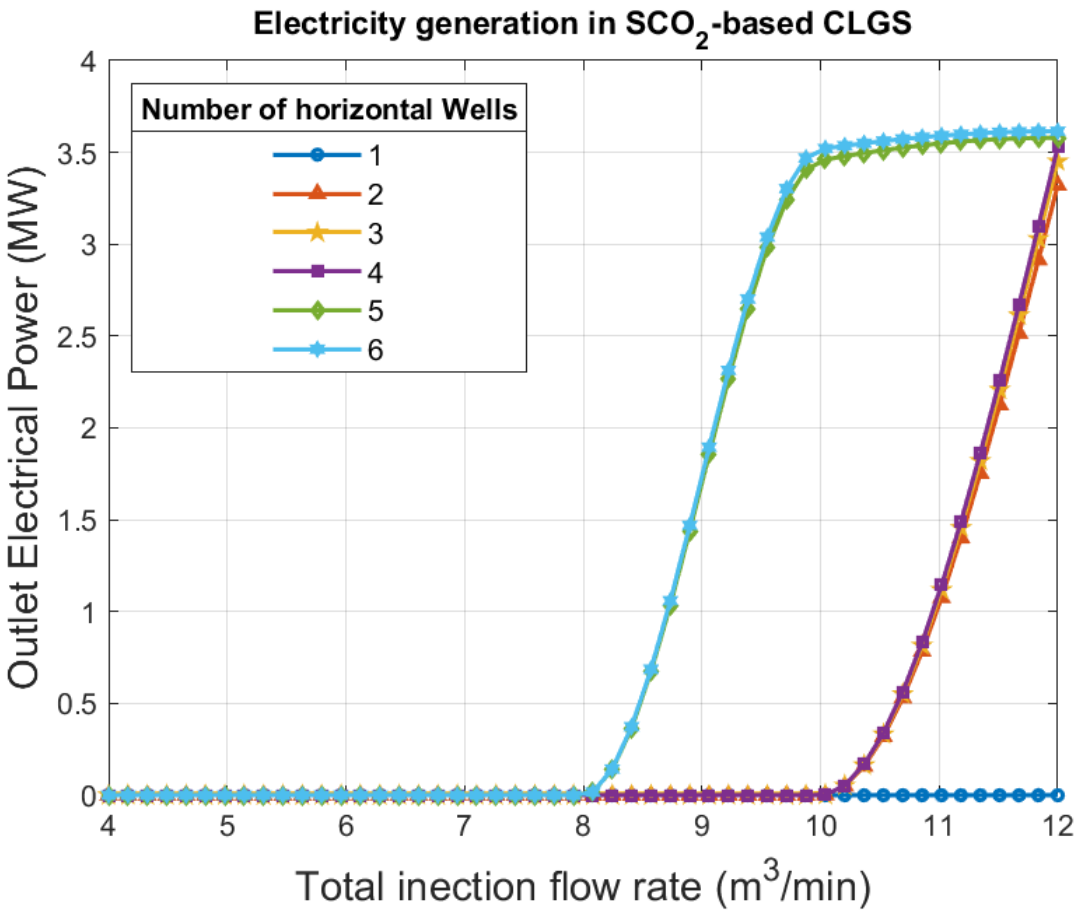

Figure 4.20: The outlet electrical power from water-based CLGS for different total injection flow rates and number of horizontal wells in the second year, with ORC working fluid mass flow rate of 40 kg/s and cooling fluid mass flow rate of 150 and 250 km/s during cold and warm months, respectively (reservoir properties from Table 4.1, injection temperature 35 ^oC, rock temperature 150 ^oC).

4.5 Conclusion

We developed a study of heat and electricity generation from a deep Closed Loop Geothermal System (CLGS) in Hot Dry Rocks (HDRs) that uses supercritical CO_2 (SCO_2) or water as the circulating fluid. The system is comprised of the injection and production wells (2 km deep), 1 km multiple horizontal wells in granite rock, and an ORC at the surface. The analysis is based on a coupled FVM/FEM/ORC model for subsurface evaluation of compressible/incompressible fluid flow and transient conductive-convective heat transfer within and between the rock and the fluid (SCO_2 and water), and surface evaluation of electricity generation at a non-constant ambient temperature. The analysis yields the following observations for 35 ^oC injection fluid and 150 ^oC initial reservoir temperature.

- The produced fluid (SCO_2/water) temperature from the CLGS over time experiences a rapid temperature rise, decline and transition periods in less than a year, and becomes approximately stable for a long time, indicating a extended lifetime (+25 years).
- Produced circulating fluid temperature in a SCO_2-based system is higher than that of a water-based system; however, the energy content of the produced SCO_2 is lower due to thermodynamic properties.
- Both water-based and SCO_2-based systems are able to generate considerable amounts of power for +25 years (water-based: 3-4 MW electrical power and 1000-2000 MW heat; and SCO_2-based: 3-3.5 MW electrical power and 100-300 MW heat).
- Seasonal surface air temperature differences can significantly affect the electrical power generation an impact ideal ORC operating parameters, such as mass flow rates. In northern climates, an ORC requires lower and higher mass flow rates during cold (October to April) and warm months (May to September), respectively, to produce a consistent level of electrical power efficiently.
- The extremely high cost of electricity combined with the great demand for heat in northern Canadian communities (e.g., Yukon, Northwest Territories, Nunavut) motivates further economic analysis into the viability of a 3-4 MW systems.
- Water-based systems tend to require fewer horizontal wells and lower flow rates than SCO_2-based systems for similar power generation. Analysis suggests that for $\sim$3.5 MW of electrical power production, a water-based system requires 2 horizontal wells with a total flow rates of 10 m^3/min, whereas a SCO_2-based system needs 4 wells

with a total flow rates of 12 m^3/min. Assuming a preference for reducing initial capital costs, the benefits of the reduced drilling costs of a water-based system are expected to outweigh the reduced operating costs (due to the thermosyphon effect) of a SCO_2-based system.

Chapter 5

Conclusions, Publications, and Future Works

5.1 Conclusions

This PhD thesis has presented a comprehensive study of design parameters for Closed Loop Geothermal Systems (CLGSs) in deep Hot Dry Rocks (HDRs) in terms of heat and electricity generation, including the reservoir rock, fluid, well geometry, and power plant parameters.

CLGS is a new method of heat extraction from HDRs, where no fluid and in-the-rock flow path are available (e.g., granite, basalt, low-porosity-permeability sedimentary rocks). In its most common design, a CLGS is a U-shaped circulation system that is comprised of two vertical sections (injection/production wells) and a horizontal section, which may include multiple horizontal wells. A fluid is circulated through the system, heating up during passage through the wells. The resulting hot fluid flowing out of the system at the surface of the production well commonly feeds a binary power plant (i.e., Organic Rankine Cycle - ORC) for electricity generation.

Analytically assessing the whole system with realistic assumptions over time is not possible because of the system's coupled multi-physics nature. Analytical solutions to only the rock temperature or the fluid temperature do exist, but only with many simplifications of these complex systems. The heat transfer process in the reservoir is a coupled transient process within and between the rock and fluid, with non-constant temperature and heat flux along the wells. The performance of the ORC, fed by a non-constant circulating outlet fluid temperature and operating in a non-constant ambient temperature (-35 ^oC to +30 ^oC in Canada) is another challenging task that has not previously been explored for CLGSs. Furthermore, the performance of the system when supercritical CO_2 (SCO_2) is circulated instead of water was poorly understood prior to this research. To address these challenges quantitatively, numerical methods must be employed, as has been done in this research. However, analytical solutions to only the rock temperature or the fluid temperature do exist, but with many simplifications.

In this PhD research, a coupled Finite Volume Method (FVM)/Finite Element Method (FEM)/ORC model has been developed to solve the problems of incompressible or compressible pipe flow (pressure and velocity), advective-convective transient heat transfer within and between the rock and fluid in the reservoir, and electrical power generation at the surface under non-constant ambient temperature. To present guidance on CLGS design (including the reservoir and ORC), the model has been implemented for a wide range of rock properties, fluid properties (compressible and incompressible), injection flow rates, and well lengths and diameters.

In Chapter 1, a general introduction and overview to geothermal systems is given. A

brief discussion was also provided on current challenges in CLGSs. The objectives of this research and the methodologies used for fulfilling each of the objectives were also briefly discussed.

Chapter 2 describes the methodology and the numerical methods used to arrive at a solution to the geothermal problem of transient heat production from HDRs using a single-horizontal well CLGS. The heat transfer process includes conduction in the rock, convection between the rock and the fluid, and advection and conduction in the fluid along the well. Dimensionless forms of the governing equations are derived, and ten rock, fluid and geometric parameters were reduced and presented as three dimensionless parameters. An axisymmetric FEM model is developed to evaluate the temperature of the rock mass and fluid over time for a wide range of system properties in terms of introduced dimensionless parameters. This chapter has been published in its entirety as a journal paper.

Chapter 3 presents a parametric study of CLGS design with multiple horizontal wells, drilled in HDRs, by developing a coupled FEM model for the problem of transient heat production in the reservoir and an ORC model for electricity generation evaluation at the surface. The design parameters include well spacing and geometry, the number of wells, injection flow rate, energy losses along the well, and ORC working and cooling fluid mass flow rates. The impacts of these parameters under a wide range of realistic conditions are assessed for the evolution of the spatial distribution of the temperature of the rock mass, the circulation fluid temperature leaving the reservoir, and the rate of electrical power generation with seasonal variations in surface air temperature. The analyses led to the presentation of an appropriate range of values for the above-mentioned parameters for an acceptable level of electricity production. The methodology and numerical examples of the chapter have been disseminated through a journal article.

Chapter 4 compares heat and electrical power production from HDRs using supercritical CO_2 (SCO_2) and water as circulating fluids in a CLGS with a hexagonal array of multiple horizontal wells. The analysis is based on a coupled FVM/FEM/ORC model, evaluating subsurface incompressible/compressible pipe flow and transient conductive-convective heat transfer within and between the rock and fluid, and surface electricity generation under non-constant ambient temperatures over time. The performances of the water-based system in comparison to the SCO_2-based system are assessed for a wide range of practical inputs to find the best range of total injection and ORC flow rates and number of horizontal wells in terms of the production fluid temperature, heat, and electrical power. Moreover, natural circulation of SCO_2 due to thermosyphon effects has also been evaluated for the system. The chapter has been reported in a journal article, now under review.

5.2 Summary of Design Parameters and Assumptions of the Model

To sum up the design process, it is identified that:

- The horizontal wells can be drilled with the smallest (practically) drillable diameter of 20 cm. However, the greater diameters are not preferred because they produce practically the same fluid temperature and power but significantly higher drilling costs.
- The horizontal wells in a hexagonal array can be placed 50-100 m apart. Interwell spacing of 100 m has a minor effect on the produced fluid temperature ($\sim$ 1%) compared to produced fluid temperature from a single well with infinite boundaries.
- Total injection flow rate of 7-8 m^3/min in a CLGS with 2-4 horizontal wells of 1 km length, located at a depth of 2 km in a moderate geothermal gradient of 65-75 $^oC/km$ can produce a significant amount of direct heat (1000-2000 MW for water-based and 100-300 MW for CO_2-based systems) and electrical power (3-4 MW), which is sufficient for a small community with 500-1000 houses.
- Water-based CLGSs may be preferred to SCO_2-based systems since water-based systems tend to require fewer horizontal wells and lower flow rates for similar power generation.

This PhD research does not directly provide a design process of CLGS for a specific case but explores a wide range of aspects of the engineering science needed for design. The study finds the optimum range of the most important parameters for maximum heat and electricity generation. The design parameters are flow rates in the wells and the ORC, length, diameter, interwell spacing, and the number of horizontal wells.

The main assumptions and simplifications of the developed FEM/FVM/ORC model that may impact the results are as follows.

- The role of casing in heat transfer analysis is ignored along all wells. In practice, the horizontal wells are chemically sealed without casing. However, the vertical wells have casing. Since the major heat transfer occurs along the horizontal section, ignoring the role of casing in analysis may have insignificant impacts on the final results.

- The HDR is assumed impermeable without saturation. However, rock may be saturated especially around the wells because of the drilling process, which may affect the final result. If the mass fraction of water in the rock is less than 1%, its impact should be negligible.

- Water is assumed as an incompressible fluid, in which its properties are assumed constant for different temperatures and pressures in the analysis. However, water properties change at high temperatures and pressures, which may impact the final output results of the system. The compressible pipe flow analysis in the last chapter is capable of circulating water in wells with variable thermodynamic properties.

5.3 CLGS Assessment in Canada

In the absence of detailed information for Canadian geothermal sites, the geothermal gradient, reservoir properties, and weather information of the FORGE site located in central Utah (350 km south of Salt Lake City) are used in this PhD thesis. The FORGE site has been extensively explored in support of geothermal development with significant available data. However, the geothermal gradient in the FORGE site is greater than that of anywhere in Canada east of the Rocky Mountains, which requires more deep drilling and an increase in cost. In Canada, high-temperature geothermal resources are mostly located in western and northwest Canada, and a vast majority of Canada has a lower geothermal gradient than that of the FORGE site [151, 106]. Therefore, to assess the possibility of power production from low geothermal gradient resources using CLGS, a geothermal gradient of 60 $^oC/km$ is assumed in this section instead of 75 $^oC/km$ (in FORGE site). Figure 5.1 shows the produced fluid temperature (red lines) and electrical power generation (blue lines) from a water-based CLGS with two different geothermal gradients of 75 $^oC/km$ (the reservoir rock temperature of 150 ^oC) and 60 $^oC/km$ (the reservoir rock temperature of 120 ^oC). The produced fluid temperature and electrical power production differences in the two scenarios are not immense, 4 ^oC and 0.2 MW, respectively. Therefore, implementation of CLGS in low geothermal gradient places like Canada also seems technically feasible.

The thermal conductivity of HDRs like granite varies widely depending on particle size distribution, porosity and permeability, degree of saturation, etc. [152]. In this section, the effects of minimum and maximum thermal conductivity used in this PhD research, based on the literature, are assessed in terms of produced fluid temperature. Figure 5.2 shows the difference in produced fluid temperature for a water-based CLGS with different thermal conductivity in the reservoir rock. The reservoir rock is assumed granite with 0.9

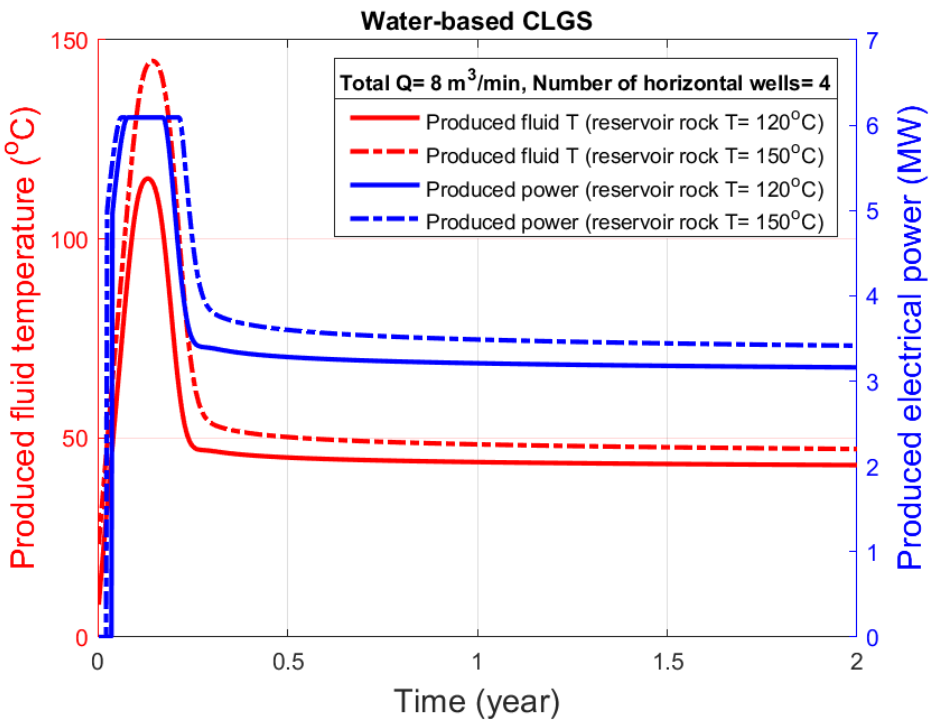

Figure 5.1: The difference between two water-based CLGSs located in low (60 $^oC/km$) and high (75 $^oC/km$) geothermal gradient places.

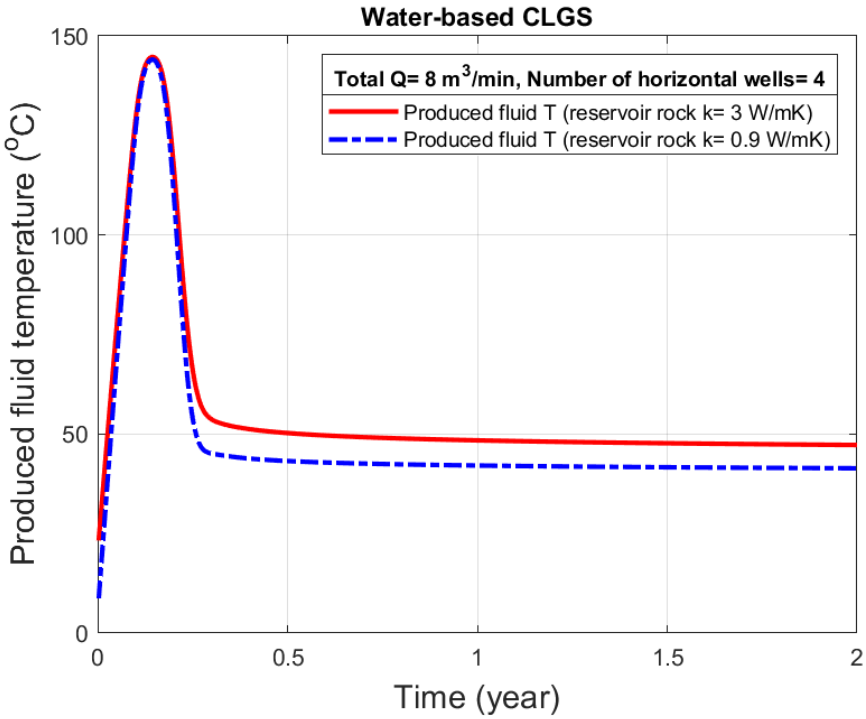

Figure 5.2: The difference between two water-based CLGSs with the assumption of two different thermal conductivity for the reservoir granite rock of 0.9 and 3 W/mK.

and 3 W/mK thermal conductivity. The difference in the produced fluid temperature is not significant.

5.4 Publications

In this section the list of peer-reviewed journal papers and conference articles emanated from this PhD research is given.

5.4.1 Journal papers

- **Ghavidel, A.**, Gracie, R., & Dusseault, M.B. (2021). Transient heat transfer in a horizontal well in hot dry rock–Model, solution, and response surfaces for practical inputs. *Applied Thermal Engineering*, 195, 117158.
- **Ghavidel, A.**, Gracie, R., & Dusseault, M.B. (2022). Design Parameter Impacting Electricity Generation From Horizontal Multilateral Closed-Loop Geothermal Systems in Hot Dry Rock. *Geothermics*.
- **Ghavidel, A.**, Dusseault, M.B., & Gracie, R. (2022). Energy From Horizontal Multilateral Closed Loop Geothermal Systems Using Supercritical CO_2 or Water. *Geothermics*.

5.4.2 Conference presentations

- **Ghavidel, A.**, Dusseault, M. B., & Gracie, R. (2021). Heat Production From Hot Dry Rocks Using Closed-Loop Horizontal Wells. *In 55th US Rock Mechanics/Geomechanics Symposium*. OnePetro.
- **Ghavidel, A.**, Dusseault, M. B., & Gracie, R. (2021). The Convective Heat Transfer Coefficient Effect on the Output Fluid Temperature From Enhanced Geothermal Systems. *In 55th US Rock Mechanics/Geomechanics Symposium*. OnePetro.
- **Ghavidel, A.**, Dusseault, M. B., & Gracie, R. (2020). Coupled Thermo-Hydro-Mechanical (THM) model for Geothermal Energy Extraction from Fractured Rock Masses, *GeoConvention*.

5.5 Future Works

The following potential topics are suggested for the extension and continuation of the research presented in this PhD dissertation:

- **Economically analyzing and optimizing the whole system, including drilling wells and surface facilities**. Economic analysis is one of the most important steps in studying the feasibility of different projects. Therefore, a full techno-economical study for such systems can be accomplished, making a comparison between different scenarios for the best option.

- **Extending the reservoir model presented in this research by adding the effects of porous media for assessing CLGS in sedimentary basins**. Sedimentary basin resources present a huge potential for geothermal energy due to a higher convective heat transfer rate (because of the presence of fluid) rather than purely slow conductive heat transfer in HDRs. Therefore, adding the effects of porous media to the existing reservoir model (fluid flow and heat transfer in porous media) allows for the assessment of sedimentary basin resources that may be more beneficial than HDRs in terms of heat and electrical power production.

- **Evaluating hybrid systems, coupling CLGS with other renewable resources, such as solar energy, wind, energy storage options, ground heat exchangers and pumps, etc.** Energy demand varies seasonally based on weather conditions in different locations. Therefore, extra demand or energy storage is necessary, especially in weather-dependent systems such as solar and wind. If CLGS can be integrated with other renewable resources based on the seasonal demands of different locations, the overall performance and flexibility of the whole system may increase significantly. The available results/model of the current study on CLGS can be integrated with any other model for further analysis to meet the requirements of different demand levels.

- **Optimization of ORC parameters for maximizing the electrical power production from CLGS with falling inlet and variable ambient temperatures.** Optimization techniques are commonly used for maximizing the output from power plants. However, they lack to consider the inlet and ambient temperatures simultaneously, which is commonly the case for geothermal systems. The available linked CLGS/ORC model in the current PhD research provides the opportunity to employ different optimization techniques, optimize the ORC parameters, and maximize electrical power production from ORC during winter and summer.

References

[1] Ali Ghavidel, Robert Gracie, and Maurice B. Dusseault. Transient heat transfer in a horizontal well in hot dry rock - model, solution, and response surfaces for practical inputs. *Applied Thermal Engineering*, pages 117–158., 2021.

[2] National Weather Service. The united state national weather service, 2021.

[3] Joseph Moore, John McLennan, Rick Allis, Kristine Pankow, Stuart Simmons, Robert Podgorney, Philip Wannamaker, and William Rickard. The utah frontier observatory for geothermal research (FORGE): results of recent drilling and geoscientific surveys. In *Geothermal Resources Council 42nd Annual Meeting-Geothermal Energy, GRC*, 2018.

[4] Benjamin K. Sovacool. How long will it take? Conceptualizing the temporal dynamics of energy transitions. *Energy Research & Social Science*, 13:202–215, March 2016.

[5] Ruth Shortall, Brynhildur Davidsdottir, and Guoni Axelsson. Geothermal energy for sustainable development: A review of sustainability impacts and assessment frameworks. *Renewable and Sustainable Energy Reviews*, 44:391–406, April 2015.

[6] Dolf Gielen, Francisco Boshell, Deger Saygin, Morgan D. Bazilian, Nicholas Wagner, and Ricardo Gorini. The role of renewable energy in the global energy transformation. *Energy Strategy Reviews*, 24:38–50, April 2019.

[7] Ruggero Bertani. Geothermal power generation in the world 2010–2014 update report. *Geothermics*, 60:31–43, 2016.

[8] Shu-Yuan Pan, Mengyao Gao, Kinjal J. Shah, Jianming Zheng, Si-Lu Pei, and Pen-Chi Chiang. Establishment of enhanced geothermal energy utilization plans: Barriers and strategies. *Renewable Energy*, 132:19–32, 2019.

[9] Marry H. Dickson and Mario Fanelli. *Geothermal Energy: Utilization and Technology.* UNESCO, 2013.

[10] John E. Mock, Jefferson W. Tester, and Michael P. Wright. Geothermal energy from the earth: its potential impact as an environmentally sustainable resource. *Annual review of Energy and the Environment*, 22(1):305–356, 1997.

[11] L. M. Edwards, George V. Chilingar, and Herman H. Rieke. *Handbook of Geothermal Energy.* Gulf Publishing Company, Houston, TX, USA, 1982.

[12] Pablo. Olasolo, M. C. Juarez, M. P. Morales, Sebastiano DAmico, and I. A. Liarte. Enhanced geothermal systems (EGS): A review. *Renewable and Sustainable Energy Reviews*, 56:133–144, April 2016.

[13] Ahmad Ghassemi, Sergejs Tarasovs, and Alexander H.D. Cheng. A 3-D study of the effects of thermomechanical loads on fracture slip in enhanced geothermal reservoirs. *International Journal of Rock Mechanics and Mining Sciences*, 44(8):1132–1148, December 2007.

[14] Ahmad Ghassemi and Xiaoxian Zhou. A three-dimensional thermo-poroelastic model for fracture response to injection/extraction in enhanced geothermal systems. *Geothermics*, 40(1):39–49, 2011.

[15] Saeed Salimzadeh, Adriana Paluszny, Hamidreza M. Nick, and Robert W. Zimmerman. A three-dimensional coupled thermo-hydro-mechanical model for deformable fractured geothermal systems. *Geothermics*, 71:212–224, January 2018.

[16] Bruce Gee, Robert Gracie, and Maurice B. Dusseault. Multiscale short-circuiting mechanisms in multiple fracture enhanced geothermal systems. *Geothermics*, 94:102094, 2021.

[17] Sachchida N. Pandey, Abhijit Chaudhuri, and Sharad Kelkar. A coupled thermo-hydro-mechanical modeling of fracture aperture alteration and reservoir deformation during heat extraction from a geothermal reservoir. *Geothermics*, 65:17–31, 2017.

[18] Bruce Gee and Robert Gracie. Comparison of fully-coupled and sequential solution methodologies for enhanced geothermal systems. *Computer Methods in Applied Mechanics and Engineering*, 373:113554, 2021.

[19] Xianzhi Song, Yu Shi, Gensheng Li, Ruiyue Yang, Gaosheng Wang, Rui Zheng, Jiacheng Li, and Zehao Lyu. Numerical simulation of heat extraction performance in

enhanced geothermal system with multilateral wells. *Applied Energy*, 218:325–337, 2018.

[20] Gaosheng Wang, Xianzhi Song, Yu Shi, Rui Zheng, Jiacheng Li, and Zhen Li. Production performance of a novel open loop geothermal system in a horizontal well. *Energy Conversion and Management*, 206:112478, 2020.

[21] Guodong Cui, Shaoran Ren, Liang Zhang, Justin Ezekiel, Chioma Enechukwu, Yi Wang, and Rui Zhang. Geothermal exploitation from hot dry rocks via recycling heat transmission fluid in a horizontal well. *Energy*, 128:366–377, 2017.

[22] Yi Wang, Liang Zhang, Guodong Cui, Jun Kang, and Shaoran Ren. Geothermal development and power generation by circulating water and isobutane via a closed-loop horizontal well from hot dry rocks. *Renewable Energy*, 136:909–922, 2019.

[23] Sven U. Schulz. *Investigations on the improvement of the energy output of a Closed Loop Geothermal System (CLGS).* PhD thesis, Technische University, Berlin (Germany), 2008.

[24] Maurice B. Dusseault. Coupled Processes and Petroleum Geomechanics. In Ove Stephanson, editor, *Elsevier Geo-Engineering Book Series*, volume 2 of *Coupled Thermo-Hydro-Mechanical-Chemical Processes in Geo-Systems*, pages 49–62. Elsevier, January 2004.

[25] Maurice B. Dusseault. Geomechanical challenges in petroleum reservoir exploitation. *KSCE Journal of Civil Engineering*, 15(4):669–678, April 2011.

[26] Yangsheng Zhao, Zijun Feng, Zengchao Feng, Dong Yang, and Weiguo Liang. THM (Thermo-hydro-mechanical) coupled mathematical model of fractured media and numerical simulation of a 3d enhanced geothermal system at 573K and buried depth 6000-7000M. *Energy*, 82:193–205, March 2015.

[27] Reza Safari and Ahmad Ghassemi. 3d thermo-poroelastic analysis of fracture network deformation and induced micro-seismicity in enhanced geothermal systems. *Geothermics*, 58:1–14, November 2015.

[28] Bin Guo, Pengcheng Fu, Yue Hao, Catherine A. Peters, and Charles R. Carrigan. Thermal drawdown-induced flow channeling in a single fracture in EGS. *Geothermics*, 61:46–62, May 2016.

[29] Qingfeng Tao and Ahmad Ghassemi. Poro-thermoelastic borehole stress analysis for determination of the in situ stress and rock strength. *Geothermics*, 39(3):250–259, September 2010.

[30] Ahmad Ghassemi. A review of some rock mechanics issues in geothermal reservoir development. *Geotechnical and Geological Engineering*, 30(3):647–664, June 2012.

[31] Lanru Jing. A review of techniques, advances and outstanding issues in numerical modelling for rock mechanics and rock engineering. *International Journal of Rock Mechanics and Mining Sciences*, 40(3):283–353, April 2003.

[32] Jahan Noorishad, Chin F. Tsang, and Paul A. Witherspoon. Theoretical and field studies of coupled hydromechanical behaviour of fractured rocks. development and verification of a numerical simulator. *International Journal of Rock Mechanics and Mining Sciences Geomechanics Abstracts*, 29(4):401–409, 1992.

[33] Jahan Noorishad and Chin F. Tsang. Coupled thermohydroelasticity phenomena in variably saturated fractured porous rocks - formulation and numerical solution. In Ove Stephansson, Lanru Jing, and Chin-Fu Tsang, editors, *Coupled Thermo-Hydro-Mechanical Processes of Fractured Media*, volume 79 of *Developments in Geotechnical Engineering*, pages 93–134. Elsevier, 1996.

[34] Lennart Borgesson, Masakazu Chijimatsu, Tomoo Fujita, Thanh S. Nguyen, Jonny Rutqvist, and Lanru Jing. Thermo-hydro-mechanical characterisation of a bentonite-based buffer material by laboratory tests and numerical back analyses. *International Journal of Rock Mechanics and Mining Sciences*, 38(1):95–104, 2001. Decovalex II.

[35] Thanh S. Nguyen, Lennart Borgesson, Masakazu Chijimatsu, Jonny Rutqvist, Tomoo Fujita, Jan Hernelind, Akira Kobayashi, Yuzo Ohnishi, Mieko Tanaka, and Lanru Jing. Hydro-mechanical response of a fractured granitic rock mass to excavation of a test pit - the kamaishi mine experiment in japan. *International Journal of Rock Mechanics and Mining Sciences*, 38(1):79–94, 2001. Decovalex II.

[36] Jonny Rutqvist, Lennart Borgesson, Masakazu Chijimatsu, Thanh S. Nguyen, Lanru Jing, Jahan Noorishad, and Chin F. Tsang. Coupled thermo-hydro-mechanical analysis of a heater test in fractured rock and bentonite at kamaishi mine — comparison of field results to predictions of four finite element codes. *International Journal of Rock Mechanics and Mining Sciences*, 38(1):129–142, 2001. Decovalex II.

[37] Jonny Rutqvist, Lennart Borgesson, Masakazu Chijimatsu, Akira Kobayashi, Lanru Jing, Thanh S. Nguyen, Jahan Noorishad, and Chin F. Tsang. Thermohydromechanics of partially saturated geological media: governing equations and formulation of four finite element models. *International Journal of Rock Mechanics and Mining Sciences*, 38(1):105–127, 2001. Decovalex II.

[38] Peter A. Cundall. Formulation of a three-dimensional distinct element model-part i. a scheme to detect and represent contacts in a system composed of many polyhedral blocks. *International Journal of Rock Mechanics and Mining Sciences Geomechanics Abstracts*, 25(3):107–116, 1988.

[39] John R. Williams and Alex P. Pentland. Superquadrics and modal dynamics for discrete elements in interactive design. *Engineering Computations*, February 1992.

[40] John R. Williams and R O'Connor. A linear complexity intersection algorithm for discrete element simulation of arbitrary geometries. *Engineering Computations*, February 1995.

[41] J. C. S. Long, J. S. Remer, C. R. Wilson, and P. A. Witherspoon. Porous media equivalents for networks of discontinuous fractures. *Water Resources Research*, 18(3):645–658, 1982.

[42] William S. Dershowitz and Herbert H. Einstein. Three Dimensional Flow Modeling In Jointed Rock Masses. International Society for Rock Mechanics and Rock Engineering, January 1987.

[43] Olgierd Cecil Zienkiewicz, Robert L. Taylor, Perumal Nithiarasu, and J. Z. Zhu. *The finite element method*, volume 3. McGraw-hill London, 1977.

[44] Matthias Bruhn. Hybrid geothermal-fossil electricity generation from low enthalpy geothermal resources: geothermal feedwater preheating in conventional power plants. *Energy*, 27(4):329–346, April 2002.

[45] Cesar R. Chamorro, Maria E. Mondejar, Roberto Ramos, Jose J. Segovia, Maria C. Martin, and Miguel A. Villamanan. World geothermal power production status: Energy, environmental and economic study of high enthalpy technologies. *Energy*, 42(1):10–18, June 2012.

[46] Enrico Barbier. Geothermal energy technology and current status: an overview. *Renewable and sustainable energy reviews*, 6(1-2):3–65, 2002.

[47] Ronald DiPippo. *Geothermal power plants: principles, applications, case studies and environmental impact*. Butterworth-Heinemann, 2012.

[48] Ronald DiPippo. Second Law assessment of binary plants generating power from low-temperature geothermal fluids. *Geothermics*, 33(5):565–586, October 2004.

[49] Ronald DiPippo. Geothermal energy Electricity generation and environmental impact. *Energy Policy*, 19(8):798–807, October 1991.

[50] Mohammed Khennich and Nicolas Galanis. Optimal Design of ORC Systems with a Low-Temperature Heat Source. *Entropy*, 14(2):370–389, February 2012.

[51] Alessandro Franco. Power production from a moderate temperature geothermal resource with regenerative Organic Rankine Cycles. *Energy for Sustainable Development*, 15(4):411–419, December 2011.

[52] Junjiang Bao and Li Zhao. *Renewable and Sustainable Energy Reviews*, 24:325–342, 2013.

[53] Alexander I. Kalina and Hank M. Leibowitz. Application of the kalina cycle technology to geothermal power generation. volume 13, pages 605–611, 1989.

[54] Henry A. Micak. An introduction to the Kalina cycle. December 1996.

[55] Xinxin Zhang, Maogang He, and Ying Zhang. A review of research on the Kalina cycle. *Renewable and Sustainable Energy Reviews*, 16(7):5309–5318, September 2012.

[56] Yunus A. Cengel and Michael A. Boles. Thermodynamics: an engineering approach. *Sea*, 1000:8862, 2002.

[57] Pall Valdimarsson. Geothermal power plant cycles and main components. *Short course on geothermal drilling, resource development and power plants*, pages 16–22, 2011.

[58] Diego Moya, Clay Aldas, and Prasad Kaparaju. Geothermal energy: Power plant technology and direct heat applications. *Renewable and Sustainable Energy Reviews*, 94:889–901, October 2018.

[59] Dariusz Mikielewicz and Jarosław Mikielewicz. A thermodynamic criterion for selection of working fluid for subcritical and supercritical domestic micro CHP. *Applied Thermal Engineering*, 30(16):2357–2362, November 2010.

[60] Sylvain Quoilin, Sebastien Declaye, Arnaud Legros, Ludovic Guillaume, and Vincent Lemort. Working fluid selection and operating maps for Organic Rankine Cycle expansion machines. 2012.

[61] Xianzhi Song, Yu Shi, Gensheng Li, Zhonghou Shen, Xiaodong Hu, Zehao Lyu, Rui Zheng, and Gaosheng Wang. Numerical analysis of the heat production performance of a closed loop geothermal system. *Renewable Energy*, 120:365–378, 2018.

[62] Koenraad F. Beckers, Nicolás Rangel-Jurado, Harish Chandrasekar, Adam J. Hawkins, Patrick M. Fulton, and Jefferson W. Tester. Techno-economic performance of closed-loop geothermal systems for heat production and electricity generation. *Geothermics*, 100:102318, 2022.

[63] JD Van Wees. draft eavor loop audit report. Technical report, 2021.

[64] Ronald DiPippo. Chapter 8 - binary cycle power plants. In Ronald DiPippo, editor, *Geothermal Power Plants*, pages 163–196. Elsevier Science, Oxford, 2005.

[65] Vase1 W. Roberts. Geothermal energy prospects for the next 50 years. Technical Report EPRI-ER-611-SR, Electric Power Research Institute (EPRI), Palo Alto, California. (USA), 1978.

[66] J C. Rowley. *Worldwide geothermal resources*. Gulf Publishing Company, Houston, TX, USA, 1982.

[67] Valgardur Stefansson. World geothermal assessment. In *Proceedings of the World Geothermal Congress*, volume 5, pages 1–6. International Geothermal Association Antalya, Turkey, 2005.

[68] Jefferson W. Tester. *Sustainable Energy: choosing among options*. The MIT Press, Cambridge, England, 2005.

[69] Shyi-Min Lu. A global review of enhanced geothermal system (egs). *Renewable and Sustainable Energy Reviews*, 81:2902–2921, 2018.

[70] John W. Lund, Derek H. Freeston, and Tonya L. Boyd. Direct utilization of geothermal energy 2010 worldwide review. *Geothermics*, 40(3):159–180, 2011.

[71] John W. Lund and Tonya L. Boyd. Direct utilization of geothermal energy 2015 worldwide review. *Geothermics*, 60:66–93, 2016.

[72] Johan Claesson and Per Eskilson. Conductive heat extraction to a deep borehole: Thermal analyses and dimensioning rules. *Energy*, 13(6):509–527, 1988.

[73] Goran A.J. Hellstrom. Ground heat storage: Thermal analyses of duct storage systems. i. theory. *Department Of Mathematical Physics, Lund Institute Of Technology, Sweden.*, 1992.

[74] Neal D. Paul. *The effect of grout thermal conductivity on vertical geothermal heat exchanger design and performance*. PhD thesis, Mechanical Engineering Department, South Dakota State University, 1996.

[75] Yian Gu and Dennis L. O'Neal. Development of an equivalent diameter expression for vertical u-tubes used in ground-coupled heat pumps. *Transaction-American Society of Heating Refrigerating and Air Conditioning Engineers*, 104:347–355, 1998.

[76] Hui Wang, Chen An, Menglan Duan, and Jian Su. Transient thermal analysis of multilayer pipeline with phase change material. *Applied Thermal Engineering*, 165:114512, 2020.

[77] Seyed Ali Ghoreishi-Madiseh, Ali Fahrettin Kuyuk, and Marco Antonio. An analytical model for transient heat transfer in ground-coupled heat exchangers of closed-loop geothermal systems. *Applied Thermal Engineering*, 150:696–705, 2019.

[78] Younes Noorollahi, Reza Saeidi, Mohammad Mohammadi, Ali Amiri, and Mehdi Hosseinzadeh. The effects of ground heat exchanger parameters changes on geothermal heat pump performance - a review. *Applied Thermal Engineering*, 129:1645–1658, 2018.

[79] Krzysztof Kupiec, Barbara Larwa, and Monika Gwadera. Heat transfer in horizontal ground heat exchangers. *Applied Thermal Engineering*, 75:270–276, 2015.

[80] Georgios Florides and Soteris Kalogirou. Ground heat exchangers - a review of systems, models and applications. *Renewable Energy*, 32(15):2461–2478, 2007.

[81] Yi Man, Hongxing Yang, Nairen Diao, Junhong Liu, and Zhaohong Fang. A new model and analytical solutions for borehole and pile ground heat exchangers. *International Journal of Heat and Mass Transfer*, 53(13):2593–2601, 2010.

[82] Ping Cui, Xin Li, Yi Man, and Zhaohong Fang. Heat transfer analysis of pile geothermal heat exchangers with spiral coils. *Applied Energy*, 88(11):4113–4119, 2011.

[83] Min Li and Alvin C.K. Lai. New temperature response functions (g functions) for pile and borehole ground heat exchangers based on composite-medium line-source theory. *Energy*, 38(1):255–263, 2012.

[84] Angelo Zarrella, Michele, and Antonio Galgaro. Thermal performance of two types of energy foundation pile: Helical pipe and triple u-tube. *Applied Thermal Engineering*, 61(2):301–310, 2013.

[85] Hossein Javadi, Seyed Soheil, Mohsen Pourfallah, and Mohammad Zaboli. Performance analysis of helical ground heat exchangers with different configurations. *Applied Thermal Engineering*, 154:24–36, 2019.

[86] Behrad Asgari, Mohammad Habibi, and Ali Hakkaki-Fard. Assessment and comparison of different arrangements of horizontal ground heat exchangers for high energy required applications. *Applied Thermal Engineering*, 167:114770, 2020.

[87] Arny Leroy and Michel Bernier. Development of a novel spiral coil ground heat exchanger model considering axial effects. *Applied Thermal Engineering*, 84:409–419, 2015.

[88] Min Li and Alvin C.K. Lai. Review of analytical models for heat transfer by vertical ground heat exchangers (ghes): A perspective of time and space scales. *Applied Energy*, 151:178–191, 2015.

[89] Mikael Philippe, Michel Bernier, and Dominique Marchio. Validity ranges of three analytical solutions to heat transfer in the vicinity of single boreholes. *Geothermics*, 38(4):407–413, 2009.

[90] Bruce Gee, Robert Gracie, and Maurice B. Dusseault. Multiscale short-circuiting mechanisms in multiple fracture enhanced geothermal systems. *Geothermics*, 94:102094, 2021.

[91] B.X. Wang and X.F. Peng. Experimental investigation on liquid forced-convection heat transfer through microchannels. *International Journal of Heat and Mass Transfer*, 37:73–82, 1994.

[92] Eugene C. Robertson. Thermal properties of rocks. Technical report, US Department of the Interior, Geological Survey Reston, Va, 1988.

[93] Won J. Cho, Sangki Kwon, and Jongwon Choi. The thermal conductivity for granite with various water contents. *Engineering Geology*, 107(3):167–171, 2009.

[94] Jean Cote and Jean M. Konrad. A generalized thermal conductivity model for soils and construction materials. *Canadian Geotechnical Journal*, 42(2):443–458, 2005.

[95] Won-Jin Cho and Sangki Kwon. Estimation of the thermal properties for partially saturated granite. *Engineering Geology*, 115(1):132–138, 2010.

[96] Michael A. Kant, Jens Ammann, Edoardo Rossi, Claudio Madonna, Dragana Hoser, and Philipp Rudolf von Rohr. Thermal properties of central aare granite for temperatures up to 500C: irreversible changes due to thermal crack formation. *Geophysical Research Letters*, 44(2):771–776, 2017.

[97] Jin Kim, Yin Lee, and Ma Koo. Thermal properties of granite from korea. *American Geophysical Union*, pages T11B–0576, 2007.

[98] M M. Miranda, C R. Matos, N V. Rodrigues, A J.S.C. Pereira, and J J. Costa. Effect of temperature on the thermal conductivity of a granite with high heat production from central portugal. *Journal of Iberian Geology*, 45(1):147–161, 2019.

[99] Christoph Clauser and Ernst Huenges. Thermal conductivity of rocks and minerals. *Rock Physics and Phase Relations: A Handbook of Physical Constants*, pages 105–126, 1995.

[100] Yuri Popov, Vladimir Tertychnyi, Raisa Romushkevich, Dmitri Korobkov, and Jean Pohl. *Interrelations Between Thermal Conductivity and Other Physical Properties of Rocks: Experimental Data*, pages 1137–1161. Birkhauser Basel, Basel, 2003.

[101] Fabrice Surma and Yves Geraud. Porosity and thermal conductivity of the soultz-sous-forêts granite. *Pure and Applied Geophysics*, 160(5-6):1125–1136, 2003.

[102] Hirofumi Sato and Fumio Hirata. Ab initio study on molecular and thermodynamic properties of water: A theoretical prediction of pkw over a wide range of temperature and density. *The Journal of Physical Chemistry B*, 103(31):6596–6604, 1999.

[103] Stuart D.C. Walsh, Nagasree Garapati, Allan M.M. Leal, and Martin O. Saar. Calculating thermophysical fluid properties during geothermal energy production with ness and reaktoro. *Geothermics*, 70:146–154, 2017.

[104] Abhijit Ramalingam and Sinnaswamy Arumugam. Experimental study on specific heat of hot brine for salt gradient solar pond application. *International Journal of ChemTech Research*, 4(3):956–961, 2012.

[105] Theodore L. Bergman, Frank P. Incropera, Adrienne S. Lavine, and David P. Dewitt. *Introduction to Heat Transfer*. John Wiley & Sons Inc., New York, USA., 2011.

[106] Dave Duchane and Don Brown. Hot dry rock (HDR) geothermal energy research and development at Fenton Hill, new mexico. *Geo-Heat Centre Quarterly Bulletin, CiteSeer*, 23(12):13–19, 2002.

[107] EAVOR Technologies. EAVOR Technologies Inc, 2020.

[108] Wilfred A. Elders and Joseph N. Moore. 2 - geology of geothermal resources. In Ronald DiPippo, editor, *Geothermal Power Generation*, pages 7–32. Woodhead Publishing, 2016.

[109] Simon Weides and Jacek Majorowicz. Implications of spatial variability in heat flow for geothermal resource evaluation in large foreland basins: The case of the western canada sedimentary basin. *Energies*, 7(4):2573–2594, 2014.

[110] William E Glassley. *Geothermal energy: renewable energy and the environment*. CRC press, 2014.

[111] Horatio Scott Carslaw and John Conrad Jaeger. Conduction of heat in solids. Technical report, Clarendon Press,, 1959.

[112] Lee R. Raymond. Temperature Distribution in a Circulating Drilling Fluid. *Journal of Petroleum Technology*, 21(03):333–341, 03 1969.

[113] A F. Van Everdingen and William Hurst. The Application of the Laplace Transformation to Flow Problems in Reservoirs. *Journal of Petroleum Technology*, 1(12):305–324, 12 1949.

[114] Henry J. Ramey. Wellbore Heat Transmission. *Journal of Petroleum Technology*, 14(04):427–435, 04 1962.

[115] JC Jaeger and Tilly Chamalaun. Heat flow in an infinite region bounded internally by a circular cylinder with forced convection at the surface. *Australian Journal of Physics*, 19(4):475–488, 1966.

[116] Koenraad F Beckers, Donald L Koch, and Jefferson W Tester. Slender-body theory for transient heat conduction: theoretical basis, numerical implementation and case studies. *Proceedings of the Royal Society A: Mathematical, Physical and Engineering Sciences*, 471(2184):20150494, 2015.

[117] Yuyang Liu, Yu Rao, and Li Yang. Numerical simulations of a double-wall cooling with internal jet impingement and external hexagonal arrangement of film cooling holes. *International Journal of Thermal Sciences*, 153:106337, 2020.

[118] Enrique Gabriel Vera, Claudio Canizares, and Mehrdad Pirnia. Renewable energy integration in canadian remote community microgrids: The feasibility of hydrogen and gas generation. *IEEE Electrification Magazine*, 8(4):36–45, 2020.

[119] Hashem Elsaraf, Mohsin Jamil, and Bishwajeet Pandey. Techno-economic design of a combined heat and power microgrid for a remote community in newfoundland canada. *IEEE Access*, 9:91548–91563, 2021.

[120] Essam A. Al-Ammar, Habib Ur Rahman Habib, Kotb M. Kotb, Shaorong Wang, Wonsuk Ko, Mahmoud F. Elmorshedy, and Asad Waqar. Residential community load management based on optimal design of standalone hres with model predictive control. *IEEE Access*, 8:12542–12572, 2020.

[121] Lewis F Moody. Friction factors for pipe flow. *Trans. Asme*, 66:671–684, 1944.

[122] Cyril Frank Colebrook, T Blench, H Chatley, EH Essex, JR Finniecome, G Lacey, J Williamson, and GG Macdonald. Correspondence. turbulent flow in pipes, with particular reference to the transition region between the smooth and rough pipe laws (includes plates). *Journal of the Institution of Civil engineers*, 12(8):393–422, 1939.

[123] Maurice Stewart. 4 - piping system components. In Maurice Stewart, editor, *Surface Production Operations*, pages 193–300. Gulf Professional Publishing, Boston, 2016.

[124] Hoss Belyadi, Ebrahim Fathi, and Fatemeh Belyadi. Chapter eight - hydraulic fracturing chemical selection and design. In Hoss Belyadi, Ebrahim Fathi, and Fatemeh Belyadi, editors, *Hydraulic Fracturing in Unconventional Reservoirs*, pages 107–120. Gulf Professional Publishing, Boston, 2017.

[125] William C. Lyons. *Air and gas drilling manual: applications for oil and gas recovery wells and geothermal fluids recovery wells*. Elsevier, 2009.

[126] Jasmine Ramsebner, Reinhard Haas, Amela Ajanovic, and Martin Wietschel. The sector coupling concept: A critical review. *Wiley Interdisciplinary Reviews: Energy and Environment*, 10(4):e396, 2021.

[127] Festus Fatai Adedoyin, Ilhan Ozturk, Mary Oluwatoyin Agboola, Phillips O. Agboola, and Festus Victor Bekun. The implications of renewable and non-renewable

energy generating in sub-saharan africa: The role of economic policy uncertainties. *Energy Policy*, 150:112115, 2021.

[128] Xiaohui Sun, Zhiyuan Wang, Youqiang Liao, Baojiang Sun, and Yonghai Gao. Geothermal energy production utilizing a u-shaped well in combination with supercritical co2 circulation. *Applied Thermal Engineering*, 151:523–535, 2019.

[129] Ali Ghavidel, Robert Gracie, and Maurice B. Dusseault. Design parameter impacting electricity generation from horizontal multilateral closed-loop geothermal systems in hot dry rock. *Geothermics*, 2022.

[130] Donald W. Brown. A hot dry rock geothermal energy concept utilizing supercritical CO2 instead of water. In *Proceedings of the twenty-fifth workshop on geothermal reservoir engineering, Stanford University*, pages 233–238, 2000.

[131] Aleks D. Atrens, Hal Gurgenci, and Victor Rudolph. Electricity generation using a carbon-dioxide thermosiphon. *Geothermics*, 39(2):161–169, 2010.

[132] Fengrui Sun, Yuedong Yao, Guozhen Li, and Xiangfang Li. Geothermal energy extraction in co2 rich basin using abandoned horizontal wells. *Energy*, 158:760–773, 2018.

[133] Xiaohui Sun, Youqiang Liao, Zhiyuan Wang, and Baojiang Sun. Geothermal exploitation by circulating supercritical co2 in a closed horizontal wellbore. *Fuel*, 254:115566, 2019.

[134] Guodong Cui, Liang Zhang, Chunyang Tan, Shaoran Ren, Yuan Zhuang, and Chioma Enechukwu. Injection of supercritical $CO_2 for geothermal exploitation from sandstone and carbonate reservoirs : CO_2 - water - rock interactions and their effects. Journal of CO_2 Utilization, 20 : 113 - -128, 2017.$

[135] Benjamin M. Adams, Thomas H. Kuehn, Jeffrey M. Bielicki, Jimmy B. Randolph, and Martin O. Saar. On the importance of the thermosiphon effect in CPG $(CO_2 plume geothermal) power systems. Energy, 69 : 409 - -418, 2014.$

[136] Benjamin M. Adams, Thomas H. Kuehn, Jeffrey M. Bielicki, Jimmy B. Randolph, and Martin O. Saar. A comparison of electric power output of co2 plume geothermal (cpg) and brine geothermal systems for varying reservoir conditions. *Applied Energy*, 140:365–377, 2015.

[137] Andrew J. Luhmann, Xiang-Zhao Kong, Benjamin M. Tutolo, Nagasree Garapati, Brian C. Bagley, Martin O. Saar, and William E. Seyfried. Experimental dissolution of dolomite by $CO_2 - chargedbrineat100Cand150bar : Evolutionofporosity, permeability, andreactivesurfacearea.ChemicalGeology, 380 : 145 - -160, 2014.$

[138] Yunus A. Cengel and John Cimbala. *Fluid Mechanics: Fundamentals And Applications (Si Units).* Tata McGraw Hill Education Private Limited, 2010.

[139] A.R.D. Thorley and C.H. Tiley. Unsteady and transient flow of compressible fluids in pipelines - a review of theoretical and some experimental studies. *International Journal of Heat and Fluid Flow*, 8(1):3–15, 1987.

[140] Jurjen K. Van Deen and Sip R. Reintsema. Modelling of high-pressure gas transmission lines. *Applied Mathematical Modelling*, 7(4):268–273, 1983.

[141] Raad I. Issa and Dudley B. Spalding. Unsteady one-dimensional compressible frictional flow with heat transfer. *Journal of Mechanical Engineering Science*, 14(6):365–369, 1972.

[142] C Bisgaard, H H. Sorensen, and S Spangenberg. A finite element method for transient compressible flow in pipelines. *International journal for numerical methods in fluids*, 7(3):291–303, 1987.

[143] John D. Anderson. Governing equations of fluid dynamics. In *Computational fluid dynamics*, chapter 2, pages 15–51. Springer, 1992.

[144] Zengyuan Guo and Xiaobo Wu. Compressibility effect on the gas flow and heat transfer in a microtube. *International Journal of Heat and Mass Transfer*, 40(13):3251–3254, 1997.

[145] Marco Cavazzuti, Mauro A. Corticelli, and Tassos G. Karayiannis. Velocity profile development and friction in compressible micro-flows. In *AIP Conference Proceedings*, volume 2191, page 20042. AIP Publishing LLC, 2019.

[146] Gideon P. Greyvenstein. An implicit method for the analysis of transient flows in pipe networks. *International journal for numerical methods in engineering*, 53(5):1127–1143, 2002.

[147] Zengyuan Guo and Xiaobo Wu. Further study on compressibility effects on the gas flow and heat transfer in a microtube. *Microscale Thermophysical Engineering*, 2(2):111–120, 1998.

[148] Ning H. Chen. An explicit equation for friction factor in pipe. *Industrial & Engineering Chemistry Fundamentals*, 18(3):296–297, 1979.

[149] Norbert Bottcher, Ashok K. Singh, Olaf Kolditz, and Rudolf Liedl. Non-isothermal, compressible gas flow for the simulation of an enhanced gas recovery application. *Journal of Computational and Applied Mathematics*, 236(18):4933–4943, 2012. FEMTEC 2011: 3rd International Conference on Computational Methods in Engineering and Science, May 9–13, 2011.

[150] Koji Fukagata, Nobuhide Kasagi, Poychat Ua-arayaporn, and Takehiro Himeno. Numerical simulation of gas–liquid two-phase flow and convective heat transfer in a micro tube. *International Journal of Heat and Fluid Flow*, 28(1):72–82, 2007. The International Conference on Heat Transfer and Fluid Flow in Microscale (HTFFM-05).

[151] Stephen E. Grasby, A. Jessop, M. Kelman, M. Ko, Z. Chen, D.M. Allen, S. Bell, G. Ferguson, J. Majorowicz, M. Moore, et al. Geothermal energy resource potential of Canada. Technical report, 2012.

[152] Podugu Nagaraju and Sukanta Roy. Effect of water saturation on rock thermal conductivity measurements. *Tectonophysics*, 626:137–143, 2014.

[153] Antonion T. Settari and Dale A. Walters. Advances in Coupled Geomechanical and Reservoir Modeling With Applications to Reservoir Compaction. *SPE Journal*, 6(03):334–342, September 2001.

[154] Rick H. Dean, Xiuli Gai, Charles M. Stone, and Susan E. Minkoff. A Comparison of Techniques for Coupling Porous Flow and Geomechanics. *SPE Journal*, 11(01):132–140, March 2006.

[155] Hou Shaobo, Zhongjin Zhang, Zhongzhou Huang, and Aixia Xie. Performance optimization of solar multi-stage flash desalination process using Pinch technology. *Desalination*, 220(1):524–530, March 2008.

[156] Chiara Piccolo and Fabrizio Bezzo. A techno-economic comparison between two technologies for bioethanol production from lignocellulose. *Biomass and Bioenergy*, 33(3):478–491, March 2009.

[157] C.P. Jawahar, Balakrishnan Raja, and Rajagopal Saravanan. Thermodynamic studies on nh3–h2o absorption cooling system using pinch point approach. *International Journal of Refrigeration*, 33(7):1377–1385, 2010.

APPENDICES

Appendix A

Numerical Solution Strategy

A.1 Numerical Solution Strategy

Strategies for solving coupled processes are typically classified into four groups: fully coupled, iteratively coupled, explicitly coupled, and loosely coupled [153, 154].

In fully coupled approach, the governing coupled equations are solved simultaneously at every time step. This approach is unconditionally stable; however, nonlinear problems (and high-order time approximations) present challenges. Moreover, it might be computationally expensive.

In iteratively coupled (sequential) method, each governing equation is solved separately, in order, at every time step. Either the thermal, flow, or mechanical part could be solved first, and using the results of the previous part, the next part is solved. This iterative process is repeated at each time step until the results converge within an acceptable tolerance; it then proceeds to the next time step.

Staggered (single-pass sequential) approach works similar to the iteratively coupled approach except that only one iteration happens at every time step. This approach can save time but is not accurate.

In loosely coupled approach, one part of the coupled process is solved after a certain number of time steps, while the other parts are solved at every time step. This approach is useful for problems on which effects of one part is negligible in the short term, e.g., THM process in an enhanced geothermal system (EGS) reservoir, where conductive heat transfer in the rock matrix occurs much slower than convective heat transfer in the fluid domain. Therefore, conductive thermal effects in the rock matrix are negligible with respect to the

stress/strain change at each time step, if time steps are small. Thus, the temperature change in the rock matrix could update the mechanical part after a certain number of time steps, while other governing equations must be solved at every time step. This approach is capable of saving computational time; however, it presents a less accurate solution and needs a reliable estimation of the number of time steps for which the mechanical part should be updated.

In this study, iteratively coupled (sequential) approach is applied to solve the equation sets for heat transfer processes for the fluid and rock mass, and SIMPLE approach is used to solve pipe flow (pressure and velocity).

A.2 Organic Rankine Cycle Model

Figure A.1 illustrates an ideal Rankine cycle, along with its components and the temperature-entropy (T-s) diagram. The components include a turbine, condenser, pump, and evaporator (heat exchanger).

Generally, the binary Rankine cycle comprises four main processes on the working fluid between every two thermodynamic states as follows: 1-2: Adiabatic expansion in the turbine 2-3: Constant-pressure heat rejection in the condenser 3-4: Adiabatic compression in the pump 4-1: Constant-pressure heat addition in the heat exchanger (preheater and evaporator).

In the Rankine cycle, the high temperature and pressure working fluid enters the turbine at state 1 as saturated vapor or superheated vapor. The working fluid expands isentropically and produces work by rotating the turbine, which is connected to a generator to produce electricity. The temperature and pressure of the working fluid drop in an isentropic process to reach state 2, as it passes through the turbine. Then, the vapor enters the condenser and is condensed under constant pressure through the heat being released to the environment. The working fluid output from the condenser reaches state 3 as a saturated liquid. At this state, the saturated liquid enters the pump and is compressed in a constant entropy to the operating pressure of the evaporator. The saturated liquid at state 4 passes through the evaporator, where its entropy increases by absorbing heat from a hot geothermal fluid under constant pressure to reaches state 1 as a saturated vapor and complete the cycle [47, 57].

The conservation of mass and energy are applied based on the first and second laws of thermodynamics, to working fluid passing through all the components. The turbine and the pump are assumed to work in irreversible adiabatic processes. The heat exchangers

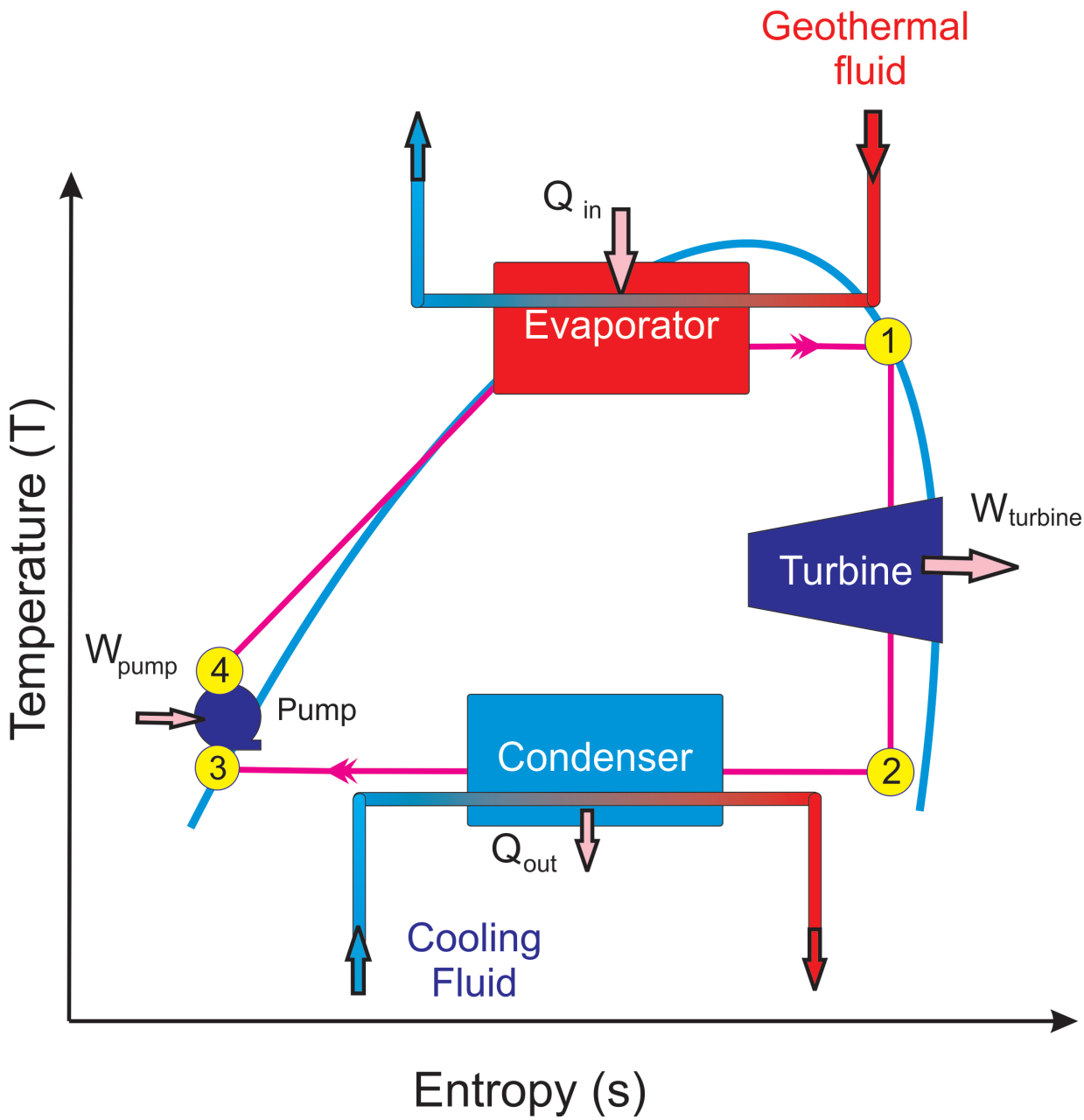

Figure A.1: Schematic diagram of an ideal Rankine cycle (T-s diagram and components).

Table A.1: Symbols used for ORC model

Properties Name	**Symbol**	**Properties Name**	**Symbol**
Turbine	tur	Outlet	out
Generator	gen	Inlet	in
Condenser	$cond$	Mass flow rate	$\dot{m}$
Evaporator	$evap$	Enthalpy	h
Pump	$pump$	Outlet work	$\dot{W}$
Working fluid	wf	Efficiency	η
Cooling fluid	cf	Specific heat	c_p
Geothermal fluid	gf	Heat transfer rate	$\dot{Q}$

are considered to no work and to be well insulated, i.e., no heat transfer occurs with the surrounding area (adiabatic processes). The kinetic and potential energy changes are ignored in the analysis because they are small in comparison to the work and heat transfer terms. It is also assumed that all components work under steady state condition.

The processes and assumptions made in the analysis of the components are explained in the following. Subscripts in numbers indicate different states of the working fluid at the inlet/outlet of each component, as shown in Figure A.1, and other subscripts stands for the name of components. All symbols are listed in Table A.1.

Turbine: The turbine converts the energy of the working fluid into the mechanical work on the turbine shaft connected to a generator, where electricity is generated. Turbines are basically designed to operate in the superheated zone to avoid the erosion caused by the presence of possible water droplets causing damage on turbine blades, which may require urgent and expensive repair or replacement. As shown in Figure A.2, in the ideal Rankine cycle, the turbine works in an isentropic process from point 1 (turbine inlet) to point 2s (turbine exit). However, in a real turbine, vapor enthalpy changes in response to turbine efficiency (state 2), i.e., it is an irreversible process. The efficiency, conservation of energy and mass in the turbine are as follows [47].

$$\dot{m}_1 = \dot{m}_2 = \dot{m}_{wf} \tag{A.1}$$

$$\eta_{tur} = (h_1 - h_2)/(h_1 - h_{2s}) \tag{A.2}$$

$$\dot{W}_{tur} = \dot{m}_{wf}(h_1 - h_2) = \dot{m}_{wf}\eta_{tur}(h_1 - h_{2s}) \tag{A.3}$$

$$\dot{W}_{gen} = \eta_{gen}\dot{W}_{tur} \tag{A.4}$$

Condenser: The condenser is a type of heat exchanger, in which the heat is released from the working fluid (vapor) to the environment (or another cooling fluid) at constant pressure (isobaric condensation). Heat rejection through the condenser, i.e., cooling of the binary cycle power plants, can be done by water or air, called wet and dry cooling systems, respectively. As seen in Figure A.1, the saturated vapor, leaving the turbine at state 2, enters the condenser, and reaches its dew point inside the condenser. Then, it starts condensing and leaves the condenser as a saturated liquid at state 3. The conservation of mass and energy in the condenser are as follows [47]

$$\dot{m}_2 = \dot{m}_3 = \dot{m}_{wf} \tag{A.5}$$

$$\dot{m}_{wf}(h_2 - h_3) = \dot{m}_{cf}(h_{out-cf} - h_{in-cf}) \tag{A.6}$$

If the cooling fluid is considered as being at a constant specific heat for the small temperature range between the inlet and outlet, Equation A.6 can be written as

$$\dot{m}_{wf}(h_2 - h_3) = \dot{m}_{cf}c_{p-cf}(T_{out-cf} - T_{in-cf}) \tag{A.7}$$

Assuming no work in the condenser, the amount of heat transfer in the condenser is given by

$$\dot{Q}_{out-cond} = \dot{Q}_{23} = \dot{m}_{wf}(h_2 - h_3) = \dot{m}_{cf}(h_{out-cf} - h_{in-cf}) \tag{A.8}$$

Pump: The pump receives the saturated liquid leaving the condenser at state 3 and compresses it at a constant entropy (i.e., isentropic process) to the evaporator operating pressure (state 4s). However, in a real system, irreversibility is taken into account, so the process is not isentropic. Therefore, as shown in Figure A.2, the compressed liquid leaving the pump reaches state 4 instead of state 4s. The conservation of mass and energy and the efficiency of the pump are defined as [47]

$$\dot{m}_3 = \dot{m}_4 = \dot{m}_{wf} \tag{A.9}$$

$$\eta_{pump} = (h_{4s} - h_3)/(h_4 - h_3) \tag{A.10}$$

$$\dot{W}_{pump} = \dot{m}_{wf}(h_{4s} - h_3) = \dot{m}_{wf}\eta_{pump}(h_4 - h_3) \tag{A.11}$$

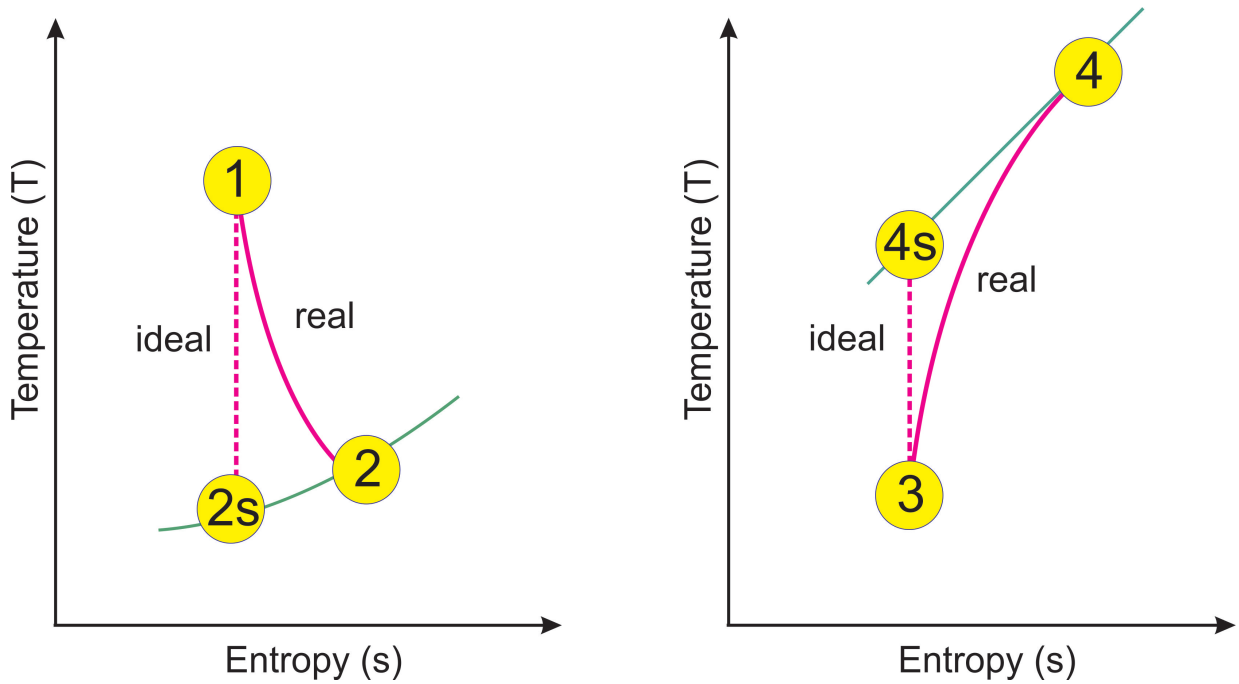

Figure A.2: Isentropic and real work of turbine and pump.

Evaporator: The evaporator act as a heat exchanger, receiving heat from the high temperature geothermal or circulating fluid in the reservoir in the primary cycle and transferring it to the working fluid in the secondary cycle. It is assumed that the evaporator work in an isobaric process, and no work is involved in the process.

In the Rankine cycle, the working fluid enters the evaporator at state 4 and receives heat from hot geothermal fluid. It then leaves the evaporator at state 1. The condition at state 1 is determined by the cycle and the turbine requirements; this state for ORC is the saturated or slightly superheated vapor. The balance equation in the heat exchanger is written as [47]

$$\dot{m}_4 = \dot{m}_1 = \dot{m}_{wf} \tag{A.12}$$

$$\dot{m}_{wf}(h_1 - h_4) = \dot{m}_{gf}(h_{in-gf} - h_{out-gf}) \tag{A.13}$$

If the specific heat of the geofluid is assumed to be known and constant for a small temperature range from the inlet to outlet (in other words, if the geofluid is incompressible like water and has low dissolved gas and solid levels, i.e., one phase) the temperature difference can be replaced by the enthalpy changes in the conservation of energy equation [47].

$$\dot{m}_{wf}(h_1 - h_4) = \dot{m}_{gf}c_{p-gf}(T_{in-gf} - T_{out-gf}) \tag{A.14}$$

Assuming no work in evaporator, the amount of heat transfer is given by

$$\dot{Q}_{in-evap} = \dot{Q}_{41} = \dot{m}_{wf}(h_1 - h_4) = \dot{m}_{gf}(h_{in-gf} - h_{out-gf}) \tag{A.15}$$

In this study, the evaporator (heat exchanger) is assumed to be comprised of two sections: a preheater and rest of the evaporator. The function of the preheater is to provide sufficient heat to raise the working fluid temperature to its boiling point. The evaporator can be designed using the temperature-heat transfer (T-q diagram) (Figure A.3). The preheater section increases the working fluid temperature to the boiling point or saturated liquid state. The working fluid continues heating up to reach saturated vapor state or a slightly superheated zone as it passes through the rest of evaporator in a phase change process. The amount of heat transfer in the preheater section and evaporator can be calculated separately by the means of the T-q diagram. Figure A.3 illustrates the heat transfer and temperature change processes in the preheater and evaporator. The minimum temperature difference between the circulating fluid and the working fluid, known as the pinch-point temperature difference (ΔT_{pp}), is a parameter determined by manufacturer specifications. The pinch-point value is helpful to determine required working fluid pressure and temperature. The pinch point temperature difference is commonly considered 2-10 ^oC in the literature [155, 156, 157]. State points 4, 4c, and 1 are known from the cycle specifications. The mass flow rate and the outlet temperature of the geofluid, therefore, can be calculated by applying the energy balance equations in the preheater/evaporator [47].

$$T_{mid-gf} = T_{4c} + \Delta T_{pp} \tag{A.16}$$

$$\dot{m}_{wf}(h_{4c} - h_4) = \dot{m}_{gf}(h_{mid-gf} - h_{out-gf}) = \dot{m}_{gf}c_{p-gf}(T_{mid-gf} - T_{out-gf}) \tag{A.17}$$

$$\dot{m}_{wf}(h_1 - h_{4c}) = \dot{m}_{gf}(h_{in-gf} - h_{mid-gf}) = \dot{m}_{gf}c_{p-gf}(T_{in-gf} - T_{mid-gf}) \tag{A.18}$$

The power plant output is calculated as

$$\dot{W}_{net} = \dot{W}_{tur} - \dot{W}_{pump} \tag{A.19}$$

Therefore, the efficiency of the Rankine cycle or ORC cab be defined as

$$\eta = \frac{\dot{W}_{net}}{\dot{Q}_{in}} \tag{A.20}$$

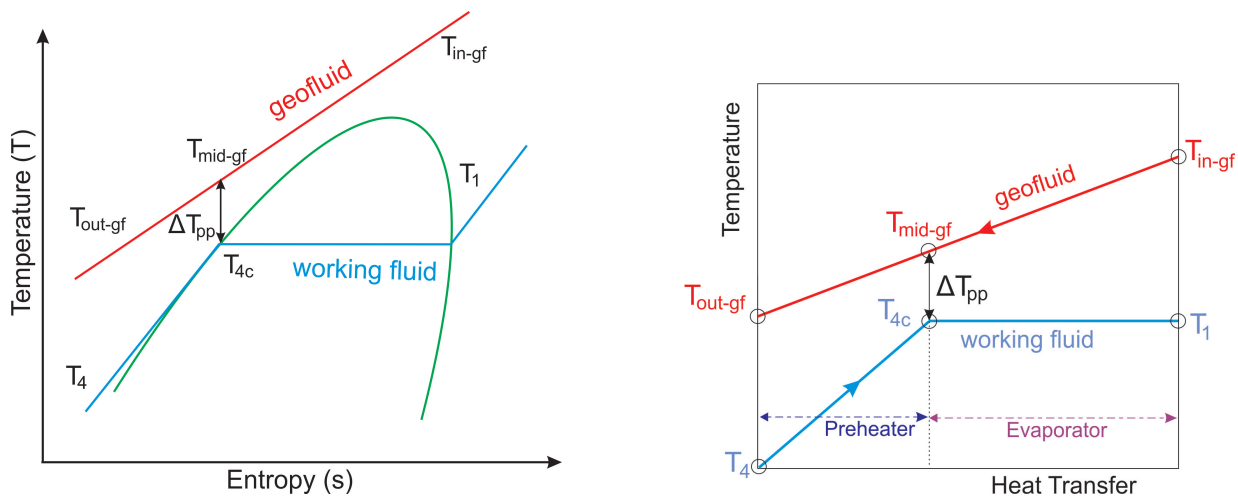

Figure A.3: The evaporator diagram T-S and T-q.

List of Abbreviations

BEM Boundary Element Method 6, 7

CLGS Closed Loop Geothermal System 4, 5, 7, 9–14

DEM Discrete Element Method 6, 7

DFN Discrete Fracture Network 6

EGS Enhanced Geothermal System 4–6, 10–12

FDM Finite Difference Method 6

FEM Finite Element Method 6, 7, 13, 14

FVM Finite Volume Method 6, 7, 13, 14

HDR Hot Dry Rock 3–5, 7, 10–13

OLGS Open Loop Geothermal System 4

ORC Organic Rankine Cycle 9, 12–14

RSM Response Surface Method 13

SCO2 supercritical CO2 6

THM Thermo-Hydro-Mechanical 6